The formation of satellite galaxies and their associated black holes

Libeskind, Noam Isaac

The Formation of Satellite Galaxies and Their Associated Black Holes

Noam Isaac Libeskind

A thesis submitted to the University of Durham
in accordance with the regulations for
admittance to the Degree of Doctor of Philosophy.

Department of Physics
University of Durham
June 2006

Teach me your mood,
O patient stars.
Who climb each night,
the ancient sky.
leaving on space no shade, no scars,
no trace of age, no fear to die.

R. W. Emerson

Contents

List of Figures

List of Tables

0.1 Declaration

The work described in this thesis was undertaken between 2003 and 2006 while the author was a research student under the supervision of Prof. Carlos Frenk and Prof. Shaun Cole in the Department of Physics at the University of Durham. This work has not been submitted for any other degree at the University of Durham or any other University.

Portions of this thesis have been published in the form of papers.

Chapter 2 has been published in the following journal:

- Libeskind N. I., Frenk C. S., Cole S., Helly J. C., Jenkins A., Navarro J. F., Power C. "The distribution of satellite galaxies: the great pancake", 2005, MNRAS, 363, 146

Chapter 3 has been submitted and accepted , and the pre-print may be obtained from astro-ph:

- Libeskind, N. I., Cole S., Frenk C. S., Okamoto T., Jenkins A. "Satellite systems around Galaxies in hydrodynamic simulations", 2006, MNRAS *accepted*, astro-ph/0607237

Chapter 4 has been published in the following journal:

- Libeskind N. I., Cole S., Frenk C. S., Helly J. C. "The effect of gravitational recoil on black holes forming in a hierarchical universe", 2006, MNRAS, 368, 1381

0.2 Acknowledgements

"All journeys have secret destinations of which the traveller is unaware."

-Martin Buber

This thesis has been a journey, and although a vague destination was always in mind, it was those secret destinations that have proven to be the most fruitful. To that end many people have helped me find my way through the, at times, labyrinthine process.

At the top of my list of people to acknowledge, are my two guides and supervisors Prof. Carlos Frenk and Prof. Shaun Cole. Together, their inspirational attitude has sought to lift my spirits and challenge my intellect. Carlos' panache for creativity and keen pedagogical instinct combined with Shaun's attention to detail through his uncompromising understanding of the problems faced by our work, not only helped me produce this thesis, but also served to teach me the virtues and integrity of scientific pursuit.

My fellow graduate students at the ICC (some of whom are now post-docs) have also provided me with help throughout the marathon of this doctorate. Among these are Claudio dalla Vecchia, Richard Whitaker, Rob Crain, and Mark Swinbank. John Helly deserves particular praise for helping me with the nuances of some of the codes I have used. Among the more senior people at the ICC, I must thank Takashi Okamoto, Adrian Jenkins, Vince Eke, Cedric Lacey and Tom Theuns for helping me understand the subtleties and peculiarities of various problems. I must also acknowledge the supervision I have received from Julio Navarro. On the computational side, Lydia Heck has been indispensable to me.

Above and beyond all the technical training I have received during my stint at Durham, this thesis would never have been possible without the support of my brother and sister, Lev and Rachel Libeskind. Together they have served as beacons of fun lighting up my horizon. Constantly beckoning me to come to New York (and giving me tsores when I refused!) they have provided me with the all the energy necessary to live away from home.

This work however, is ultimately indebted to my loving parents Nina and Daniel

Libeskind, who have served as a constant reminder of the important things in life: being healthy and having fun. They have closely followed my progress as a top priority, despite working harder then anyone I know while bearing the responsibility for many other people (not to mention a few cities!) on their shoulders. My father's creative imagination and my mother's realistic approach to facing challenging situations, are attributes that I aspire towards. I hope that in some form or another I have been able to reflect some of these characteristics in the completion of this thesis.

Finally, I *dedicate* this work to Cilia, whose cool and collected attitude has seen me through the ups and downs associated with such a project. I strive to have her tireless optimistic insight into the world as well as her indefatigability, realism, genuineness, sincerity, and love for life. Without her, this cosmos would not be interesting enough to study.

Chapter 1

Introduction to the Standard Model of Cosmology

1.1 Background

According to the modern interpretation of astronomical data, the Universe originated in a hot, uniform and homogeneous state. The cosmos we see today however, is anything but homogeneous lending creed to the idea that tiny density fluctuations must have been present in the Universe's nearly uniform origin. As the Universe expands, these primordial fluctuations grow according to the laws of gravity to form the rich and complicated Universe we see today.

This theory is known as the hot Big Bang model and much of the past half century of cosmological research has been dedicated to testing its implications. One of the central problems this theory poses, is how galaxies form in such an expanding Universe. Modern ideas of galaxy formation invoke radical forms of energy such as non-baryonic dark matter and cosmological dark energy in a bid to balance the cosmic budget and to indirectly, provide the right (empirically motivated) environment in which gas can turn into stars. The sites of galaxy formation are thought to be deep within the potential wells of large dark matter halos, strewn across the universe in a complex filamentary network known as the cosmic web.

In this introduction we[1] provide a justification for the hot Big Bang model via a review of the current status of the theory. We review the central problems of

[1] As dictated by convention, the term "we" will be used throughout this thesis to refer to the first person singular.

galaxy formation and highlight the sophisticated computational achievements that have been made in tackling the galaxy formation problem.

1.1.1 The birth of modern cosmology

The study of the Universe - *cosmology*, is perhaps one of the oldest pursuits of science. Modern cosmology however, is, relatively speaking, one of the younger branches of physics. Its roots were laid less then a century ago, when A. Einstein published *Die Allgemeine Relativitätstheorie* (the general theory of relativity, Einstein 1916), in which he wrote down the field equations: the fundamental relationship between space-time and matter-energy. The science of cosmology may be said to have been born in 1922, when A. Friedmann, G. Lemâitre, H. P. Robertson and A. G. Walker all contributed to solving the field equations under the assumption of the Cosmological Principle - that our Universe is isotropic and homogeneous. The Cosmological Principle led to the Robertson-Walker metric (or the Friedman-Lemâitre Robertson-Walker metric) which may be used to solve the Einstein field equations. The Friedman equations, which describe the dynamics of such a universe, are

$$H^2 \equiv \left(\frac{\dot{a}}{a}\right)^2 = \frac{8\pi G}{3}\rho + \frac{\Lambda}{3} - \frac{kc^2}{a^2} \tag{1.1}$$

$$\frac{\ddot{a}}{a} = -\frac{4\pi G}{3}(\rho + 3p) + \frac{\Lambda}{3}. \tag{1.2}$$

In this model, matter is described as a fluid with density ρ, that exerts a pressure p, in a universe with a curvature k and expansion factor $a = a(t)$; c is the speed of light. Models where the curvature $k = 0, 1, -1$ represents flat, closed and open geometries, respectively. Λ represents the cosmological constant, arbitrarily added by Einstein to the field equations in order to allow for a static Universe. An important cosmological parameter is obtained by setting the global curvature and cosmological constant both to zero ($k = \Lambda = 0$). The critical density then needed to balance the Hubble expansion, and thus 'close' the universe is defined as:

$$\rho_{\rm crit} = \frac{3H^2}{8\pi \rm G}. \tag{1.3}$$

We may also define a dimensionless density parameter

$$\Omega_x = \frac{\rho_x}{\rho_{\rm crit}}, \tag{1.4}$$

where x represents an energy component (e.g. matter, radiation, etc.); note that this is an epoch dependent parameter.

Although ideas about the size and nature of the Universe originated at least since I. Kant posited that the spiral nebulae observed through telescopes were in fact "island universes" (Kant 1798), the real theoretical necessity to understand the behaviour of the Universe began after the advent of General Relativity and the Friedman solution. Observations however, lagged behind: evidence for the existence of extragalactic sources did not surface until Hubble painstakingly collated 18 years of observations of M31 (Hubble 1929b). Using a Period-Luminosity relationship for a Cepheid variable star in M31, Hubble inferred that its distance was roughly $\sim$275 kpc (the distance to M31 is today thought to be $\sim$ 770 kpc), and therefore that it must be external to our Galaxy, whose diameter, although unknown at the time, was not thought to exceed 70-80 kpc.

In the same year that Hubble published the existence of at least one extragalactic source (the implication of which was that all spiral nebulae were extragalactic), he also found a linear relationship between a galaxy's distance and its recessional velocity described by the red Doppler shift in its spectra (Hubble 1929a). The discovery of what has become known as "the Hubble law" indicated that the Universe was expanding, providing evidence for the instability of the cosmos and for the Friedman solutions. This milestone paved the way for the birth of modern cosmology: the study of what the Universe is made out of (galaxies) and how galaxies and the Universe evolve in time.

1.1.2 The Hot Big Bang

The Einstein field equations, solved by assuming the Cosmological Principle, requires that at some finite time in the past, t_0, the scale factor, a, must have been zero. Thus, any homogeneous and isotropic universe must necessarily originate from a singularity of infinite density, known as the Big Bang. Hubble's redshift versus distance relation is exactly what one would expect to see if the Universe has been expanding since the Big Bang.

Implicit in Hubble's redshift versus distance relation is the question, "How fast

is the Universe expanding?", embodied today by the value of the so-called *Hubble constant*[2], H_0. Hubble himself estimated its value to be 500 km s^{-1} Mpc^{-1} (Hubble 1929a), while modern studies indicate the value is closer to 70 km s^{-1} Mpc^{-1} (e.g. Freedman et al. 2001). Measurements of the expansion rate of the Universe generally rely on measuring the distances to galaxies via well known empirical relations such as the Tully-Fisher relation, which correlates galactic circular velocity with luminosity (e.g. Tully and Fisher 1977). So-called "standard candles", objects whose absolute magnitude may be inferred from well known relations, may also be used as distance indicators.

As the Universe expands, the expansion rate is regulated by the Universe's constituent composition: it is decelerated by gravity and accelerated by dark energy. The expansion rate at any given epoch (the Hubble constant, $H_i = H(t_i)$) may be measured in terms of the scale factor and its first derivative ($H_1 \equiv \dot{a}_1/a_1$), as defined in equation 1.1. Thus, in order to measure the rate of change of H, we need to measure H_0 today and compare it with H_1 at some time in the past. Recently, observations of the light curves of distant type Ia Supernovae by Perlmutter et al. (1997) ($z > 0.38$) and Riess et al. (1998) ($0.16 < z < 0.62$) indicate that the expansion rate of the Universe was slower at these redshifts and is thus accelerating, providing the first detection of the effects of a Λ dominated universe.

1.1.3 The Cosmic Microwave background

Shortly after the Big Bang, the density, pressure and temperature of the Universe were all very high. The high temperature allowed matter (composed mainly of protons, simple atomic nuclei and free electrons) and radiation to be in thermal equilibrium. As the Universe expands adiabatically, the density decreased allowing both matter and radiation to cool. When the temperature dropped to $\sim$ 3000 K (at a redshift of $z \sim 1000$) protons were able to recombine with free electrons making the Universe transparent to radiation. The existence of a relic radiation field from the epoch of recombination was first predicted by G. Gamow who estimated that

[2]Throughout this thesis the Hubble constant shall be parameterised by "*little h*" in the conventional way: $H_0 = 100\ h$ km s^{-1} Mpc^{-1}

since recombination the light emitted by the dense plasma that permeated the early Universe, will have been redshifted to lower energies due to the expansion of space. Gamow (1956) calculated that the spectrum of this relic radiation today should be that of a black body at a temperature of 6 K from the He to H ratio predicted by early calculations of primordial nucleosynthesis (see section 1.1.4). The cosmic microwave background (CMB) was serendipitously discovered by Penzias and Wilson (1965), who could not find the cause of an excess 3.5 K temperature noise, in their horn shaped radiometer. They found the signal to be isotropic and therefore most likely of extra-galactic origin.

The Cosmic Background Explorer (COBE) satellite launched in 1989, confirmed the temperature of the background radiation to be 2.7 K and its spectrum to be that of a black body (Smoot et al. 1992). Before the launch of COBE, earlier balloon based experiments had discovered that a major anisotropy in the CMB signal is a dipole, resulting from the earth's motion through space. Besides the dipole, the only departure from isotropy in the CMB is due to the inhomogeneities in the primordial density field. COBE found that after the dipole is subtracted, the CMB's strength doesn't vary with direction: it found fluctuations, but only to one part in 10^5 (Smoot et al. 1992). The next generation of high precision CMB anisotropy research has been conducted by the Wilkinson Microwave Anisotropy Probe (WMAP; Spergel et al. 2003; Spergel et al. 2006).

The acoustic horizon scale, namely the distance an acoustic oscillation can travel through the dense plasma at the time of last scattering, determines the characteristic scale of the CMB temperature fluctuations. The observed angular scale then constrains the geometry of the Universe, albeit with a dependence on h. For accepted values of $h = 0.7$, WMAP points to a flat $k = 0$ universe providing us with evidence that the total energy density of the Universe is close to the critical value (i.e. $\Omega_{\rm tot} = 1$). In the case of a flat universe WMAP data in conjunction with large scale structure surveys, are able to constrain the parameters (e.g. Ω, h) of the current cosmological model and provide us with the first standard cosmological paradigm.

1.1.4 Big Bang Nucleosynthesis

Explaining the relative abundance of the chemical elements has long been a problem considered by astrophysicists. If stars are formed out of primeval Hydrogen, their dense hot centres may be responsible for the fusion of Hydrogen into Helium, and Helium into heavier elements. This mechanism, known as stellar nucleosynthesis, was first addressed by Salpeter (1952) and Burbidge et al. (1957). However it was soon found to drastically under predict the abundance of Helium, which makes up $\sim 25\%$ of the Universe.

The hot, dense state of the early Universe would have been conducive to nuclear fusion. If protons are pushed sufficiently close together, the attractive strong nuclear force dominates the repulsive electromagnetic force, and the protons may fuse. Since the capture of free neutrons is essential in the fusion process, Deuterium and Helium must be produced before the abundance of free neutrons drops due to neutron decay[3]. The presence of high energy gamma rays at early times will have a negative influence and may destroy any newly formed Deuterium. Thus the Universe needs to cool to below 10^{10} K, such that the abundance of photons capable of photo-dissociating Deuterium is low. This occurs when the universe is $\sim$ 2s old (e.g. Zeilik and Gregory 1998). The fusion process cannot run rampant and elements heavier then ^{4}He are not produced in large abundances (trace abundances of ^{7}Li and ^{7}Be are produced) because of a bottleneck due to the instability of nuclei with atomic number 5 and 8. As the Universe cools further, the kinetic energy of the nuclei becomes insufficient to overcome the Coulomb barrier ending nucleosynthesis preventing heavier nuclei from being created. Nucleosynthesis lasts a mere 10^3 seconds, after which fusion ceases and the relative abundances of primordial chemical elements are fixed.

The first reaction in the chain that leads to the production of ^{4}He doesn't build up a lot of D since it is reversible due to the emission of a γ-ray, capable of photodissociation. The low binding energy of D is thus the first 'bottleneck' in that it prevents any Tritium, ^{3}He or ^{4}He from forming until the Universe has cooled and

[3]The nuclear reactions needed to produce ^{4}He are: $p+n \rightarrow \gamma$+D; D+D $\rightarrow n+^3$He; ^{3}He$+n \rightarrow ^3$H $+p$; $^3\mathrm{H} + \mathrm{D} \rightarrow n+^4$He

the chance of photodissociation drops; D + D reactions can then advance at a faster rate. Since Deuterium is only produced as a byproduct, its final abundance is very sensitive to whether the reactions that follow it are able to come to completion - that is, its abundance depends on the reaction rates and the density of baryons, Ω_b. The fraction of baryons locked up in Deuterium (and ^{3}He) is thus constant and provides a mechanism for weighing the baryonic component of the Universe. The production of Deuterium freezes out with a certain number density subject only to the number of baryons per high energy gamma rays (known as the photon per baryon ratio, η) capable of photodissociation. The photon per baryon ratio is defined as:

$$\eta \equiv \frac{\rho_\gamma}{\rho_b} \propto \frac{T_{CMB}^3}{\Omega_b \rho_{crit}} \tag{1.5}$$

where the last step follows since the density of a radiation gas $\rho_\gamma \propto T_{CMB}^3$. Since ρ_{crit} depends on h^2 (e.g. see equation 1.3), and we may accurately measure T_{CMB}, we find that constraints on η may be translated into constraints on $\Omega_b h^2$.

Big Bang nucleosynthesis makes strong predictions for the relative abundances of primordial Deuterium, ^{3}He (produced as a byproduct), ^{4}He, ^{7}Li and ^{7}Be as a function of the photon per baryon value. Although complicated by stellar nucleosynthesis, the fraction of ^{4}He expected from Big Bang nucleosynthesis closely matches that which is observed (e.g. Izotov et al. 1994). Furthermore, measurements of the D/H ratio have been used by Kurki-Suonio (2002) to constrain the baryon fraction of the Universe, Ω_b to $0.005 \leq \Omega_b h^2 \leq 0.022$. Also, Burles and Tytler (1998) measured the D/H ratio in metal poor, high redshift absorption clouds near quasars to estimate that $\Omega_b h^2 = 0.019^{\pm}0.001$. The success of Big Bang nucleosynthesis in explaining the abundance of primordial chemical elements cannot be ignored and must be credited as a significant contribution to the current cosmological paradigm.

1.1.5 Inflation

As successful as the Big Bang model is in explaining the relative abundance of the chemical elements, the existence of the CMB, and the recession of galaxies, before A. Guth developed the theory of inflation in the 1980s (Guth 1981), at least four fundamental problems challenged the Big Bang. These are posed and explained

below:

1. *Why is the density of the Universe today so close to the critical value needed to 'close' the Universe?* As mentioned in section 1.1.2, the amount of matter in the Universe determines whether its ultimate fate is to collapse under gravity in a big crunch (closed), to expand forever (open), or to expand with an ever decreasing expansion rate (flat). As the Universe expands its density quickly evolves away from the critical value. Like a pencil standing on its point, any deviation from the vertical (critical density) is rapidly exacerbated. From the angular scale of CMB anisotropies, we know that the Universe is close to flat (from WMAP results alone $\Omega_k = -0.003^{+0.013}_{-0.017}$; Spergel et al. 2006), implying that in the past the density parameter of the Universe must have been even closer to the critical value. In fact if the density parameter differed by more then only one part in 10^{55} at an age of 10^{-35}s, then by today the Universe would have either already collapsed in a big crunch, or the density of galaxies would have dropped to more then a magnitude below current observational limits. The fine tuning of the density parameter is a highly unlikely result of the Big Bang and is indicative of hidden physics.

2. *Why is the temperature of the CMB so close to being perfectly uniform in every direction?* If one looks at two regions of the sky that are separated by more then $\sim ct$, where c is the speed of light and t is the age of the universe, then these two regions are not and never have been in casual contact[4]. Two regions that are not in casual contact can never have come into thermal equilibrium with each other. At the time of recombination, when the CMB was emitted, the horizon within which regions were at thermal equilibrium was small, and amounts to $\sim$ 1 degree on the sky. Since regions separated by more than this were not in thermal equilibrium at the time the CMB was emitted, the CMB should exhibit large scale anisotropies which are not seen.

3. *Grand Unified Theories predict the existence of topological defects and massive relic particles, yet why are none observed?* In the early universe Grand Unified

[4]The horizon scale in a mass dominated universe is $3ct$.

Theories (GUTs) predict that magnetic monopoles and other relic particles will have been created. These relic particles would have been so massive and contribute so much to the total density parameter, that they would have dominated the young Universe. By today they would have easily caused the universe to collapse. Yet, no GUT relic particle particle has ever been observed and, far from being a dominant source of mass, their contribution to the density parameter is negligible.

4. *What is the origin of the large scale structure of the Universe?* As stated in section 1.1.3, the Universe is not homogeneous and the large scale structure we observe grew out of the existence of density fluctuations present in the early Universe.

The theory of inflation posits that the Universe underwent a period of rapid exponential growth ($a \propto e^{Ht}$) within the first 10^{-32}s. The expansion rate accelerated ($\ddot{a} > 0$), and the Universe doubled in size roughly $\sim$80 times from a size of 10^{-25}m to 0.1m. This occurred because the inflaton's quantum (scalar) field had a non-zero vacuum energy density which acted like a cosmological constant. This simple picture explains the uniformity of the CMB: regions outside of each others horizon's at the time the CMB was emitted were within casual contact before inflation. Inflation also drives the density parameter towards the critical value. This occurs because as the Universe inflates, any regions of curvature are necessarily ironed out during the inflationary stage. Inflation ends when the scalar field's vacuum energy eventually decays. This reheats the Universe and creates the matter that permeates space-time. Inflation dilutes the number of massive relic particles such that the number within our horizon today is estimated to be $\lesssim 1$. As long as $T_{\text{reheat}} < T_{\text{GUT}}$, no additional relic particles are created by GUTs. Finally, quantum fluctuations of the inflaton's scalar field in the pre-inflationary Universe are stretched into the primordial density fluctuations which, through gravitational instability, grow into the large scale structure of galaxies and clusters.

It is remarkable that by allowing for a period of inflationary expansion in the early universe, these four very serious problems are all easily solved. Although it is not yet part of the so-called "standard model of particle physics" nor any proposed Grand Unified extension, inflation has been heralded as one of the saviours of the

Big Bang theory.

1.1.6 Dark Matter

The existence of non-luminous dark matter was first hypothesised by F. Zwicky (Zwicky 1933) to account for the kinematics of galaxies in the Coma cluster. By looking at the motions of the galaxies on the periphery of the Coma cluster, Zwicky used Newtonian dynamics to estimate the cluster's dynamical mass assuming that the galaxies were all bound to the cluster. When compared to the luminous mass estimated using a fiducial value for the mass per unit luminosity, Zwicky found that the dynamical mass is roughly 400 times larger then its luminous counterpart.

This idea gained firm observational support on smaller scales when the rotation curves of individual galaxies were measured (e.g. Rubin et al. 1980). Instead of falling of as $r^{-1/2}$ as expected from Keplerian dynamics, the velocity of stars orbiting at large distances from the centre of galaxies remains constant. The high orbital velocity of stars at large radii may be explained either by the existence of a non-luminous, galaxy encompassing contribution to the mass, or by modifying the laws of gravity (e.g. Milgrom 1983).

Although a relativistic theory of Modified Newtonian Dynamics (MOND), in which the interaction between light and matter is well described, has been formulated (Bekenstein 2004), it has yet to predict the observed large scale structure of the Universe starting from the initial conditions of the CMB. Also, arguments against MOND have been made by by looking at the density of Ly-α absorbers (Aguirre et al. 2001) and direct evidence for the necessity of dark matter, even within a MONDian framework, exists from weak lensing studies of galaxy clusters (e.g. Gavazzi 2002; Clowe et al. 2004). In light of the hypothetical nature of MONDian cosmogonies, in this thesis we focus on CDM.

To make matters worse, the dark matter inferred from rotation curves and cluster dynamics may be dominated by a non-baryonic component. As mentioned in section 1.1.4, Big Bang nucleosynthesis places firm constraints on the baryonic density of the Universe. Uncertainties and factors of h aside, Big Bang nucleosynthesis provides at the most $\Omega_{\rm b} \simeq 0.06$. The total value of $\Omega_{\rm m}$ as measured dynamically

from the motion of clusters is at least 0.2, strongly suggesting that the invisible matter dominating the dynamics of galaxies and clusters is non-baryonic. Furthermore, X-ray measurements of intra-cluster gas in the Coma cluster have shown that the baryonic component, while making a significant contribution to the cluster, is nevertheless limited to $\Omega_b/\Omega_m \leq 0.09$. In combination with estimates of Ω_b from nucleosynthesis and assuming that the baryon fraction of the Coma cluster is representative of the universal value, White et al. (1993) were able to constrain $\Omega_m < 0.2$. Thus this measurement of the baryon fraction in the Coma cluster, when combined with both the baryonic component of the density predicted by Big Bang nucleosynthesis and the flat geometry suggested by the CMB, provides a strong indication of the existence of dark energy, namely a cosmological constant, Λ.

Depending on whether the velocity of the dark matter particle is relativistic or not at the time of decoupling (from the radiation dominated early universe), non-baryonic dark matter may be divided into two flavours: "hot" and "cold". The most obvious first candidate for dark matter was the massive neutrino. Neutrinos decouple from the primordial photon bath at very high energies, making them a potential type of Hot Dark Matter. Since neutrinos were created in great abundance during the Big Bang (10^9 neutrinos per baryon), assigning them even a small mass would help balance the cosmic density budget and raise the global value of Ω_m . While perhaps the most natural explanation for dark matter, one argument for dismissing massive neutrinos (or indeed any form of Hot Dark Matter) as the dark matter particle is that they they wash away small scale structures due to a process known as free streaming (Bond et al. 1980). Free streaming occurs because collisionless neutrinos can stream from the high density regions into the low density regions uninhibited, thereby smoothing out the density field (i.e. $v_\nu >> v_{esc}$). Thus any small scale structures in a universe dominated by Hot Dark Matter must have been formed in a top-down way (i.e. fragmentation when a density perturbation becomes non-linear) later on in cosmic history. Yet small scale power is observed in the high redshift Universe, and Hot Dark Matter can therefore be ruled out by the existence of many non-linear structures (e.g. Quasars at $z > 4$) which would not have had the time to fragment if the dominant form of dark matter were relativistic.

Cold Dark Matter (CDM) is composed of particles massive enough to be moving

at non-relativistic speeds when they decouple from the radiation dominating the early Universe. Supersymmetry may provide candidates for the CDM particle (e.g. the axion), although none of these candidates have ever been observed and their motivation is purely theoretical. Yet, the non-relativistic nature of CDM provides an attractive model of structure formation. Since CDM is non-relativistic, it is able to form clumps at high redshift that are then able to merge in a roughly hierarchical fashion. The large scale structure of the Universe as observed in large sky surveys such as the 2dFGRS (Colless et al. 2003; Cole et al. 2005) and SDSS (Abazajian et al. and The SDSS collaboration 2005) is well modelled by CDM. Claims that CDM does not produce enough large scale power (e.g. filaments and voids) has been successfully addressed by White et al. (1987).

1.1.7 The Growth of Perturbations and Structure Formation

The inhomogeneities visible in the CMB are a result of a primordially inhomogeneous density field. Inflation conveniently provides a mechanism for creating these density fluctuations. Since inflation does not end everywhere simultaneously and since it is during the reheating phase of inflation which comes at the end of the inflationary epoch that matter and energy are created, after inflation is over the Universe will be clumpy. In the linear regime, these density perturbations are amplified during the expansion of the Universe, as regions that are over-dense grow slower than the expansion (owing to gravitational effects), while regions that are under dense expand more rapidly than the global expansion.

The perturbations produced during inflation have a power law spectrum

$$|\delta_k|^2 \propto k^n, \tag{1.6}$$

where δ_k is the Fourier transform of the density fluctuation $\delta = \Delta\rho/\rho$, and k is the wave number which denotes the physical size of the fluctuation. The spectral index $n \approx 0.95$, (Spergel et al. 2006) is thought to be close to unity and power is distributed over many scales. As mentioned in section 1.1.6 the shape of the power spectrum can constrain the nature of the dark matter which permeates the Universe.

The growth of the primordial perturbations into the structures we see today, is primarily driven by the *hierarchical* nature of the clustering of CDM, on which gravity acts. The first objects to form in a CDM universe are small dark matter halo progenitors. These small haloes grow by successive mergers and accretion into the large $z = 0$ haloes that host galaxies and clusters. Some of the first N-body calculations made to simulate this process were performed by Davis et al. (1985) who found that under the right cosmological assumptions the clustering of galaxies may be reproduced.

Recently, two major redshift surveys (2dFGRS and SDSS) have completed surveying hundreds of thousands of galaxies in a bid to measure the large scale distribution of galaxies. Clustering statistics of the galaxy distribution can be used to constrain $\Omega_{\rm m}h$ as well as the baryon fraction $\Omega_{\rm b}/\Omega_{\rm m}$. These surveys provide strong evidence for a low, but non-negligible baryon fraction by detecting the existence of so-called "baryon wiggles", oscillations in the galaxy power spectrum resulting from the non-zero baryonic contribution to the growth of structure (Cole et al. 2005, Eisenstein et al. 2005). Also, these surveys have allowed us to measure the contribution to Ω from dark matter which which as mentioned in section 1.1.6, falls short of unity.

1.1.8 Towards a standard model

The numerous successes of the Big Bang model have created a cosmological paradigm, now being called "The Standard model of Cosmology". The paradigm is built up by the convincing measurement of suite a of cosmological numbers (including h, k, $\Omega_{\rm b}$, $\Omega_{\rm m}$, Λ), combined with theoretical justification for the values these numbers may assume. Measurements of the recessional velocity of distant galaxies have shown that the Universe is expanding at a rate of 70 kms^{-1} per Mpc ($h \approx 0.7$, Freedman et al. 2001). Highly precise measurements of the anisotropies in the CMB point to flat $k = 0$ Universe (Spergel et al. 2006), implying that the the density of the Universe may be expressed as $\Omega_{\rm m} + \Omega_\Lambda = 1$. Large scale sky surveys (such as 2dFGRS and SDSS) allow us to measure the fraction of the Universe made out of matter (multiplied by h: i.e. $\Omega_{\rm m}h$). Since the value of $\Omega_{\rm m} = 0.27$ measured in this

way falls short of unity (e.g. Cole et al. 2005), the value of $\Omega_\Lambda = 0.73$ is needed to obtain a flat Universe and be consistent with the geometry measurements of the CMB. A positive value for Λ is also needed to explain the apparent acceleration of the expansion rate as mentioned in section 1.1.2. Finally, the theory of Big Bang nucleosynthesis allows us to constrain the baryonic contribution to the mass density of the Universe (multiplied by the hubble constant squared: $\Omega_b h^2$) by measuring the cosmic abundance of Deuterium. The CMB also allows us to measure the baryonic mass contribution via the location of the first acoustic peak in its power spectrum. Both methods are consistent and indicate that baryonic mass contributes a mere 4% to the energy budget of the Universe, implying that 23% of the Universe's matter is weakly or non-interacting dark matter. (A minor role is also played by the Ly-α forest, many of whose properties are predicted by this model.)

Although, by no means agreed on by all cosmologists, this model explains many features of the observable Universe. Its successes include being able to predict quantitative and qualitative aspects of the Universe starting from the initial conditions of inflation. Although highly successful in reproducing many attributes of the local and high-z universe, the model invokes physically motivated yet at times uncomfortable forms of matter and energy that have yet to be directly detected. While providing a robust framework within which galaxies may be studied, the ΛCDM model cannot independently predict all the nuances of the galaxy population. Perhaps now, the most interesting tests of the paradigm are found not on the large scales of the Universe, but on the small scales of galaxies. This thesis focuses on the predictions the ΛCDM cosmological model makes on the small scales probed by haloes of Milky Way galaxies. In particular we are interested in the sites of satellite galaxy formation, their luminosity function, the orientation of Milky Way type galaxies with respect to their haloes and the impact the presence of naked black holes has on galaxies. In the next section we review the current status of galaxy formation in ΛCDM cosmogonies.

1.2 Phenomenological Galaxy Formation

The baryonic matter of which galaxies are composed and the dark matter that dominates the formation of large scale structure, are likely to behave quite differently on the small scales of galaxy formation. Baryonic gas for example, is susceptible to radiative cooling and shock heating. These thermodynamic processes influence the properties of the baryonic halo material, and are thus instrumental in determining the distribution of halo gas. Rees and Ostriker (1977), Silk (1977) and Binney (1977) were the first to realise that the atomic processes associated with radiative cooling would have a dramatic effect on gas in a halo. In the absence of any form of heating (i.e. shock heating due to mergers) the baryonic gas will radiate away its thermal energy, lose its pressure support, and collapse to the centre of the halo. The density of this cold gas will eventually reach a critical value where star formation may occur.

In section 1.1.7 we described the hierarchical nature of structure formation in a universe dominated by CDM. White and Rees (1978) incorporated the ideas of radiative cooling into a hierarchical model wherein gas is able to cool in the centres of dark matter haloes. The efficiency of a galaxy to form in a dark halo is dependent on the ability of the halo gas to cool. This in turn is sensitive to a number of effects including the merger history of its dark matter halo (as mergers are likely to shock heat the halo's gas reservoir to the virial temperature) and the presence of energetic supernovae.

The merger history of a particular halo may be quantised by the halo's "merger tree". White and Rees (1978) based their galaxy formation calculations on the mass functions analytically derived by the Press-Schechter formalism (Press and Schechter 1974) and succeeded in predicting properties of the galaxy population in a number of ways, including reproducing the observed galaxy luminosity function's shape. Despite its successes, the galaxy formation models of White and Rees (1978) suffered from producing an over-abundance of faint galaxies, and indicated that some additional form of heating was necessary to suppress halo gas from cooling. White and Frenk (1991) elaborated on previous ideas and constructed some of the first analytic models of galaxy formation, while Cole (1991) used the merger

tree formula obtained by Bond et al. (1991) to construct the first semi-analytical models of galaxy formation in a CDM universe. Both reached similar conclusions to White and Rees (1978) and inferred that galaxy-galaxy mergers were an important process needed to help avoid the over abundance of galaxies. Bond et al. (1991) produced a phenomenological model where observationally motivated assumptions and analytical approximations are used together in order to predict a wide range of galaxy properties. As more and more physical effects have been recognised as important processes in the galaxy formation puzzle, the phenomenological models have become more and more complicated. Other advances include the ramifications of satellite-satellite mergers first studied by Somerville and Primack (1999), while the effect of dust extinction on morphologies and luminosities of galaxies was first addressed by Kauffmann et al. (1999). Quasar activity in the nucleus of a galaxy was studied by Kauffmann and Haehnelt (2000) who modelled Quasars using a physically motivated recipe for black hole growth. The properties of the Lyman break galaxy population (Baugh et al. 1998, Governato et al. 1998), the clustering dependence on redshift, luminosity and morphology (Kauffmann et al. 1997, Baugh et al. 1999), and the evolution of galaxy clusters (e.g. Kauffmann and Charlot 1998) have all been studied in this phenomenological way.

Models of this type, known as "semi-analytical models", use a combination of physically motivated prescriptions with analytical calculations to predict a wide variety of galaxy characteristics. Although galaxies are simulated "phenomenologically", the advantage of semi-analytical modelling is that the user can readily measure the sensitivity of the galaxy population to one particular parameter. Theoretical constraints on otherwise free parameters (e.g. feedback) can be set.

While much of galaxy formation research was focusing on calculations performed on a halo's merger tree (known as semi-analytical modelling), the advent of computer simulations was getting underway as well. Aarseth et al. (1979) ran the first N-body simulations of cluster formation using 1000 point masses each representing a single galaxy. The problem of galaxy formation is best addressed by using these two powerful tools (N-body simulations and semi-analytical modelling) in conjunction with each other. Below we explain the state of the art of both of these tools.

1.3 Semi-analytical modelling

Throughout this thesis, we have made extensive use (see Chapters 2 and 4) of the GALFORM semi-analytical model. This code, first developed by Cole et al. (1994) and subsequently extended by Cole et al. (2000), Benson et al. (2002b) and Bower et al. (2005) among others, combines physically motivated prescriptions with analytical calculations to give a phenomenological method of predicting a wide variety of galaxy characteristics. Below we summarise the physics implemented in the model, emphasising those aspects most important for this thesis.

1.3.1 Dark Matter halo merger trees

In order to predict certain characteristics of a galaxy at any time during its assembly, the GALFORM semi-analytical model starts with a given $z = 0$ galaxy halo mass. The haloes merger history is then calculated by using an analytical extension (Cole 1989; Cole 1991; Bower 1991; Bond et al. 1991; Lacey and Cole 1993) to the Press-Schechter formalism (Press and Schechter 1974)[5]. Equation 2.15 of Lacey and Cole (1993) gives the fraction of mass, $f_{12}(M_1, M_2)$, in haloes of mass M_2 at a time t_2, which at a previous time t_1, was in haloes of mass in the range $M_1 \rightarrow M_1 + dM_1$:

$$f_{12}(M_1, M_2)dM_1 = \frac{1}{\sqrt{2\pi}} \frac{(\delta_{c1} - \delta_{c2})}{(\sigma_1^2 - \sigma_2^2)^{3/2}} \times \exp\left(-\frac{(\delta_{c1} - \delta_{c2})^2}{2(\sigma_1^2 - \sigma_2^2)}\right) \frac{d\sigma_1^2}{d\mathrm{M}_1} d\mathrm{M}_1. \quad (1.7)$$

The quantities σ_1 and σ_2 are the linear theory root mean square overdensities in spheres of mass M_1 and M_2. The quantities δ_{c1} and δ_{c2} represent the critical linear theory over density thresholds for collapse at times t_1 and t_2 respectively. $\sigma(M)$ is computed from the density fluctuation power spectrum which is well constrained by large sky surveys, while δ_c depends on the cosmology and is computed assuming a spherical collapse model.

Equation 1.7 is used to construct *binary* merger trees. In order to ensure that each halo is composed of only two progenitors and that multiple mergers do not occur, we ensure that each time step, dt_1, is sufficiently small. The binary merger

[5]Although in this thesis we have made extensive use of extracting merger trees directly from N-body simulations (see sec. 1.4.2) we have also used the analytical method based on Cole et al. (2000), and as such its description is included.

tree is created by following the procedure described in Cole et al. (2000) on every fragment of the halo. The time resolution used to ensure each halo has no more then two progenitors is accordingly, very high. Yet, the binary merger tree may be used to produce a more realistic merger tree with reduced time resolution by placing each node on a pre-defined grid of time steps. A sequence of fast, rapid, binary mergers, will thus appear as simultaneous multiple mergers in the new discretzed tree.

We thus start by specifying a mass M_0 and a time $z = z_0$ at which we wish to calculate certain galaxy properties. We construct the merger tree "backwards" in time, generation by generation, until we reach $z_{start} > z_0$. The rules of star formation, however progress "forwards" in time, starting at the top of the halo merger tree and moving down to the bottom.

1.3.2 Halo properties

In order to calculate the physical properties of galaxies that form within dark matter haloes, we need a detailed model for the internal structure of haloes. Below we describe how we model these internal properties which include the distribution of spins, the interior density profile and the halo's rotation. Many parameters needed to describe the internal structure of haloes are taken from results obtained in N-body simulations.

Spin Distribution

The spin of a dark matter halo is quantified by a dimensionless spin parameter:

$$\lambda_{\rm H} = \frac{J_{\rm H}|E_{\rm H}|^{1/2}}{{\rm G}M_{\rm H}^{5/2}} \tag{1.8}$$

where G is Newton's gravitational constant and where $J_{\rm H}$, $M_{\rm H}$, and $E_{\rm H}$ are the total angular momentum, mass, and energy of a halo. According to Cole and Lacey (1996), we may assign each newly formed halo a spin parameter drawn at random from a log-normal distribution of $\lambda_{\rm H}$:

$$P(\lambda_{\rm H})d\lambda_{\rm H} = \frac{1}{\sqrt{2\pi}\sigma_\lambda}\exp\left(\frac{(\ln\lambda - \ln\lambda_{\rm med})^2}{2\sigma_\lambda^2}\right)\frac{d\lambda_{\rm H}}{\lambda_{\rm H}} \tag{1.9}$$

with the median spin value of $\lambda_{\rm H} = 0.039$ and a deviation of $\sigma_\lambda = 0.53$. These fits were obtained for a specific halo mass in a CDM cosmology, however they only

weakly depend on mass and power spectrum slope.

Halo density Profile

All haloes that form in the merger tree are assumed to be spherically symmetric and have a dark mass distribution described by the "NFW" profile (Navarro, Frenk & White 1996, 1997):

$$\rho(r) = \frac{\Delta_{\rm vir}\rho_{\rm crit}}{f(a_{\rm NFW})} \frac{1}{r/r_{\rm vir}(r/r_{\rm vir} + a_{\rm NFW})^2} \tag{1.10}$$

Here $f(a_{\rm NFW}) = \ln(1 + 1/a_{\rm NFW}) - 1/(1 + a_{\rm NFW})$. The density profile is valid only interior to the virial radius ($r \leq r_{\rm vir}$) which is defined as the radius at which the mean interior density is $\Delta_{\rm vir}\rho_{\rm crit}$. The value of the virial over density, $\Delta_{\rm vir}$ depends on both the background cosmological model as well as the geometry of halo collapse (e.g. see Eke et al. 1996). The concentration of the halo is described by $a_{\rm NFW}$, and is correlated to the halo mass (e.g. see Navarro et al. 1997) albeit with a considerable scatter (e.g. Jing 2000 and Bullock et al. 2001). The scatter in the correlation is ignored in our model, but we note that if we introduce some scatter by perturbing $a_{\rm NFW}$ about the mean, we find a negligible effect on the statistics of galaxy properties.

Halo Rotation Velocity

We assume that the mean rotational velocity $v_{\rm rot}$, of concentric shells of halo material is constant with radius and always aligned in the same direction (motivated by N-body studies; see Warren et al. 1992). We relate $v_{\rm rot}$ to the halo's spin parameter, $\lambda_{\rm H}$ by:

$$v_{\rm rot} = A(a_{\rm NFW})\lambda_{\rm H} V_{\rm H} \tag{1.11}$$

where $V_{\rm H} \equiv \sqrt{GM/r_{\rm vir}}$ is the halo's circular velocity at the virial radius, and $A(a_{\rm NFW})$ is a dimensionless coefficient, weakly dependent on $a_{\rm NFW}$ ($A \approx 3.9$ for $a_{\rm NFW} = 0.01$, while $A \approx 4.5$ for $a_{\rm NFW} = 0.3$; see appendix A of Cole et al. 2000).

1.3.3 Gas Distribution and Cooling

In the GALFORM model, gas is assumed to be either "hot" halo gas, or "cold" galactic gas. The hot halo gas will cool into the cold galactic gas during the galaxy formation

process. During mergers or halo collapse, all diffuse halo gas is assumed to be shock heated to the virial temperature given by

$$T_{\rm vir} = \frac{\mu m_{\rm H} V_{\rm H}^2}{2k_{\rm B}} \tag{1.12}$$

where $k_{\rm B}$ is Boltzmann's constant, μ is the mean molecular mass and $m_{\rm H}$ is the mass of the Hydrogen atom. This shock heated gas settles into a spherically symmetric distribution and is typically less concentrated than the dark matter. Its distribution is well approximated by the β-model (Cavaliere and Fusco-Femiano 1976) where the choice of β (motivated by the simulation results of Navarro et al. 1995 and Eke et al. 1998) yields a hot gas density profile,

$$\rho_{\rm gas}(r) \propto \frac{1}{r^2 + r_{\rm core}^2}, \tag{1.13}$$

where the first generation of haloes have an initial core radius $r_{\rm core} = a_{\rm NFW} r_{\rm vir}/3$. This value of the core radius is allowed to change as the halo gas cools. The analytical work by Evrard and Henry (1991), Kay and Bower (1999), and Wu et al. (2000) indicates that increasing the minimum entropy of the gas can increase the core radius. The cooling has little effect in the outer areas of the halo as the pressure at the virial radius is controlled by shocks from infalling matter.

When a new halo forms, we determine if any gas has already cooled by looking at the fraction of mass in hot gas. If some gas has already cooled (and the hot mass fraction is less than the global value $\Omega_{\rm b}/\Omega_{\rm m}$) the core radius is increased until we recover the same density at the virial radius that we would have found had no gas cooled.

The cooling time for a halo is calculated as:

$$\tau_{\rm cool}(r) = \frac{3}{2}\frac{1}{\mu m_{\rm H}}\frac{k_{\rm B} T_{\rm gas}}{\rho_{\rm gas}(r)\Lambda(T_{\rm gas}, Z_{\rm gas})} \tag{1.14}$$

where $\rho_{\rm gas}(r)$ is the gas density a distance r from the halo centre, $T_{\rm gas}$ is the gas temperature and $Z_{\rm gas}$ its the metallicity. The cooling function $\Lambda(T_{\rm gas}, Z_{\rm gas})$ depends on both gas temperature and metallicity and we use the values tabulated by Sutherland and Dopita (1993).

We define a cooling radius $r_{\rm cool}(t)$ which allows us to calculate the amount of gas that can cool in the halo within a time $t = \tau_{\rm cool}$. However the gas must also have

enough time to be accreted by the disc. We estimate the time needed for accretion as the free fall time. We define a free fall radius $r_{\rm ff}(t)$ beyond which material does not have enough time to fall onto the galaxy. To calculate the amount of mass that cools onto the disc during a single time step Δt, we calculate $r_{\rm min}(t) = \min[{\rm r_{cool}}, {\rm r_{ff}}]$ at the beginning and end of each time step. The amount of gas that is able to cool onto the disc is then set to the mass of hot gas in the shell defined by the two values that determine $r_{\rm min}$ (that is, $r_{\rm ff}$ and $r_{\rm cool}$) and is equal to $\dot{M}_{\rm cool}\Delta t$. This process defines a cooling rate $\dot{M}_{\rm cool}$, which is important for calculating metal enrichment, star formation and feedback (see sec. 1.4.2).

Disc sizes are calculated assuming angular momentum to be conserved during the cooling of hot halo gas. Thus, the specific angular momentum added to a galaxy during its formation is equal to that which the gas within $r_{\rm min}(t) = \min[{\rm r_{cool}}, {\rm r_{ff}}]$ originally had. This assumption is non-trivial and has a dramatic effect on sizes of discs that form. In Chapter 3 we use hydrodynamic methods to test the reliability of this angular momentum assumption. The so-called "angular momentum catastrophe" (first identified by Navarro and Benz 1991) indicates that in hydrodynamic simulations discs are too small. This occurs in their simulations since the diffuse halo gas first cools into clumps. These clumps are very efficient in merging with a central galaxy via the loss of angular momentum by dynamical friction against the dark matter halo. Angular momentum is more likely to be conserved if feedback can prevent halo gas from cooling into small clumps, and instead the gas radiatively cools directly on to the disc (see Weil et al. 1998, Sommer-Larsen et al. 1999, Eke et al. 2000).

1.3.4 Star and Disc Formation

The process of star formation begins with the cooling of hot gas. However as cold gas is turned into stars many effects need to be taken into account. The formation (and rapid death) of large Super Novae (SNe) will inject metals and energy into the interstellar medium (ISM). The outflows from SNe are a form of feedback and can heat up cold gas and inhibit star formation. Enriching the ISM will also have an effect on the cooling times and allow more gas to cool at later times. If powerful

enough, SNe can drive material out of the galaxy via strong hot stellar winds. Below we summarise how we treat all these effects.

We assume that the instantaneous star formation rate, ψ is directly proportional to the cold gas mass:

$$\psi = M_{\rm cold}/\tau_{\star}, \tag{1.15}$$

where $\tau_{\star}$ is the star formation time scale. We model feedback by young stars by assuming that cold gas mass is reheated and ejected from the disc at a rate of:

$$\dot{M}_{\rm eject} = \beta\psi, \tag{1.16}$$

where β is the feedback efficiency whose value, like $\tau_{\star}$, depends on the global properties of the galaxy. The star formation timescale is related to the disc's circular velocity by:

$$\tau_{\star} = \epsilon_{\star}^{-1}\tau_{\rm disk}(V_{\rm disk}/200\ {\rm kms}^{-1})^{\alpha_{\star}}, \tag{1.17}$$

where $\tau_{\rm disk}$ is the dynamical time of the disk defined at its half mass radius as $\tau_{\rm disk} \equiv r_{\rm disk}/V_{\rm disk}$. The feedback efficiency is defined as

$$\beta = (V_{\rm disk}/V_{\rm hot})^{-\alpha_{\rm hot}}, \tag{1.18}$$

where $\epsilon_{\star}$, $\alpha_{\star}$, and $\alpha_{\rm hot}$ are all dimensionless parameters while $V_{\rm hot}$ has the dimensions of velocity. In the Cole et al. (2000) model these parameters are set to 0.005, -1.5, 2.0 and 150 km s^{-1} respectively. These values were selected in order to reproduced physical characteristics of the galaxy population such as the Tully-Fisher relation and the faint end of the galaxy luminosity function.

1.3.5 Chemical enrichment

Cooling of hot halo gas, the formation of stars and the ejection and reheating of gas due to SNe, are all processes which are assumed to occur instantaneously. We therefore use an instantaneous recycling approximation to model these effects. Over one time step of the merger tree, the cooling rate $\dot{M}_{\rm cool}$ and hot gas metallicity $Z_{\rm hot}$, is assumed to be constant. The differential equations we use to describe the metal enrichment due to star formation are:

$$\dot{M}_\star = (1-R)\psi \tag{1.19}$$

$$\dot{M}_{\rm hot} = -\dot{M}_{\rm cool} + \beta\psi \tag{1.20}$$

$$\dot{M}_{\rm cold} = \dot{M}_{\rm cool} - (1-R+\beta)\psi \tag{1.21}$$

$$\dot{M}^Z_\star = (1-R)Z_{\rm cold}\psi \tag{1.22}$$

$$\dot{M}^Z_{\rm hot} = -\dot{M}_{\rm cool}Z_{\rm hot} + \beta Z_{\rm cold}\psi \tag{1.23}$$

$$\dot{M}^Z_{\rm cold} = \dot{M}_{\rm cool}Z_{\rm hot} + (p-(1+\beta-R)Z_{\rm cold})\psi \tag{1.24}$$

where the metallicity of cold gas is

$$Z_{\rm cold} = M^Z_{\rm cold}/M_{\rm cold} \tag{1.25}$$

and likewise, the metallicity of hot gas is given by

$$Z_{\rm hot} = M^Z_{\rm hot}/M_{\rm hot}. \tag{1.26}$$

R represents the fraction of mass recycled by stars and p represents the yield: the fraction of mass that is converted into stars and then returned to the ISM as metals. These differential equations are easily solved (see Appendix B of Cole et al. 2000) and we can obtain analytical solutions to the time evolution of most of these quantities.

1.3.6 Spheroid formation and Galaxy mergers

Dynamical Friction

The spherical bulges of spiral galaxies, as well as large elliptical galaxies are formed primarily through galaxy mergers. When two dark haloes merge, the largest of the two galaxies becomes the new "central" galaxy, while the rest of the galaxies present in each halo fall into orbit around the central galaxy. Their orbits will gradually decay as they lose energy and angular momentum to the dark halo via dynamical friction. The timescale for merging satellites is based on Chandrasekhar's dynamical friction formula (Chandrasekhar 1943), and is calculated as:

$$\tau_{\rm mrg} = f_{\rm df}\Theta_{\rm orbit}\tau_{\rm dyn}\frac{0.3722}{\ln(M_{\rm H}/M_{\rm sat})}\frac{M_{\rm H}}{M_{\rm sat}} \tag{1.27}$$

where $M_{\rm H}$ is the halo mass, $M_{\rm sat}$ is the mass of both the satellite and the halo in which it formed, and $\tau_{\rm dyn} \equiv \pi r_{\rm vir}/V_{\rm H}$ is the halo's dynamical time. $f_{\rm df}$ is a free parameter which may be adjusted depending on the uncertainties assumed in the model (set by Cole et al. 2000 to be unity).

The orbital parameters of the satellite experiencing dynamical friction are contained in the term $\Theta_{\rm orbit}$ and defined as

$$\Theta_{\rm orbit} = \left(\frac{J}{J_{\rm c}(E)}\right)^{0.76} \left(\frac{r_{\rm c}(E)}{r_{\rm vir}}\right)^{2}, \tag{1.28}$$

where E, and J are the satellite's initial energy and angular momentum, and $r_{\rm c}(E)$ and $J_{\rm c}(E)$ are the radius and angular momentum of a circular orbit with the same energy. The orbital parameters of infalling satellites have been studied by Tormen (1997) (see also Benson 2005) who find that the distribution of $\Theta_{\rm orbit}$ is well fit by a log-normal distribution. Thus infalling satellites will merge with the central galaxy when their merger timescale is shorter than the age of the halo. Not all satellites will merge during the lifetime of a halo: when a new halo forms, each satellite is given a random value of $\Theta_{\rm orbit}$ according to a log-normal distribution. $\tau_{\rm mrg}$ is calculated and the satellite merges with the central galaxy after this period, provided that during this time the halo has not itself merged to become part of a larger halo. Any satellites that have not already merged are then re-assigned a value of $\Theta_{\rm orbit}$ and $\tau_{\rm mrg}$ is re-calculated.

Spheroids: Mergers, Bursts and Disc Instabilities

The morphology of the product of a merger between a central galaxy and a satellite will depend on (among other things such as gas content metallicity, etc.) the mass ratio of the merging satellite $M_{\rm sat}$ to the mass of the central galaxy $M_{\rm cen}$. We make use of the prescription used in Kauffmann et al. (1993) to divide mergers into two categories: "major" and "minor". We define a threshold, $f_{\rm ellip} = 0.3$ and term a merger as "major" if $M_{\rm sat}/M_{\rm cen} \geq f_{\rm ellip}$ and "minor" if $M_{\rm sat}/M_{\rm cen} < f_{\rm ellip}$. During a major merger, a single bulge of stars is produced. All the cold gas in both discs is turned into stars in a burst of star formation. If the merger is minor, the stars of the satellite are merged onto the bulge of the central galaxy. Any gas present in the satellite is added to the gaseous disk of the central galaxy.

We also allow spheroids to form via the additional route of disk instabilities. Strongly self gravitating discs are likely to be unstable to the formation of a bar which will evolve into a bulge (e.g. see Efstathiou et al. 1982, Binney and Tremaine 1987, Mo et al. 1998). This occurs because there is a maximum rotation velocity that an axis-symmetric disc can obtain before the disc structure becomes disrupted. In order to estimate the stability of a given galactic disc, we calculate the number

$$\epsilon_{\rm m} \equiv \frac{V_{\rm max}}{\sqrt{{\rm G}M_{\rm disk}/r_{\rm disk}}} \tag{1.29}$$

where $V_{\rm max}$ is the circular velocity at the half mass radius $r_{\rm disk}$. Efstathiou et al. (1982) have set $\epsilon_{\rm m} \gtrsim \epsilon_{\rm crit} = 1.1$ for a disc to be unstable, however we will use a value ($\epsilon_{\rm crit} = 1.05$) that reproduces a more realistic distribution of bulge to total luminosity ratios (see Sec. 4.3.2). If a given disc satisfies the bar instability criteria, we assume that all the disc stars evolve into a bar which is dynamically unstable and which subsequently evolves into a bulge (Combes et al. 1990). The bar instability also causes any gas present in the disc to be funnelled towards the centre and then undergo a burst of star formation. The gas that gets channelled towards the centre may provide fuel for the black hole that rests in the centre of the bulge. While some of this cold gas will be transformed into stars, some of it may equally be available for black hole growth.

1.3.7 Galaxy Sizes

In order to calculate the sizes of the two (disc + bulge) component galaxy we are guided by the following two principles:

a) The size of a stellar disc is determined by the conservation of angular momentum and centrifugal equilibrium.

b) The size of a stellar bulge is determined by the conservation of energy and virial equilibrium.

For discs, we idealistically assume an exponential surface density profile (see Eqn. 4.3) while for bulges we assume an $r^{1/4}$ deVaucolouers profile in projection (see Eqn. 4.7). As discs form by conserving the angular momentum of the halo gas that cools, their sizes are relatively straight forward to calculate. Spheroids formed

by the merger of two galaxies however, are said to ultimately "merge" when the separation of each component equals the sum of their half mass radii. Conservation of energy and the virial theorem lead to:

$$\frac{(M_1+M_2)^2}{r_{\rm new}} = \frac{M_1^2}{r_1} + \frac{M_2^2}{r_2} + \frac{f_{\rm orbit}}{c} + \frac{M_1 M_2}{r_1+r_2} \tag{1.30}$$

where $r_{\rm new}$, r_1 and r_2 are the half mass radii of the product and of the merging partners whose total mass is M_1 and M_2. The factor c and $f_{\rm orbit}$ relate to the binding and orbital energy of each component:

$$E_{\rm bind} = -c\frac{{\rm G}(M_1+M_2)^2}{r} \tag{1.31}$$

$$E_{\rm orbit} = -\frac{f_{\rm orbit}}{2}\frac{{\rm G}M_1 M_2}{r_1+r_2} \tag{1.32}$$

The value of $f_{\rm orbit} = 1$ is adopted such that the orbital energy corresponds to that of two point masses in a circular orbit. The value of c depends weakly on the density profile of the galaxy ($c \approx 0.49$ for an exponential disc and $c \approx 0.45$ for a deVacolouer's spheroid) and for simplicity we use $c = 0.5$.

When a bulge is formed due to a bar instability, its size is computed using a slightly different equation. If the mass of the unstable disc and the existing bulge (if there is one) before the formation of a bar is $M_{\rm disc}$ and $M_{\rm bulge}$, and their half mass radius are $r_{\rm disc}$ and $r_{\rm bulge}$ then the final bulge half mass radius will be:

$$\frac{c_{\rm B}(M_{\rm disc}+M_{\rm bulge})^2}{r_{\rm new}} = \frac{c_{\rm B}M_{\rm bulge}^2}{r_{\rm bulge}} + \frac{c_{\rm D}M_{\rm disc}^2}{r_{\rm disc}} + f_{\rm int}\frac{M_{\rm bulge}M_{\rm disc}}{r_{\rm bulge}+r_{\rm disc}} \tag{1.33}$$

The factors $c_{\rm D} = 0.49$ and $c_{\rm B} = 0.45$ are adopted for an exponential disc and a deVaucolouers spheroid, as mentioned above. The final term represents the gravitational interaction energy between the disc and bulge and we use $f_{\rm int} = 2$ in order to approximate the values of the interaction energy over a realistic range of $r_{\rm bulge}/r_{\rm disc}$.

1.3.8 Stellar Population Synthesis and Dust Extinction

As shown above, the GALFORM model is able to produce a range of galaxy characteristics including star formation histories, sizes and masses of bulge and disc components, chemical enrichment and metallicities. However in order to compare

these properties with observations, we need to model the spectra and photometric properties of the galaxies as well as including the effects of interstellar dust extinction.

In order to compute the properties of a stellar population we need to combine the star formation history of that population with an assumed initial mass function (IMF). The models of Bruzual and Charlot (1993, 2003) provide a spectral energy distribution (SED) for a single stellar population, $l_\lambda(Z,t)$, which depends on the metallicity Z and age t. The entire galaxy's SED may be obtained by convolving this with the galaxy's star formation history:

$$L_\lambda(t) = \int_0^t l_\lambda(t-t', Z(t'))\psi(t')dt' \tag{1.34}$$

where $Z(t')$ and $\psi(t')$ are the metallicity and star formation rate of the stars which formed at a time t'. As stated earlier, an assumption regarding the IMF of the stars must be made. We assume that all galaxies have the same IMF at all times. The form Cole et al. (2000) adopt for the IMF is known as the "Kennicut" IMF (Kennicutt 1983):

$$\frac{dN}{d\ln m} \propto m^{-x} \tag{1.35}$$

where $x = 0.4$ for $m < M_\odot$ and $x = 1.35$ for $m > M_\odot$. Some of the star forming mass will form brown dwarfs ($m < 0.1M_\odot$), which will not contribute to the SED of the galaxy. The fraction of brown dwarfs is represented by Υ, defined as:

$$\Upsilon = \frac{\text{mass in visible stars + brown dwarfs}}{\text{mass in visible stars}} \tag{1.36}$$

The masses used here are the masses at the moment the stellar population forms, i.e. before accounting for the fraction of mass recycled back into the ISM. Brown dwarfs reduce all luminosities by a factor of $\sim 1/\Upsilon$. Observational estimates constrain Υ to fall in the range $1 < \Upsilon \lesssim 2$ (Broeils 1992; Mobasher et al. 1999).

The effect of dust on starlight is treated using the models of Ferrara et al. (1999) who include both the absorption and the scattering of starlight by inter-galactic dust grains for a realistic three dimensional distribution of stars and dust.

1.4 N-body simulations

As we have seen in the previous section semi-analytical galaxy formation models rely on constraining unknown parameters from the results obtained by N-body simulations (such as the distribution of $\lambda_{\rm H}$). N-body simulations are also a powerful tool in the cosmologists arsenal because they provide a spatial context within which one may study the assembly of a single galaxy, a group of galaxies or a cluster. N-body techniques have come a long way since their inception, and there now exists a myriad of N-body codes as well as software to interpret the (at times) massive data output. In this thesis we have made extensive use of N-body simulations of galaxy haloes. Here, we briefly review the codes used and the state-of-the art in hydrodynamic and N-body methods.

1.4.1 N-body codes

All the simulations used in this thesis were performed with the parallel N-body code known as GADGET (Springel et al. 2001b)[6]. GADGET evaluates the forces (accelerations) on each individual particle due to all the other particles in the simulation, by using a hierarchical tree data structure (Barnes and Hut 1986). A gravitational 'softening' length is introduced to prevent the force between two neighbouring particles from becoming infinite, since this would cause an unphysical two-body scattering between closely separated CDM particles. The dark matter particles are thus assumed to be collisionless.

Initial Conditions

The cosmological simulations we use are performed in periodic boxes. The effect of periodicity is that the box must have a total density exactly equal to the mean density of the universe. Also periodic boundary conditions allow the density field to be easily expanded in terms of Fourier transforms, allowing for a simple representation in Fourier space. The box however, must be large enough such that perturbations on scales comparable to the box size must still be linear by $z = 0$.

[6]Not all the simulations used herein were performed with the exact same version of GADGET, and this is explicitly stated where pertinent.

The initial conditions (initial positions and velocities) of each particle is generated in order to recover a Gaussian density field with a specified power spectrum at times when linear theory is still a valid approximation. Each particle is displaced from its position in an initially smooth distribution. The amount by which each particle is perturbed is calculated following the Zel'dovich approximation (Zel'Dovich 1970) for linear theory (see Efstathiou et al. 1985). The peculiar velocity assigned to each particle is proportional to its displacement and matched to the growing mode of linear perturbation theory.

Mass refinement

We are able to achieve a high resolution (low particle mass) region embedded in a lower resolution background by a mass refinement technique (e.g. see Katz and White 1993; Navarro and White 1994). First, a low resolution simulation in a periodic box is run to $z = 0$. The final output is examined and a region of interest (where it is believed a galaxy will form) is targeted. Those particles that fall within this region ($\sim 2r_{\rm vir}$) of interest are traced back to the initial conditions, where their positions and velocities on the original cubic grid are noted. A box is then drawn around all these particles. This box is then filled with low mass particles. Appropriate small scale power is added to the initial condition's power spectrum. The simulation is then re-executed to $z = 0$ providing us with two different dark matter particle resolutions: a high resolution population (concentrated within a region of interest) embedded in a low resolution (high mass "boundary" particles) region. This process may also be carried out recursively with the highest resolution particles concentrated in the centre of an 'onion shell' configuration, while multiple species of lower resolution particles are confined, in decreasing resolution, to outer concentric shells.

In this thesis we concentrate on the high resolution regions of galactic halo simulations. It is these regions which will have enough small scale power to resolve subhalos within which it is believed satellite galaxies may form. How these subhalos are identified is explained below.

Identifying substructures

In order to identify small bound substructures within large parent haloes we use the algorithm SUBFIND (Springel et al. 2001a). The algorithm starts by identifying "Friends-of Friends" (FOF) groups (e.g. Davis et al. 1985) by linking together into the same group, particles whose mean inter-particle separation is less than some "linking length", b. Particles linked together in this manner form groups approximately enclosed by surfaces of constant isodensity ($\rho \propto 1/b^3$). By setting $b = 0.2$, FOF returns groups whose over density roughly corresponds to that predicted by the spherical collapse model, i.e. virialised haloes. However, besides having a tendency to link two haloes via "bridges", FOF has no way of selecting bound substructures from within a larger halo. If sufficient numerical resolution is used, many studies (e.g. Tormen 1997; Ghigna et al. 1998; Moore et al. 1999; Ghigna et al. 2000) have shown that the dense cores of small CDM haloes are able to survive the mass loss effects (such as tidal stripping) associated with merging (i.e. the "over-merging problem"). These dense cores must be identified as they are likely to be the sites of satellite galaxy formation.

SUBFIND demands that a substructure satisfies the following two criteria: that it is locally over dense and that it is self bound. The algorithm starts by assigning a density ρ to each particle (by calculating the distance r_n to its nth neighbour) as $\rho \sim 1/r_n^3$. Substructures are locally over dense regions that are contained within an isodensity contour that traverses a saddle point. In order to find these saddle points, imagine ordering the particles by density and (conceptually) replacing them one by one in order of decreasing density. When a particle i with density ρ_i is considered, the $N_{\rm ngb}$ nearest neighbours (within the entire simulation) are identified. We call this set of $N_{\rm ngb}$ particles Ξ_i. Within Ξ_i we define the subset of particles whose density is *higher* than ρ_i as Ψ_i. We define the set Π_i as the subset of Ψ_i containing the two particles closest to particle i. The set Π_i may either contain two particles, one particle or be empty. We examine each of these cases:

i) $\Pi_i = 0$. If Π_i is empty, then none of the $N_{\rm ngb}$ nearest neighbours have a larger density than particle i. Particle i is considered to be a local density maximum and a new subgroup is grown around it.

ii) $\Pi_i = 1$. If Π_i contains a single particle (or two particles belonging to the same group) than particle i is also a member of this subgroup.

iii) $\Pi_i = 2$. If Π_i contains two particles that are members of two different groups, than particle i is a saddle point. The two groups defined by the two particles in Π_i are labelled as "subhalo candidates". The two groups are then joined and particle i is added to the new group.

Using this algorithm provides us with a list of groups and subgroups. In order to ensure that each group meets the self-bound criteria, a binding energy calculation is performed on each subhalo and unbound particles are stripped of group membership. We then impose a $N_{\rm ngb} = 10$ particle limit on each subhalo and reject subhalos with fewer particles.

In this algorithm, a particle may easily be a member of more then one subgroup and there is, in effect, no limit to the number of "haloes within haloes" we can find. However for our purposes we wish each particle to be a member of only one subgroup at any given time. In order to achieve this we only consider the smaller of the two groups each time a particle is thought to be a saddle point (case (iii) above). This decision is motivated by the fact that we are interested in looking at small groups within larger parent haloes, and the mass of the larger halo is assumed to be greater than that of the subhalo.

1.4.2 Extracting Merger trees from N-body simulations

We use `GADGET` to run simulations of galactic sized haloes, and apply the algorithm `SUBFIND` in order to identify bound subhalos for each redshift output. We then wish to link subgroups of the main halo through the simulation outputs, in order to extract the merger history of each subhalo as well as the formation of the main halo.

We begin by looking at subhalo catalogues for two sequential time steps $t_1 < t_2$. A halo at time t_1 is considered to be the progenitor of any halo at time t_2 which contains the largest fraction of its particles. We perform this linking for all adjacent simulation snapshot outputs and it is then straight forward to construct a merger history for each halo.

This process relies on identifying each halo in a given simulation output, and being able to trace it forwards in time by assuming it can only increase in mass. In an idealised hierarchical universe this idea holds as halos grow via mergers. However in practise a halo can lose mass as well (due to, for example, tidal stripping and the arbitrary boundary imposed by FOF). Thus in the linking algorithm discussed above, we occasionally find haloes that are less massive than the sum of their progenitors, corresponding to the unphysical case wherein a halo accretes *negative* mass. The two ways of dealing with these (rare) situations is to either add mass to the halo, or subtract mass from its progenitors. Both of these simple methods cause similar concerns. Adding mass to the halo may be problematic if the halo itself is a progenitor, of a halo which is now less massive then the sum of its progenitors. Similarly the problem is propagated throughout early times if the mass of the progenitors is reduced as it will become less massive than its progenitors. When we reduce the mass of a halo, we do so such that we minimise the effect on early output times. This can be accomplished since each halo has a certain excess mass (mass accreted in the form of small unresolved dark matter halos), which when removed will have no effect on its progenitors at earlier times. If a halo is found which is less massive than the sum of its progenitors, then first the excess mass of its largest progenitor is removed. If this is not enough the excess mass of the second largest progenitor is removed and so on. If the excess mass from all progenitors has been removed, yet the halo in question is still less massive then the sum of its progenitors, we scale the masses of all of its progenitors down be a certain factor. Although one may be inclined to think that the problem of mass conservation may be serious, in practice serious violations rarely occur. Additionally, it has been shown that the reassignment of mass in halos has little effect on the galaxy properties (Helly et al. 2003).

1.4.3 Smooth Particle Hydrodynamics

In Chapter 3 we make use of gas dynamical (SPH) simulations. These differ from simulations of collisionless CDM in that in addition to the dark matter particles, gas is treated by using pseudo particles that are assumed to represent the gas

distribution in a fluid cell (Gingold and Monaghan 1977; Lucy 1977; Monaghan 1992). At every given time step, each SPH particle has a well defined mass, thermal energy, and velocity. The properties of the gas that the discrete SPH particles are designed to represent (e.g. temperature, density, etc.), are determined by averaging (smoothing) over all other particles within a characteristic length scale (known as the "smoothing length") using a kernel function, which gives a different weight to each particle depending on its distance (e.g. a Gaussian). One of the advantages of SPH simulations is that this smoothing length is allowed to vary depending on the local conditions, thus optimising computational efficiency. The Lagrangian nature of SPH means that in dense regions, the smoothing length is very small and results in a high spatial resolution, whereas in regions of low density the smoothing length is large and the computational cost in these regions is minimised.

The thermodynamic properties of the gas and accelerations ('forces') on each particle, are calculated by solving smoothed versions of the differential hydrodynamical equation (these are: the momentum equation, the continuity equation, and the thermal energy transfer equation). Star formation is made to occur when a gas particle meets a certain (temperature and density) criteria. Gas particles then undergo star formation and spawn star particles. The star particle's own properties (e.g. metallicity, mass, etc.) are assigned in a self-consistent way. Each star particle is assumed to represent a star cluster and as such has a pre-defined initial mass function (depending on how it was created; see Chapter 3). Unlike dark matter, the number of SPH particles is not conserved. Although SPH particles may not be created, one gas particle may spawn multiple star particles depending on the pre-starbursting mass of the gas particle, and the nature of the star burst. Star particles differ from their SPH counterparts in that they are assumed to be collisionless.

1.5 Motivation for this Thesis

The motivation for this work grew out of three open problems facing the ΛCDM model: the "missing satellite problem", the "satellite orientation problem" and the effect of gravitational recoil on black holes forming in a hierarchical universe. Below, I will review each of these problems and summarise the work that follows in the

succeeding chapters.

1.5.1 The "Missing satellite" Problem

N-body simulations of galactic halos forming in a ΛCDM universe, have consistently shown that the number of dark matter haloes that survive (as subhalos) the mass loss effects due to merging, is at least an order of magnitude more than the number of satellite galaxies seen orbiting the Milky Way (Moore et al. 1999, Klypin et al. 1999). The discrepancy exists over a large range of satellite masses. Observations of Milky Way satellites are however likely to be incomplete. Willman et al. (2004) claim that low-latitude observations of satellites will be incomplete due to Galactic obscuration. Additionally, observations of dwarf satellites in the outer halo will likewise be incomplete due to their inherent dimness. Unfortunately, these biases are likely to increase the number of faint satellites in the Milky Way's neighbourhood by only a factor of ~ 2 and not fully solve the discrepancy between the number of predicted subhalos and the number of observed satellites in a galactic halo. Nevertheless, the entire population of satellites of the Milky Way is far from being fully observed, and faint new satellites are being identified at an ever increasing rate (eight in 2006 alone: Zucker et al. 2006, Belokurov et al. 2006a, Belokurov et al. 2006b, Willman et al. 2006). However, the discovery of new satellites is only likely to affect that faint end of the luminosity function and the problem will persist as large bright satellites orbiting the Galaxy are unlikely to be discovered.

An alternative approach is to prevent galaxies from forming in all subhalos. Benson et al. (2002a), used a very detailed model of reionization to calculate the flux of UV ionizing photons emitted by hot young OB stars (see also Gnedin 2000). While photo-ionization of halo gas can inhibit gas from radiatively cooling and forming stars in the central regions of subhalos, Benson et al found that they were unable to prevent enough galaxies from forming using only reionization.

A somewhat related problem is how the Milky Way satellites are distributed about the Galaxy. The first observations of the distribution of the Milky Way satellites were made by Kunkel and Demers (1976). Later, Lynden-Bell (1982) noted that instead of being spherically distributed about the Galaxy, the satellite

galaxies appeared anisotropically situated along polar orbits. Kroupa et al. (2005) claim that this anisotropy is at odds with the spherical CDM prediction. Indeed N-body simulations indicate that subhalos are themselves close to being spherically distributed inside galactic sized dark matter halos. In Chapter 2 we attempt to tackle this problem by examining the distribution of satellites in N-body simulations populated by using the semi-analytical model presented in section. 1.3.

1.5.2 The Alignment and angular momentum problem

It has been known since the pioneering gas dynamical work of Navarro and Benz (1991) that simulations have a hard time reproducing disc galaxies whose size is similar to that observed. For the most part, this is due to the fact that most discs in their simulations form by gas cooling into small clumps which then merge via dynamical friction with a central bulge. The size of a disc is determined by the angular momentum of the material which forms it. However if gas is allowed to cool at high redshift, then much of the angular momentum will be lost as the clumps spiral in due to dynamical friction, and the resulting discs that are formed are too small. In this thesis, we make use of the galaxy formation model of Okamoto et al. (2005) that successfully prevents excessive gas cooling in small clumps by including photoionization, as well as a top-heavy IMF in bursts that injects sufficient energy as to regulate cooling. In these simulations, the angular momentum problem is solved and realistically sized discs are created. We study the alignment between the discs and the satellite distribution as well as the alignments between the angular momenta of the dark halo, the galaxy, and the satellite distribution. In Chapter 3 we study the shape distribution of satellites and both the spatial and angular momentum alignment of various components of the galactic halo.

1.5.3 Gravitational recoil in a Hierarchical Universe

Nearly all galactic bulges are thought to harbour a black hole, whose mass correlates remarkably very well with the velocity dispersion and mass of the bulge itself. The bulges of galaxies are made up by successive mergers of a combination of disc and bulge dominated galaxies. If the black holes that reside in the centre of each bulge

are assumed to merge as well, some very interesting effects will come into play. For example, the merging of two black holes will cause gravitational radiation to be emitted from the final inner most stable orbit. If the black holes are of unequal mass, this gravitational radiation will be beamed anisotropically and result in changing the system's net linear angular momentum. The consequence of such a black hole merger is a large linear momentum kick in a direction specified by the final orbit. We investigate the effect of this gravitational recoil on galacto-centric black holes. Can black holes be ejected from galaxies in this way? What fraction of the total black hole mass is in ejected black holes and can we constrain the uncertain physics of kicks by looking at the scatter about the empirical $M_{\rm bh} - M_{\rm bulge}$ relation? In Chapter 4 we address this problem by incorporating the growth of black holes in to GALFORM. We also model the kick velocity, and use N-body simulations to track the spatial distribution of black hole.

Chapter 2

The Great Pancake of Milky Way Satellites

2.1 Introduction

In the cold dark matter (CDM) cosmology, structure builds up through fragments merging together in a roughly hierarchical way. High resolution N-body simulations of the formation of dark matter halos in the ΛCDM cosmology have demonstrated that the cores of tightly bound fragments often survive the merging process and remain as distinct substructures orbiting inside a parent halo (Klypin et al. 1999, Moore et al. 1999). The centre of the main halo and the accompanying substructures are naturally identified with the formation sites of central and satellite galaxies respectively. The N-body simulations suggest that the mass functions of surviving substructures in galactic and cluster halos are roughly self-similar. Yet, the luminosity function of galaxies in rich clusters has a very different shape from the luminosity function of satellites in smaller systems such as the Milky Way or the Local Group (Kauffmann et al. 1993; Mateo 1998; Trentham and Hodgkin 2002; Benson et al. 2002b, Eke et al. 2004). Not only is the central galaxy much more prominent in Milky-Way systems than in galaxy clusters, but the number of surviving subhalos in simulations of galaxy-sized halos far exceeds the number of the known satellites of the Milky Way.

The discrepancy between the small number of satellites around the Milky Way and the large number of surviving substructures, once regarded as a major challenge to the cold dark matter cosmology, is now thought to be due to the astrophysical processes that regulate the cooling of gas in halos and its subsequent transformation into stars. The increase in the entropy of the intergalactic medium brought about

by the reionization of the gas at early times has been identified as a possible solution to the so-called "satellite problem" (Kauffmann et al. 1993; Bullock 2002; Benson et al. 2002a; see also Stoehr et al. 2002). Reionization sharply reduces the efficiency of gas cooling in small halos so that galaxies that formed prior to reionization are preferentially those that end up as satellites in systems like the Local Group. The detailed model calculated by Benson et al. (2002a), which includes the effects of early reionization as well as other forms of feedback, reproduces many observed properties of the Local Group's satellite system, including the distribution function of circular velocity, the luminosity function and the colour distribution.

While the original satellite problem is no longer deemed a serious challenge, another related potential problem for the cosmological paradigm has recently been highlighted by Kroupa, Thies & Boily (2005). These authors argue that the strongly flattened spatial distribution of the 11 brightest dwarf satellites of the Milky Way, a feature known, but not understood, for many years (Lynden-Bell 1976; Kunkel and Demers 1976; Kunkel and Demers 1977; Lynden-Bell 1982; Majewski 1994), is inconsistent with the ΛCDM model. According to Kroupa et al. (2005), CDM models predict a roughly isotropic distribution of satellites. They based this conclusion on the assumption that the spatial distribution of satellites resembles the spatial distribution of the halo dark matter which indeed, as N-body simulations have demonstrated, is approximately (although not exactly) spherical (e.g. Frenk et al. 1988; Jing and Suto 2002; Bullock 2002).

In this Chapter, we demonstrate that the satellites of systems like the Local Group do *not* trace the distribution of halo mass. On the contrary, the satellites in our suite of high resolution N-body simulations are generally arranged in highly flattened configurations which have similar properties to those of the Milky Way satellite system. This, at first sight surprising, result is a reflection of the anisotropic accretion of subhalos which generally stream into the main halo along the filaments of the cosmic web. The flattened structure in which the brightest Milky Way satellites lie traces a great circle on the sky and is approximately perpendicular to the Galactic Plane (throughout this Chapter we use the terms "brightest" and "most luminous" satellite galaxies; strictly speaking these satellites were selected according to the mass of the stellar component). In our simulations, the satellite structures

tend to be aligned with the major axis of the triaxial halo mass distribution, that is, the longest axis of the halo is close to lying in the principal plane of the satellite distribution.

As the work in this Chapter was nearing completion, two related papers appeared on astro-ph. Both of them used high-resolution simulations of galaxy halos similar to those that we have performed. Kang et al. (2005) identified "satellites" in their 4 simulations with randomly chosen dark matter particles taken either from the halo as a whole or exclusively from substructures. They were able to find flattened satellite systems similar to that of the Milky Way in the former case but not in the latter. Zentner et al. (2005) found satellites in three N-body simulations of Milky-Way type systems also in two different ways. In the first, they used the semi-analytic model of Kravtsov, Gnedin & Klypin (2004) which is based on similar principles as those applied by Benson et al. (2002a). In their second model, they identified satellites with the most massive subhalos. Zentner et al. (2005) found that in both cases, the satellite systems had a planar distribution similar to that in the Milky Way and argued that the degree of central concentration of the satellite systems plays an important role in this result. They also showed that the population of subhalos as a whole is anisotropic and preferentially aligned with the major axis of the triaxial halo.

Like Zentner et al. (2005), our study employs a semi-analytic model to follow the formation of the visible satellites. In this respect, both these studies are quite different from that of Kang et al. (2005) who based their conclusions purely on dark matter particles. Our model differs from that of Zentner et al. (2005) in several important respects. Our simulation codes and methods for identifying substructure are different. While they considered three halos specifically chosen to lie on a filament, we used 6 simulations randomly chosen from a large cosmological volume. The biggest difference, however, concerns the semi-analytic models used in the two studies. While both of them give a reasonable match to several observed properties of the Milky Way's satellites, our semi-analytic model has been applied and tested much more extensively than that of Kravtsov et al. (2004). The model we use is based on the GALFORM code of Cole et al. (2000) as extended by Benson et al. (2002b). This model has been shown to give an acceptable account of many properties of the

galaxy population as a whole including the luminosity function in various passbands, from the UV to the far infrared, and in various environments, distributions of colour, size and morphological type, etc. The model is also relatively successful at matching the properties of galaxies at high-redshift, as discussed in Baugh et al. (2004). Finally, the two studies use somewhat different methods to quantify the distribution of Milky Way satellites and to compare the results with the observations. On the whole, the conclusions of the two studies are consistent although there remain some differences as we discuss in Section 5.

The remainder of this Chapter is organised as follows: in Section 2.2 we outline the methods used; in Section 2.3.1 we present our results which we interpret in Section 2.3.2; in Section 5 we discuss the implications of our findings.

2.2 Simulations and galaxy formation model

We have analyzed 6 high-resolution N-body simulations of galactic-size dark matter halos carried out with the GADGET code (Springel et al. 2001b). The halos, chosen to have a mass $\sim 10^{12}\mathrm{M}_{\odot}$, were otherwise randomly selected from a large cosmological simulation of a cubic region of side 35.325 h^{-1}Mpc in a flat ΛCDM universe (with $\Omega_{\mathrm{m}} = 0.3, h = 0.7, \sigma_8 = 0.9$). The simulation was executed a second time adding "high resolution" (i.e. small mass) particles, and appropriate small scale power in the initial conditions, to a region surrounding the halo under consideration. These simulations have been studied extensively in previous papers (Power et al. 2003, Hayashi et al. 2004, Navarro et al. 2004b) and we refer the reader to those papers for specific details of how the simulations were carried out. Table 2.2 summarizes the important parameters of the simulations.

We identified bound substructures in the simulation using the algorithm SUBFIND (Springel et al. 2001a). First, "friends-of-friends" groups (Davis et al. 1985) are found by linking together particles whose separation is less than 0.2 times the mean interparticle separation, corresponding roughly to particles within the virialized region of the halo. SUBFIND then identifies substructures within these halos based on an excursion set approach, using the spatial and velocity information for each particle in order to define self-bound objects.

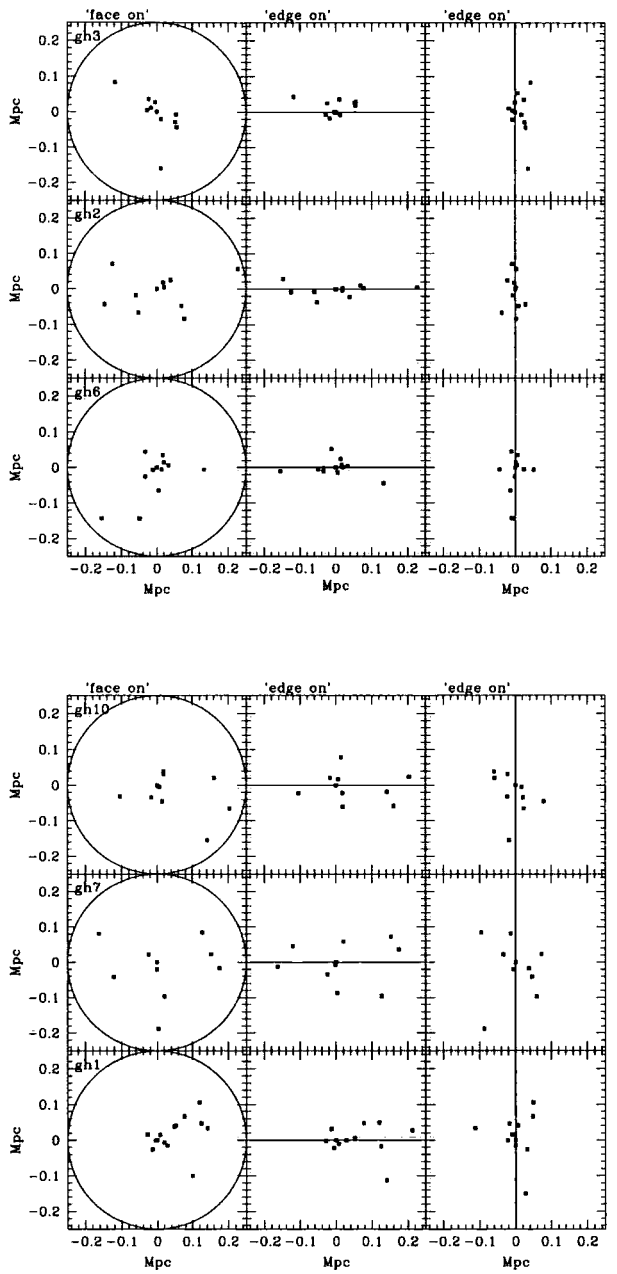

Figure 2.1: Projections of the positions of the 11 most massive satellites within 250 kpc of the central galaxy along the principal axes of the inertia tensor in simulations gh3, gh2 and gh6 (above) and in simulations gh10, gh7 and gh1 (below).

	$N_{\rm tot}$ (10^6)	$N_{\rm hr}$ (10^6)	$R_{\rm vir}$ (h^{-1} kpc)	$N_{\rm vir}$ (10^6)
gh1	14.6	12.9	110	1.07
gh2	18.1	16.2	131	1.74
gh3	18.0	16.2	170	3.73
gh6	25.5	22.2	169	3.76
gh7	19.2	17.3	156	2.99
gh10	13.4	12.1	133	1.86

Table 2.1: Parameters for the six N-body halo simulations. The columns give: (1) halo label; (2) total number of particles in the simulation cube; (3) number of high resolution particles; (4) virial radius of the halo in h^{-1} Mpc defined as the distance from the centre to the radius at which the mean interior density is 200 times the critical density; (5) number of particles within the virial radius. All halos were simulated in a cube of comoving length $35.325\,h^{-1}$Mpc in a ΛCDM universe, with a particle mass of $2.64 \times 10^5 h^{-1} M_\odot$ in the 'high resolution' region.

For each halo, we generate a complete merger history, identifying all progenitor and descendant halos, as described in Helly et al. (2003). The semi-analytic galaxy formation model is calculated along each branch of the merger tree. This is based on the model described in detail in Cole et al. (2000) and Benson et al. (2002b) and summarised in section 1.3. The model includes the following physical processes: (i) the shock-heating and virialization of gas within the gravitational potential well of each halo; (ii) radiative cooling of gas onto a galactic disk; (iii) the formation of stars from the cooled gas; (iv) the effects of photoionization on the thermal state and cooling properties of the intergalactic medium; (v) reheating and expulsion of cooled gas through feedback processes associated with stellar winds and supernovae explosions (see Benson et al. 2003b); (vi) the evolution of the stellar populations; (vii) the effects of dust absorption and radiation; (viii) the chemical evolution of the stars and gas; (ix) galaxy mergers (which, depending on the violence of the merger, may be accompanied by starbursts and the formation of a bulge – see Baugh et al. 2004); (x) the evolution of the size of the disk and bulge.

Our model differs from that of Cole et al. (2000) and Helly et al. (2003) in the way in which galaxy mergers are treated. In the current model, the positions of satellite galaxies and the time when they merge is determined by using information from SUBFIND. Central galaxies are placed on the most bound particle of the most massive subgroup in the halo. (SUBFIND identifies the background mass distribution of the halo as a separate subgroup, so this is generally a robust way to define the centre of the halo.) Satellite galaxies are placed on the descendant subhalo of the progenitor halo in which they formed. If the subhalo ceases to be identified by SUBFIND at some later output time, we continue to trace its constituent particles and place the galaxy at the centre of mass of this group of particles. A galaxy is considered to have merged onto the central galaxy if its distance from the central galaxy is less than the spatial extent of the set of particles it is associated with.

An overview of the results of our semi-analytic model as regards the evolution of the galaxy population as a whole may be found in Benson et al. (2003a) and Baugh et al. (2004) while results relevant to the satellites of the Milky Way may be found in Benson et al. (2002a).

2.3 Results

We begin by quantifying the shapes of dark matter halos in the simulations and sub-sytems within them. We then interpret the results in terms of the formation histories of the halos and their subsystems.

2.3.1 The morphology of halos and their subsystems

The semi-analytic model applied to the N-body simulations provides the position and internal properties of the central galaxy in each halo and its satellites. According to the semi-analytic model, three of the central galaxies are spirals and three ellipticals. For the purpose of comparing with the analysis of Kroupa et al. (2005), we select the 11 most luminous satellites in each halo within a distance of 250 kpc from the central galaxy. We calculate the moment of inertia tensor of this satellite subsample, weighting each object equally, and obtain the principal axes of

the distributions.

Fig. 2.1 shows three orthogonal projections along the principal axes of the satellite systems in our six simulations. The figure reveals, remarkably, that the loci of the 11 brightest satellites define a thin, disk-like structure around the central galaxy. As we show below, in most cases, the satellite structure is aligned with the major axis of its triaxial host dark matter halo.

The distribution of the luminous satellites differs significantly from the distribution of the dark matter substructures identified by SUBFIND. Fig. 2.2 is analogous to Fig. 2.1 but the points plotted now correspond to the most massive 1000 substructures found within 250 kpc of the central galaxy. The projections are along the principal axes of the inertia tensor of the substructure systems. It is evident that the distribution of substructures is much less anisotropic than that of the satellites in Fig. 2.1.

The eigenvalues of the diagonalised inertia tensor are proportional to the root mean square deviation of the x, y and z coordinates relative to the principal axes. Denoting the major, intermediate and minor axes by a, b and c respectively ($a > b > c$), the flattening of the system may be quantified by the ratios c/a and b/a. The early N-body simulations of Frenk et al. (1988) showed that CDM halos are triaxial and recent work indicates that c/a= 0.7 ± 0.17, and b/a> 0.7 (Bullock 2002).

The axial ratios, found by diagonalising the moment of inertia tensor, of the dark matter halos and various subsystems of objects within them are plotted Fig. 2.3. Fig. 2.3a shows that our simulated halos have axial ratios consistent with those found in previous simulations and tend to congregate near the top right of the panel corresponding to nearly spherical objects. This is also the region populated by the systems composed of the 1000 most massive subhalos.

The axial ratios of the systems consisting of the 11 most luminous satellites are plotted in Fig. 2.3b. The triangles correspond to our full semi-analytic model (shown in Fig. 2.1) and the squares to a variant in which the early reionization of the intergalactic medium is not included. The satellite systems in the two models have similar flattening because more than 80 % of the subhalos that host the brightest satellites in the two cases are the same. However, as discussed by Benson

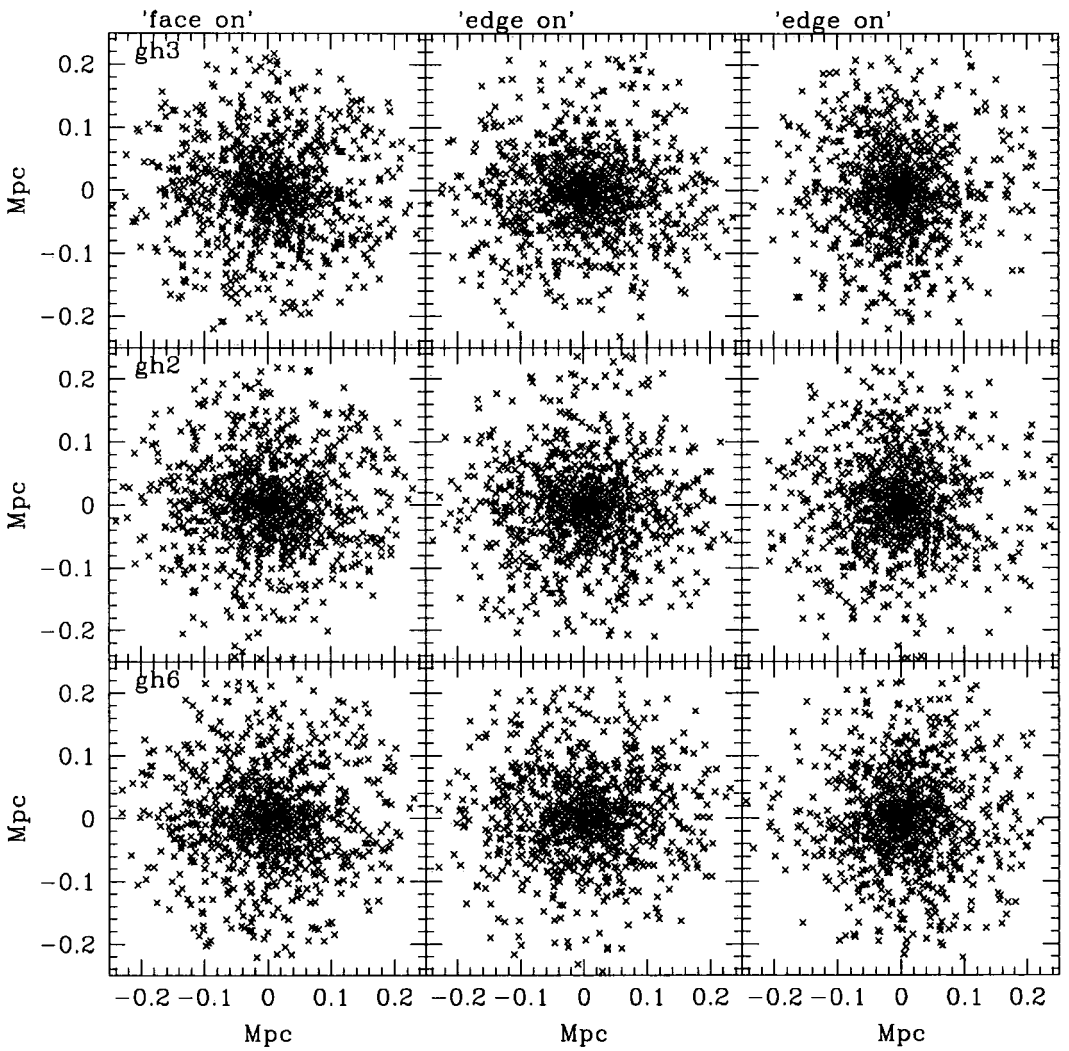

Figure 2.2: Projections of the positions of the 1000 most massive dark matter substructures within 250 kpc of the central galaxy along the principal axes of the inertia tensor in simulations gh3, gh2, and gh6

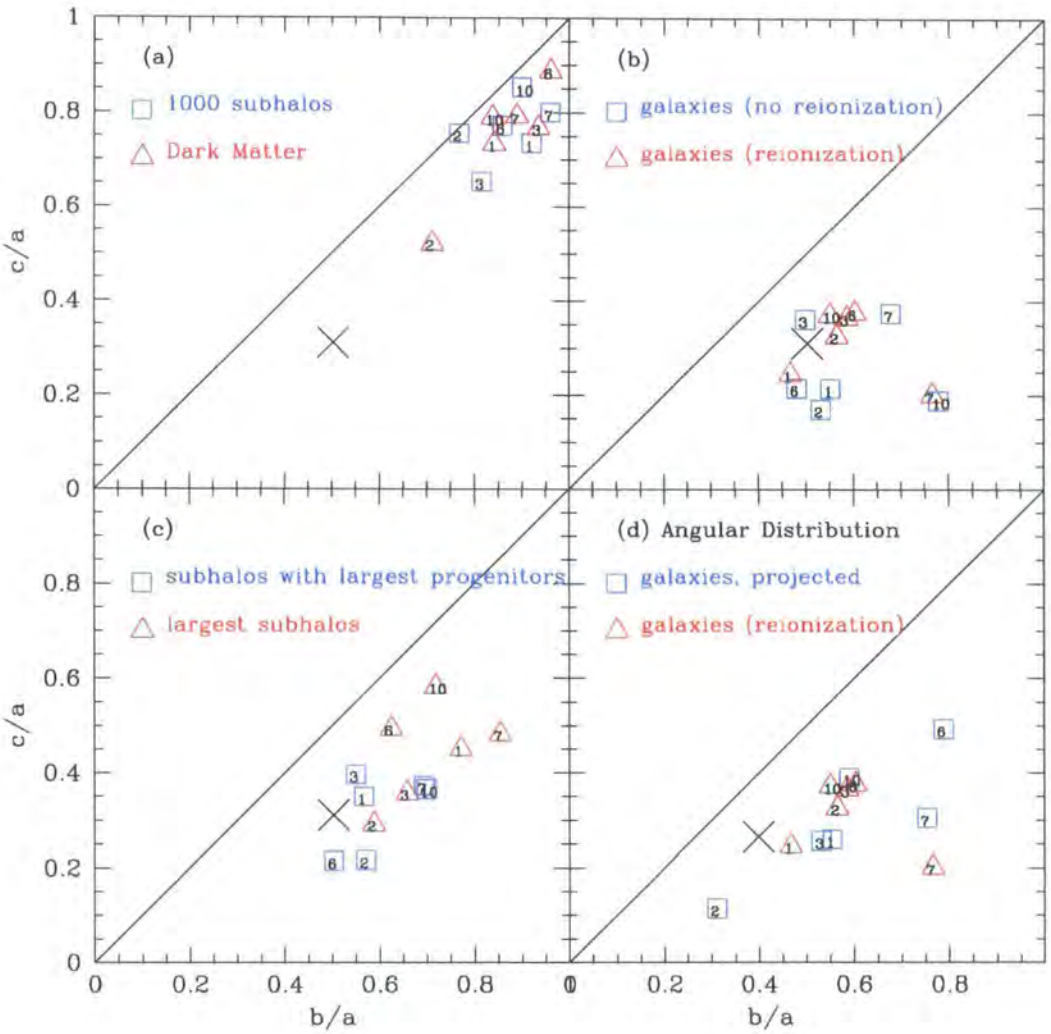

Figure 2.3: Minor-to-major (c/a) versus intermediate-to-major (b/a) axial ratios. The numbers inside each symbol identify the simulated halo. The '$\times$' indicates the axial ratios of the Milky Way's satellite system. Only data out to a radius of 250 kpc is used in all cases. Panel (a) compares the axial ratios of the dark matter halos (triangles) with those of the system consisting of the 1000 most massive dark matter substructures (squares). Panel (b) compares the axial ratios of the systems made up of the 11 most luminous galaxies in models with and without early reionization (triangles and squares respectively). Panel (c) compares the axial ratios of the systems of 11 most massive substructures with those of the systems consisting of the 11 substructures that had the most massive progenitors. Panel (d) compares the axial ratios of the systems made up of the 11 most luminous satellites in our full semi-analytic model (triangles) with those of the same systems but with the radial distances of each satellite normalised to a common value.

et al. (2002a), neglecting the effects of reionization leads to an overprediction of the number of faint galaxies, including satellites in the Milky Way. Whether reionization is included or not, the satellites in our simulations cluster around the location of the Milky Way data marked by a cross in Fig. 2.3. This is the main result of our analysis: the flattening of the satellite system in our simulations is in excellent agreement with that of the Milky Way satellite system.

It is clear from Fig. 2.3a and Fig. 2.3b that the brightest satellites inhabit a biased subset of subhalos. To explore the origin of this bias, we select two subsets of subhalos: the 11 most massive subhalos at $z = 0$ and the 11 subhalos which had the most massive *progenitors* prior to being incorporated within the virial radius of the main halo. The flattening of these two systems is compared in Fig. 2.3c. The figure shows that the crucial factor in establishing a highly flattened system *is not* the final mass of the subhalo but *the mass of the largest progenitor.* It is the latter that correlates well with the final stellar mass or luminosity of the visible satellite, as shown in Fig. 2.4a. Here we plot the stellar mass of each satellite galaxy against the mass of its largest progenitor. This strong correlation is a result of the GALFORM model readily making the most luminous galaxies in the most massive progenitor halos. In contrast, Fig. 2.4b shows there is no correlation between the stellar mass of each satellite and the mass of its host substructure. This is due to the subhalos having been subjected to various amounts of tidal stripping.

Comparison of Fig. 2.3b and Fig. 2.3c indicates that the flattening of the systems consisting of the 11 most luminous satellites and the 11 subhalos that had the most massive progenitors are very similar. This is an important result because it demonstrates that our main conclusion regarding the compatibility of the Kroupa et al. (2005) data with the CDM cosmology does not depend on the details of our semi-analytic modelling of galaxy formation. So long as the brightest satellites form in those subhalos with the most massive progenitors, our conclusions stand.

With only 11 satellites in our main samples, the possibility that estimates of the inertia moments might be unduly affected by the presence of outliers is a concern. We investigate the sensitivity of our results to outliers by scaling all radial positions to a common value while keeping the angles of each radius vector fixed. The axial ratios of the rescaled data are compared to the original axial ratios of the 11 "reion-

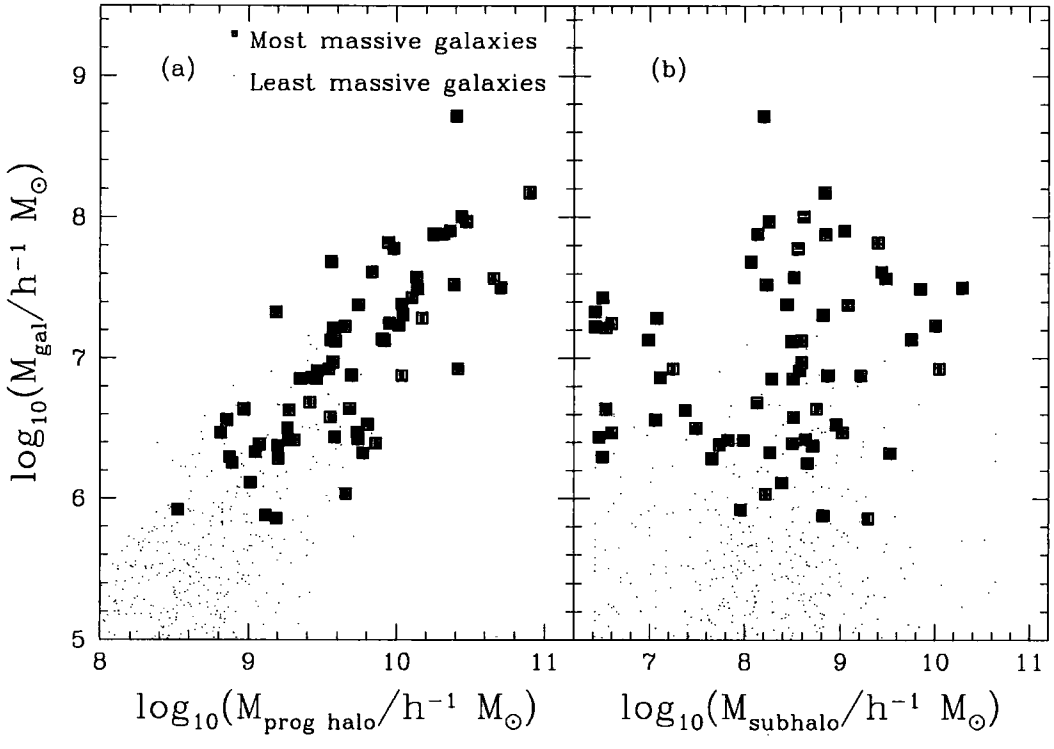

Figure 2.4: (a) Stellar mass in each satellite galaxy as a function of the mass that its largest progenitor halo had before becoming incorporated into the main halo. (b) Stellar mass in each satellite galaxy as a function of the mass of the substructure the galaxy currently resides in. The squares show results for the 11 most massive satellites in each of our 6 simulations, while the dots show results for the less massive satellites.

ization" satellites in Fig. 2.3d. Rescaling the satellite radial distances scatters the axial ratios somewhat but does not, on average, lower the overall flattening of the systems. As shown in the figure, rescaling the Milky Way data in the same way also has a small effect on the axial ratios.

Another concern is that the small number of satellites may introduce a bias in the axial ratio estimates. Indeed, our procedure would consistently give $c/a = 0$ for samples of 3 satellites (as they would lie on a plane), so it is important to check that the axial ratios of satellites shown in Fig. 2.3 are not driven by the size of the sample. We have compared the satellites with samples of the same size (11 objects) drawn from either the dark matter halos or the 1000 subhalo sample. The dark matter particles were drawn at random from a smooth, triaxial NFW distribution (Navarro, Frenk, and White 1996, 1997) with axial ratios set equal to the mean of that of our dark matter halos: $\langle b/a \rangle = 0.86$, $\langle c/a \rangle = 0.74$. The distribution of c/a ratios thus obtained is fairly broad and biased; indeed, the average c/a of 6000 random trials is ~ 0.44 with a dispersion of ~ 0.12. Similarly, for the parent sample of 1000 subhalos we find that random samples of 11 objects give, for a total of 6000 trials (1000 per halo), a combined average $\langle c/a \rangle$ of ~ 0.41, with similar dispersion, ~ 0.12 [1].

Despite the sizeable dispersion, a KS test shows that the likelihood of obtaining the values of c/a for the satellite systems shown in Fig. 2.3b by chance is quite small. This is shown in Table 2.2, where we list the probability that the c/a axial ratio for the various samples of satellites shown in Fig. 2.3 is consistent with the shape of the distribution of dark matter or of the 1000 subhalo population. The probabilities are very low for our satellite galaxies sample (regardless of whether or not reionization is included), as well as for subhalos with the most massive progenitors. On the other hand, samples of the 11 most massive subhalos are seen to be fully consistent with either the dark matter or the 1000 subhalo sample as a whole.

Finally, we consider the connection between the highly anisotropic distribution of satellites and the orientation of their host dark matter halo. Consider the vector

[1] Just over 3% of the dark matter trials with 11 particles produce ratios in which both b/a and c/a are comparable or smaller than the Milky Way values; the figure is just over 7% for samples drawn for the 1000 subhalo system.

system	dark matter	1000 subhalos
subhalos w/largest prog.	7.4×10^{-3}	3.6×10^{-2}
galaxies (reionization)	2.4×10^{-3}	1.3×10^{-2}
galaxies (no reionization)	2.2×10^{-3}	9.7×10^{-3}
largest subhalos	0.95	0.61

Table 2.2: KS probabilities that the axial ratio c/a for various samples of satellites and subhalos shown in Fig. 2.3 are consistent with those for the dark matter or the 1000 subhalo sample. Only the set of the most massive subhalos at present is consistent with being randomly drawn from these distributions.

pointing along the major axis of the distribution (i.e. along $a_{\rm sat}$). Let θ denote the angle between this vector and a vector pointing along the major axis of the halo, $a_{\rm DM}$. For our six simulations, we find that $\cos(\theta)$ equals to 0.768, 0.979, 0.702, 0.747, 0.387, 0.942 for galaxy halos gh1, gh2, gh3, gh6, gh7 and gh10 respectively. Thus, apart from gh7, there is a strong alignment between the major axis of the disk-like satellite systems and the major axis of the parent dark matter halo. In the Milky Way, the major axis of the satellite disk-like structure is perpendicular to the galactic disk. Thus, if our galaxy resides in a dark matter halo similar to those that we have simulated, then the disk must be aligned such that its normal vector points in the direction of the halo major axis.

2.3.2 Interpretation

The highly anisotropic distribution of satellite galaxies in Milky Way type systems is a somewhat surprising outcome of galaxy formation in a CDM universe. This is particularly so in view of the fact that the population of subhalos as a whole is much less anisotropic and has axial ratios similar to those of the halo dark matter. The key to understanding the origin of the anisotropic satellite distribution lies in the connection between halos and the cosmic web and, in particular, in the way in which satellites are accreted into the main halo. Fig. 2.5 illustrates the anisotropic nature of satellite accretion. The dots show a random 1% of the dark matter particles that end up in the main halo at the final time. The circles mark the locations of

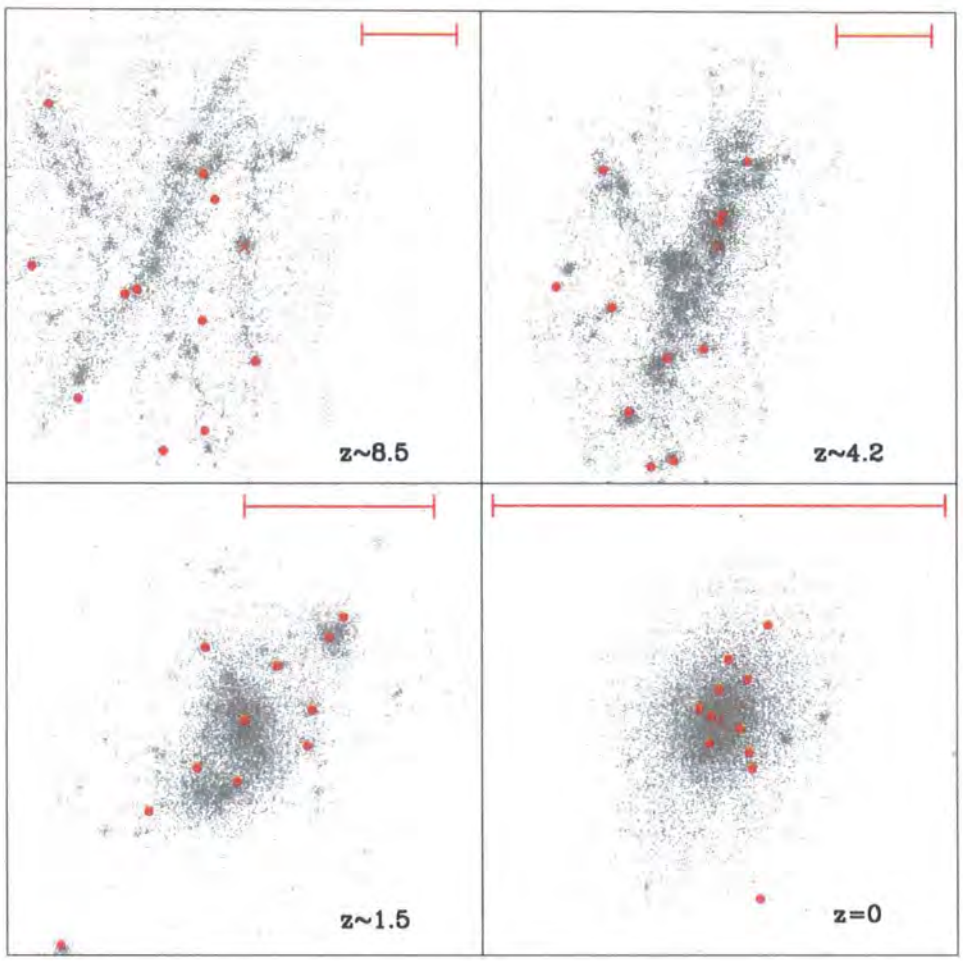

Figure 2.5: The formation of a galactic halo and its satellites. The points show a random 1% of the dark matter particles that end up in the main halo and the circles the positions of the 11 most luminous satellites that end up within 250 kpc of the main galaxy by the present day. The scale of each plot is indicated by the line which has a co-moving length of 400 kpc. The initial collapse produces a 2D structure – a large pancake of dark matter.

the most massive progenitors of the 11 most luminous satellites at the final time. Rather than originating isotropically, those halos destined to become bright visible satellites are accreted primarily along one or two of the cosmic web filaments.

This figure illustrates the highly anisotropic collapse typical of CDM structures on galactic scales. Careful inspection of the time evolution of the system shows that the collapse occurs first along 2D sheet-like structures which subsequently wrap up into filamentary streams of dark matter (Navarro et al. 2004a). By $z \sim 4.2$, these filamentary "highways" along which proto-satellite galaxies form are well established. The filaments are generally thicker than the locus of the largest proto-galactic halos which tend to concentrate towards the central, densest parts of the filament in a near 1-dimensional configuration. As the most massive halo progenitors collapse to form the main galaxy, this alignment is largely preserved. Smaller halos are more widely scattered across the thick filaments, reflecting their weaker clustering strength (Cole and Kaiser 1989; Mo, Mao, and White 1999). In addition, they are often accreted over a longer period and from a larger range of directions. Their distribution, now lacking a preferred orientation, ends up being much less anisotropic than that of the most massive halos. Whether reionization is included or not, satellite galaxies in the semi-analytic model form preferentially in the subhalos with the most massive progenitors and thus inherit their highly flattened configuration.

2.4 Discussion and conclusions

We have shown that the, at first sight surprising, flattened distribution of satellites in the Milky Way is the natural outcome of the anisotropic accretion of matter along a small number of filaments, characteristic of halo formation in the CDM cosmology. Kroupa et al. (2005) reached the opposite conclusion, that the observed satellite distribution is incompatible with the CDM model, because they neglected the fact that the satellites do not trace the distribution of halo dark matter but form instead in the most massive halos (prior to accretion) whose spatial distribution is biased.

Our results are not directly comparable to those of Kang et al. (2005) who also attempted to interpret the flattened distribution of Milky Way satellites with the

aid of high-resolution N-body simulations. Kang et al. (2005) assumed that the satellites follow the dark matter distribution in the halo and did not consider the formation sites of satellites in detail. Zentner et al. (2005), on the other hand, implemented a semi-analytic model similar to ours in N-body simulations also similar to those of Kang et al. (2005).

Our results are broadly consistent with those of Zentner et al. (2005). Unlike them, we did not choose halos specifically lying along filaments but selected them at random from a large cosmological simulation. In the event, three of our halos would, according to our semi-analytic model, host spiral galaxies and the other three elliptical galaxies. One difference between the two studies is that Zentner et al. (2005) found an acceptable match to the Milky Way satellite distribution both in their semi-analytic model and in a model in which the satellites are identified with the most massive subhalos at the final time. We have shown that the distribution of the latter is not as flattened as the distribution of Milky Way satellites. The crucial factor is not the final mass of the halo, which is affected by tidal stripping, but the mass of the largest progenitor before it is accreted into the main halo. Indeed, if the satellites are identified with the halos that had the largest progenitors, then their flattened distribution is very similar to that of the satellites identified by our semi-analytic model. Thus, our conclusions are independent of the details of our galaxy formation modelling.

As was also found by Zentner et al. (2005) and Knebe et al. (2004), the major axis of the flattened satellite distribution in our simulations points close to the direction of the major axis of the parent halo. This alignment reflects the preferential accretion of mass onto the halo along the dominant filament. An important consequence of this result is that if the Milky Way resembles the systems we have simulated, then the Galactic disk should lie in the plane perpendicular to the major axis of the halo because the observed satellite system itself is perpendicular to the Galactic disk. This inference is consistent with the conclusion reached by Helmi (2004) from an analysis of the kinematics of the Sagittarius dwarf streams.

The satellite alignment that we have found in our simulations is almost certainly related to the "Holmberg effect," (Holmberg 1969) the observation that the satellites of external galaxies within a projected radius of $r_{\rm p} \sim 50$ kpc tend to lie

preferentially in a cone along the galaxies' minor axis, avoiding the equatorial regions. To test this observation requires a larger number of simulations than those we have performed. Similarly, our current simulations are inadequate to test the extension of the Holmberg effect uncovered by Zaritsky et al. (1997) from a study of isolated spirals which also revealed an excess of satellites along the minor axis of the galaxy, now out to projected distances of $r_{\rm p} \sim 500$ kpc. A similar result was found by Sales and Lambas (2004)[2] from a much larger sample of galaxies drawn from the 2 degree field galaxy redshift survey. They too found an anisotropic distribution for $r_{\rm p} < 500$ kpc, but only for satellites moving with a velocity relative to their host of $\Delta v < 160$ km s $^{-1}$. In contrast, Brainerd (2005) found the opposite effect in a sample of satellites from the Sloan Digital Sky Survey, an alignment along the major axis at small radii ($r_{\rm p} < 100$ kpc) and an isotropic distribution beyond.

Although our simulations are not large enough to study the distribution of satellites beyond the inner 250 kpc of the galactic centre, it seems likely that the anisotropic distribution of satellites will continue out to larger separations. We intend to study this problem in a larger set of simulations.

In summary, we have found that the flattened distribution of the Milky Way satellites, first noted by Lynden-Bell (1976), and most recently highlighted by Kroupa et al. (2005), turns out to have a simple explanation in the context of structure formation in the CDM model. It is merely a reflection of the intimate connection between galactic dark matter halos and the cosmic web.

[2]Recently however, private communication with Yang et al. (2006) casts doubt on this result and indicates that the sense of the satellite anisotropy may be along the minor axis of the galaxy.

Chapter 3

The Spatial and Angular Momenta Alignment of Dark Matter Halos, Galactic Discs and their Satellite Distributions

3.1 Introduction

Any successful theory of galaxy formation will necessarily have to explain a wide variety of physical phenomena across many scales. On the Galactic mass scale, the problem of how small satellites form around galaxies such as the Milky Way, poses two interesting, and as yet not fully answered questions. These are:

1) What determines the number of Milky Way satellites and the shape of their luminosity function?

2) Why are the Milky Way's satellites aligned on a great circle in the sky and why is this great circle nearly perfectly perpendicular to the disc of the Milky Way?

At present, it is unclear whether the shape of the Milky Way's satellite luminosity function and their peculiar spatial distribution are unique to the Galaxy, or whether these are generic features that arise during the formation of a galactic halo. By virtue of their small size, extragalactic satellites are difficult to observe, and most studies are hampered by either resolution limits, completeness, or sample

size. However, recent advances using large sky surveys have produced large samples – albeit with only very few satellites per primary – and have shed some light on these questions.

In a universe in which the gravitationally dominant component consists of cold dark matter (CDM), the existence of small-scale power in the initial conditions causes the early collapse of matter and cosmological simulations show that small, dense, CDM haloes are able to form at early times. These low mass haloes grow by successive mergers and smooth accretion giving rise to the large-scale structures we see today (e.g Frenk et al. 1985; Wechsler et al. 2002; Zhao et al. 2003). High resolution N-body simulations of the growth of CDM halos have shown that the dense cores of merging clumps often survive the disruptive effects associated with mergers and remain as distinct substructures (or subhalos) embedded within a larger, smooth main halo (Klypin et al. 1999; Moore et al. 1999). Although the total mass attached to subhalos is only of order $\sim$ 10% of the total halo mass (Ghigna et al. 1998; Gao et al. 2004; Springel et al. 2001a; Stoehr et al. 2002), both N-body simulations and semi-analytical calculations of the assembly of dark matter haloes based on the extended Press-Schechter theory (e.g. Bond et al. 1991; Bower 1991; Lacey and Cole 1993), show that many more embedded substructures survive than there are visible satellites in galactic halos (e.g. Kauffmann et al. 1993; Moore et al. 1999; Klypin et al. 1999).

Many authors have argued that this so-called "missing satellite problem" poses a severe challenge to the CDM cosmology and encourages the study of alternative forms of dark matter (Craig and Davis 2001; Moore et al. 2000; Spergel and Steinhardt 2000; Yoshida et al. 2000) or of different cosmological initial conditions (Kamionkowski and Liddle 2000). Other authors have argued that the paucity of satellites in the Local Group is a natural byproduct of the physics of galaxy formation that regulate the cooling of gas in small halos (e.g. Kauffmann et al. 1993; Bullock et al. 2000; Benson et al. 2002b) or merely the result of a misidentification of substructures in the simulations with satellites in the Milky Way (Stoehr et al. 2002). The semianalytical model of galaxy formation of Benson et al. (2002a) included a detailed treatment of the reionization of hydrogen in the early universe which, by altering the thermodynamic state of primordial gas, inhibits the forma-

tion of small satellite galaxies. In this model, the increase in the entropy of the gas has two effects: it inhibits the cooling of new gas into small halos and it delays star formation in gas that has already cooled. The end result is a satellite population with about the observed numbers seen in the Local Group and with a luminosity function that matches the faint end of the observed function but not its bright end where the model fails to produce enough large, LMC-like satellites.

The spatial distribution of satellite galaxies poses another interesting problem within the CDM paradigm. Whereas N-body simulations show that the substructures that survive within halos tend to be nearly spherically distributed, the galactic satellites about the Milky Way are confined to a highly flattened structure, a puzzling fact first recognised 30 years ago (Lynden-Bell 1976; Kunkel and Demers 1976; see also Lynden-Bell 1982). Kroupa et al. (2005) drew attention to this discrepancy and concluded that the anisotropic alignment of the Galaxy's satellites contradicts the CDM model. Recent work including Chapter 2 however, has shown that the satellite galaxies do not populate a random selection of subhalos but are preferentially found in a biased subset which is arranged in a flattened configuration. This bias partly reflects the preferential infall of the most massive dark matter clumps along the filaments of the cosmic web. This phenomenon is clearly seen (to various degrees) in the N-body simulations analysed in Chapter 2, and by Kang et al. (2005), and Zentner et al. (2005) (and in the cluster mass simulations of Knebe et al. 2004). These studies differ in the precise way in which subhalos are identified with satellites but they all agree that flattened satellite configurations such as that seen in the Milky Way are not uncommon. In particular, Chapter 2 and Zentner et al. followed the formation of satellites by applying a semi-analytic galaxy formation model to high-resolution N-body simulations. Both studies found not only flattenings consistent with that seen in the Local Group but also that the long axis of the flattened satellite distribution tends to be aligned with the long axis of the parent dark matter halo.

Beyond the Local Group, a number of studies have claimed correlations between the orientation of central galaxies and the distribution of their satellites. Holmberg (1969) first identified a lack of satellites in the plane of a coadded sample of central galaxies out to a projected radius of $r_p \lesssim 50$ kpc. Zaritsky et al.

(1997) found evidence for this "Holmberg effect" but only on much larger scales ($300 \gtrsim r_p \gtrsim 500$ kpc). The reality of the Holmberg effect remains controversial. Early authors claimed that if an anisotropy exists at all, it is, if even significant, at best small (Hawley and Peebles 1975; Sharp et al. 1979; MacGillivray et al. 1982). An anisotropy perpendicular to the disc was recently inferred in the distribution of satellites identified in the 2dFGRS by Sales and Lambas (2004) but a private communication quoted in Yang et al. (2006) indicates that the original analysis was incorrect and that the anisotropy is, in fact, along the disc, not perpendicular to it. Brainerd (2005) and Yang et al. (2006) have claimed to see an alignment of satellites in the SDSS[1] in the opposite direction to Holmberg's, that is along the plane of the galaxy disc rather than orthogonal to it. Yang et al. (2006) found that the planar distribution is detectable only in red satellites but the blue population is consistent with an isotropic distribution. These apparently conflicting observational studies all seem to suggest anisotropic distributions of satellites but they disagree on how the plane of satellites is oriented relative to the central galaxy.

In principle, simulations are an ideal way to investigate the sort of issues just discussed. Since their introduction to cosmology in the 1970s (Peebles 1971; Aarseth et al. 1979), N-body simulations have been extremely useful in revealing how cosmic structures emerge out of small primordial perturbations (e.g. Springel et al. 2006 and references therein). To investigate questions such as the alignment between satellites and central galaxies, however, it is necessary to follow not only the evolution of dark matter, but the coupled evolution of the baryonic component as well. Until recently, progress in this area was hampered by the inability of hydrodynamic simulations to produce realistic discs from CDM initial conditions. Without some form of feedback to prevent most of the gas from cooling into subgalactic fragments, the outward transfer of orbital angular momentum to the dark halo as these fragments merge results in discs that are much too small (Navarro and Benz 1991; Weil et al. 1998; Sommer-Larsen et al. 1999; Eke et al. 2000)

The "disc angular momentum problem" has recently been overcome, at least partially, in a number of simulations which include plausible forms of feedback and are able to produce relatively realistic galactic discs (e.g. Governato et al. 2004;

[1] http://www.sdss.org/

Robertson et al. 2004; Bailin et al. 2005; Okamoto et al. 2005). In this Chapter, we analyse the simulations carried out by Okamoto et al. (2005). Specifically, we investigate the properties of satellite galaxies orbiting central galaxies of mass similar to that of the Milky Way. We derive the satellite luminosity function over a limited, but still interesting, range of luminosity. We search for anisotropy in the satellite galaxy distribution, and study the alignment of satellite systems with their central baryonic discs, as well as the alignment of the disc with the its dark matter halo.

This Chapter is organized as follows: in Section 3.2.1 we describe the simulations we have used as well as our method for selecting a complete satellite samples. In Section 3.3 we derive the satellite galaxy luminosity function as well as look at the gas fraction of the largest satellites. We show our results concerning the relative alignments in Section 3.4. In Section 3.5 we show our results regarding the angular momenta of the various components. We conclude in Section 3.6.

3.2 Identifying galaxies and satellites

In this section, we briefly describe the simulations that we have analysed and the methods that we have developed in order to identify central and satellite galaxies.

3.2.1 The simulations

We have analysed two simulations of galaxy formation, both carried out using the parallel PM-TreeSPH code GADGET2 (Springel 2005), as modified by Okamoto et al. (2005). GADGET2 calculates the evolution of dark matter using N-body techniques and the evolution of gas using smooth particle hydrodynamics (SPH).

Initially, the two simulations followed the evolution of dark matter in a cosmological cubical volume of length $L_{\rm box} = 35.325h^{-1}$Mpc in a ΛCDM model with cosmological parameters Λ=0.7, $\Omega_{\rm m}$=0.3, $H_0 = 70$ km s^{-1} and σ_8=0.9. For the first simulation (hereafter SD), a region around a suitably chosen dark matter halo was identified at the final time and the simulation was run again, this time adding many more dark matter particles and SPH particles in the region of the halo and

perturbing these with additional high frequency power drawn from the same power spectrum of the original simulation following the general method outlined by Frenk et al. (1996). Since the goal of this simulation was to investigate the formation of a galactic disk, the halo chosen for resimulation was selected to have a quiet recent merger history, with no major mergers since $z \approx 1$. A preliminary semi-analytical calculation applied to the merger tree of this halo, using the methods of Helly et al. (2003), indicated that a disk galaxy was likely to form in this halo. The high resolution region enclosed a spherical volume of radius 0.9 Mpc around the halo at $z = 0$.

Simulation SD did indeed form a reasonably realistic disk, as discussed by Okamoto et al. (2005) (in their "shock-burst" model). Encouraged by this success, we ran a second simulation (hereafter SR) with the same code, this time populating several regions of the same volume with high resolution dark matter and gas particles. The high resolution regions consisted of a large sphere of radius $5h^{-1}$Mpc and four smaller overlapping spheres each of radius $r = 1h^{-1}$Mpc. This arrangement ensured coverage of all the large galaxies that formed out to the virial radii of their halos. The same cosmological parameters were used in both simulations, except that the baryon density in SD was taken to be Ω_b=0.040 and slightly larger, Ω_b=0.044, in SR. In both simulations, the mass per particle was $\sim 2.6 \times 10^6 h^{-1}$ $M_\odot$ for gas and $\sim 1.7 \times 10^7 h^{-1}$ $M_\odot$ for dark matter.

The various physical processes included in our simulations are described in detail in Okamoto et al. (2005). Here, we summarise the salient points. The interstellar medium (ISM) is modelled, following Springel and Hernquist (2003), as a two phase medium composed of hot ambient gas and cold gas clouds in pressure equilibrium. Gas heating and cooling rates are computed assuming collisional ionization equilibrium, in the presence of a uniform and evolving ultra-violet (UV) background, which is assumed to be generated by hot OB stars and is switched on at $z = 6$ (Haardt and Madau 1996). The cooling rates, which depend on the metallicity of the gas, are computed from the tables given by Sutherland and Dopita (1993); molecular cooling and other forms of cooling below $T \approx 10^4$ K are ignored.

Star formation can occur in a "quiescent" and a "burst" mode. In the quiescent mode, gas particles that meet a specified density criteria, are turned into stars

according to a pre-determined probability. These stars form with a standard initial mass function (IMF; Kennicutt 1983). Bursts of star formation are triggered by major mergers which are identified by tracking large changes in the entropy of the gas. In a burst, stars form on a shorter timescale than in the quiescent mode and with a top-heavy IMF. This model of star formation is motivated by the semi-analytical work of Baugh et al. (2005) who argue that only a top-heavy IMF in bursts can explain the number density of sub-millimetre and Lyman-break galaxies at high redshift. Nagashima et al. (2005b,a) argue, similarly, that this model is also required to explain the metallicity of the intracluster medium and of elliptical galaxies.

In the Okamoto et al. (2005) model, the evolution of the stellar populations that form is followed in detail, tracking both type-II and type-Ia supernovae. This requires abandoning the instantaneous recycling approximation (IRA) assumed by Springel and Hernquist (2003), whereby star formation, cold gas cloud formation by thermal instability, the evaporation of gas clouds and the heating of ambient gas by supernovae explosions all occur simultaneously. Instead, following each star formation event, supernovae energy and metals are injected back into the ISM on a timescale which is computed from the mass-dependent stellar lifetime (Portinari et al. 1998; Marigo 2001) and the assumed IMF.

A top heavy IMF in bursts increases the number of supernovae that explode per unit of mass turned into stars, thereby generating stronger feedback. This, in turn, inhibits the early collapse of cold gas clouds in small subgalactic halos, helping to maintain an abundant reservoir of hot halo gas. Following the last major merger and accompanying starburst, radiative cooling of hot gas from the reservoir flows inwards and settles into a centrifugally supported disc which becomes unstable to star formation. This is the key to the formation of a realistic disc galaxy in the simulations of Okamoto et al. (2005).

3.2.2 Identifying central and satellite galaxies

We begin the process of finding central and satellite galaxies by identifying "friends-of-friends" (FOF) groups in the dark matter, linking together particles whose sep-

aration is less than 0.2 times the mean interparticle separation, corresponding roughly to particles within the virialised halo (Davis et al. 1985). We then identify bound substructures ("subhalos") in the simulation with the algorithm SUBFIND (Springel et al. 2001a). Using particle positions and velocities, SUBFIND calculates the binding energy of each FOF group (stripping unbound particles of group membership) and then identifies bound substructures inside the parent halo. We consider only halos with ten or more dark matter particles, corresponding to a subhalo mass resolution of $M_{\rm res,sub} = 1.7 \times 10^8 h^{-1} M_\odot$. For each subhalo, we calculate the centre of mass, as well the size, $r_{\rm sub}$, defined as the rms distance of its particles from the centre.

Substructures within the parent halo are thus identified as locally overdense, self-bound, regions in the dark matter density field that fall within the high resolution region of the simulation. In order to identify clumps of star particles as individual galaxies, we associate each star particle with a unique dark matter substructure. For each gas and star particle, we find the substructure whose centre of mass is closest and assign the SPH particle to that substructure if it is within $r_{\rm sub}$. As star clumps tend to be dense and centrally concentrated, our results are robust to the choice of subhalo radius (for example, increasing $r_{\rm sub}$ by 50% has a negligible effect on our results). We also impose a ten star particle lower limit, corresponding to $M_{\rm res,gal} \sim 2.6 \times 10^7 h^{-1} {\rm M}_\odot$, on the stellar mass of any galaxy. With this resolution limit, our galaxy samples become incomplete at magnitudes fainter than $M_V \sim -12$.

We identify "central" galaxies of luminosity similar to the Milky Way with galaxies brighter then -20.4 in the V band. We calculate their virial radius by growing concentric spheres around the galaxy and noting where the mean internal density falls below $200\rho_{\rm crit}$, where $\rho_{\rm crit}$ is the critical density. Galaxies that fall within this radius are considered satellite galaxies. In order to obtain isolated systems similar to the Milky Way, we ensure that no two central galaxy candidates are within each other's virial radius.

Fig. 3.1 shows an illustrative example of how our algorithm selects central and satellite galaxies. We plot all the star particles within the virial radius projected onto the principal planes of the central galaxy, i.e. the planes on which the galaxy is face-on and edge-on. In red, we plot the star particles that are associated with

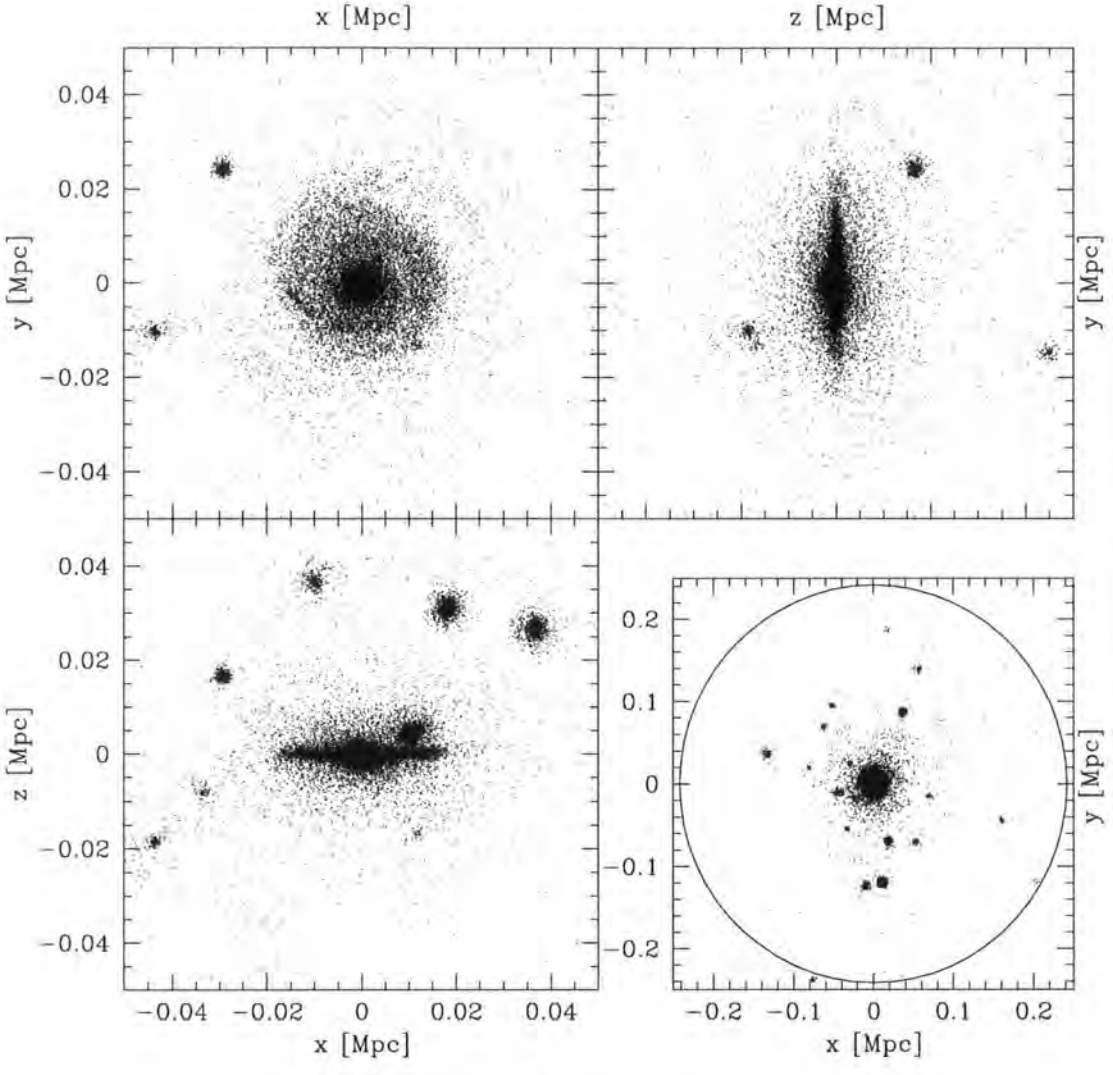

Figure 3.1: A central galaxy and its satellite system. The black dots denote all the star particles associated with the galaxy, while the red dots denote the star particles associated with satellites located within the virial radius of the central galaxy. The top two and the bottom left panels show a zoomed-in projection of the distribution of stars near the central galaxy, in the three principal planes, i. e. in the planes in which the galaxy is face-on and edge-on. The *bottom right* panel shows a face-on projection out to 250 kpc. The virial radius, defined by $\bar{\rho}(< r_{\rm vir}) = 200\rho_{\rm crit}$, is marked by the green circle.

Table 3.1: Properties of the 9 galaxy haloes (gh). We show the virial radius ($r_{\rm vir}$), the dark halo mass internal to this radius ($M_{\rm dm}$), the stellar mass of the galaxy ($M_\star$), the gas mass of the galaxy ($M_{\rm gas}$), the V band magnitude (M_V), the number of satellites orbiting within the virial radius ($N_{\rm sat}$), and the bulge ($M_{\rm bulge}$) and disc ($M_{\rm disc}$) mass of the galaxy.

	gh1	gh2	gh3	gh4	gh5	gh6	gh7	gh8	gh9
$r_{\rm vir}$ (h^{-1}Mpc)	0.244	0.243	0.242	0.209	0.152	0.190	0.171	0.152	0.215
$M_{\rm dm}(10^{12}M_\odot)$	1.672	1.648	1.136	1.045	0.402	0.783	0.567	0.400	1.610
$M_\star(10^{10}M_\odot)$	6.63	9.61	6.49	5.19	2.31	3.26	2.42	1.73	5.54
$M_{\rm gas}(10^{10}M_\odot)$	3.13	5.02	5.40	2.66	0.77	2.66	1.75	1.27	3.43
M_V	-21.3	-22.1	-21.2	-20.9	-20.4	-20.5	-20.4	-20.4	-21.6
$N_{\rm sats}$	20	13	16	4	5	5	8	5	2
$M_{\rm bulge}(10^{10}M_\odot)$	3.77	2.46	2.51	2.56	1.01	1.86	1.49	1.44	2.87
$M_{\rm disk}(10^{10}M_\odot)$	2.86	7.15	3.98	2.63	1.31	1.42	0.95	0.29	2.67

satellite galaxies. There are different numbers of satellites in each projection because we are plotting all the star particles in projection through the virial radius, which is larger than the plotted box. In the bottom right panel, we show the face-on projection of the system out to the virial radius. The central galaxy has a very extended stellar halo (black points in the figure) made up of stars that lie within the $r_{\rm sub}$ of the central galaxy' subhalo and not within the $r_{\rm sub}$ of any satellite subhalo. This extended halo makes up only a small fraction of the stellar mass of the central galaxy. Below, when we calculate the shape of the central galaxy we remove the extended halo by considering only the innermost 98% of the stars.

3.3 The luminosity function of satellite galaxies

Our simulations produced a sample of 9 central galaxies with $M_V < -20.4$, 8 from simulation SR and one from simulation SD. In Table 3.1 we present various

properties of these nine systems.

The V-band luminosity function of the satellites in this sample is shown in Fig. 3.2. The luminosity function is nearly flat in the range $-13.5 > M_V > -16.5$ and drops off sharply at fainter and brighter magnitudes. The nominal resolution limit of our simulations corresponds to a satellite absolute magnitude $M_V \sim -12$ and it is important to check whether the decline in the luminosity function in the range $-12 > M_V > -13.5$ is the result of feedback processes, such a photoionization or supernova feedback, which affect the number of faint galaxies in the simulations or whether it is affected by resolution effects.

To investigate the likely effects of resolution in our estimate of the satellite luminosity function we have used the semi-analytic model GALFORM described in Cole et al. (2000) and Benson et al. (2002b). The semi-analytic model includes all the standard physical effects present in the simulation: gas cooling according to a metallicity-dependent cooling function, star formation, feedback due to supernovae explosions, the injection of metals ejected in supernovae into the interstellar medium, etc. Photoionization is included in an approximate way by assuming that gas cannot cool in halos with circular velocity $v_{\rm circ} < 60$ km s^{-1} after the assumed epoch of recombination, $z < 6$. Baugh et al. (2005) have shown that this simple approximation gives an excellent match to a detailed calculation based on the idea of a filtering mass.

We proceed as follows. In the semi-analytic model, it is possible to specify the mass of the smallest halo to be considered and this allows us to model the effects of resolution in the SPH simulation (Helly et al. 2003). We recall that in the simulation itself we only considered halos with at least ten particles, corresponding to $M_{\rm res,sub} = 1.7 \times 10^8 h^{-1}$ M$_\odot$. We ran a series of semi-analytic models with resolution varying by 4 orders of magnitude, from $\sim 10^{-2} M_{\rm res,sub}$ to $10^2 M_{\rm res,sub}$. In all cases, we found that the shape of the luminosity function brightwards of $M_V = -12$ was essentially unaffected. If the resolution is degraded further, then the faint end of the luminosity function becomes truncated at increasingly bright magnitudes. We conclude from this test that our satellite sample is likely to be complete for magnitudes brighter $M_V = -12$ and that our estimate of the satellite luminosity function in this regime is unlikely to be affected by resolution.

In Fig. 3.2, we compare our estimated luminosity function with data for satellites in the Local Group obtained from the sample compiled by Mateo (1998), supplemented with data from Irwin[2]. Unlike Mateo (1998), we include the SMC, the LMC and M33 in our sample. Brighter than our estimated resolution limit of $M_V < -12$, we find that the luminosity function in our simulations is in excellent agreement with the data over a range of 7 magnitudes, down to $M_V = -19$. Of course, in the Local Groups, the statistics at the bright end are rather poor: the last two data points (centred on -18 and -19.75) contain only one galaxy each (the LMC and M33, respectively). However, within the errors, the simulations are consistent with the data.

We also compare our results in Fig. 3.2 with those in the semi-analytic model of Benson et al. (2002a). The simulations and the semi-analytic model are broadly in agreement over most of the luminosity range, from the resolution limit of the simulations to the brightest two bins. However, there is a significant difference at the bright end: while we find a satellite as bright as the LMC one third of the time, Benson et al. only find one 5% of the time. In the simulations, satellites as bright as M33 are produced in about 5% of systems, while the frequency in the Benson et al. model is less than 1%. The reasons for the disagreement between the semi-analytic model and the simulations (and Local Group data) are probably a reflection of the different treatment of various physical processes in the methods. However, the fact that our simulations match the observed satellite luminosity function over a large range of magnitudes indicates that the relatively small observed number of satellites in the Local Group is not, in principle, difficult to explain within the CDM model. The much publicised "satellite problem" exists, as other authors have remarked (e.g. Bullock et al. 2000; Benson et al. 2002a), only when the astrophysical processes involved in the formation of visible galaxies are neglected.

In order to investigate how realistic the satellites in our simulations are, particularly the bright ones, we compare, in Fig. 3.3, their gas fractions with those of real satellites. Panel (a) shows the gas fractions as a function of the magnitude difference between the satellite and the parent galaxy in the V-band. Only satellites with $M_V < -12$ in the simulations, the Milky Way and M31 are shown and, for the

[2]http://www.ast.cam.ac.uk/~mike/local_members.html

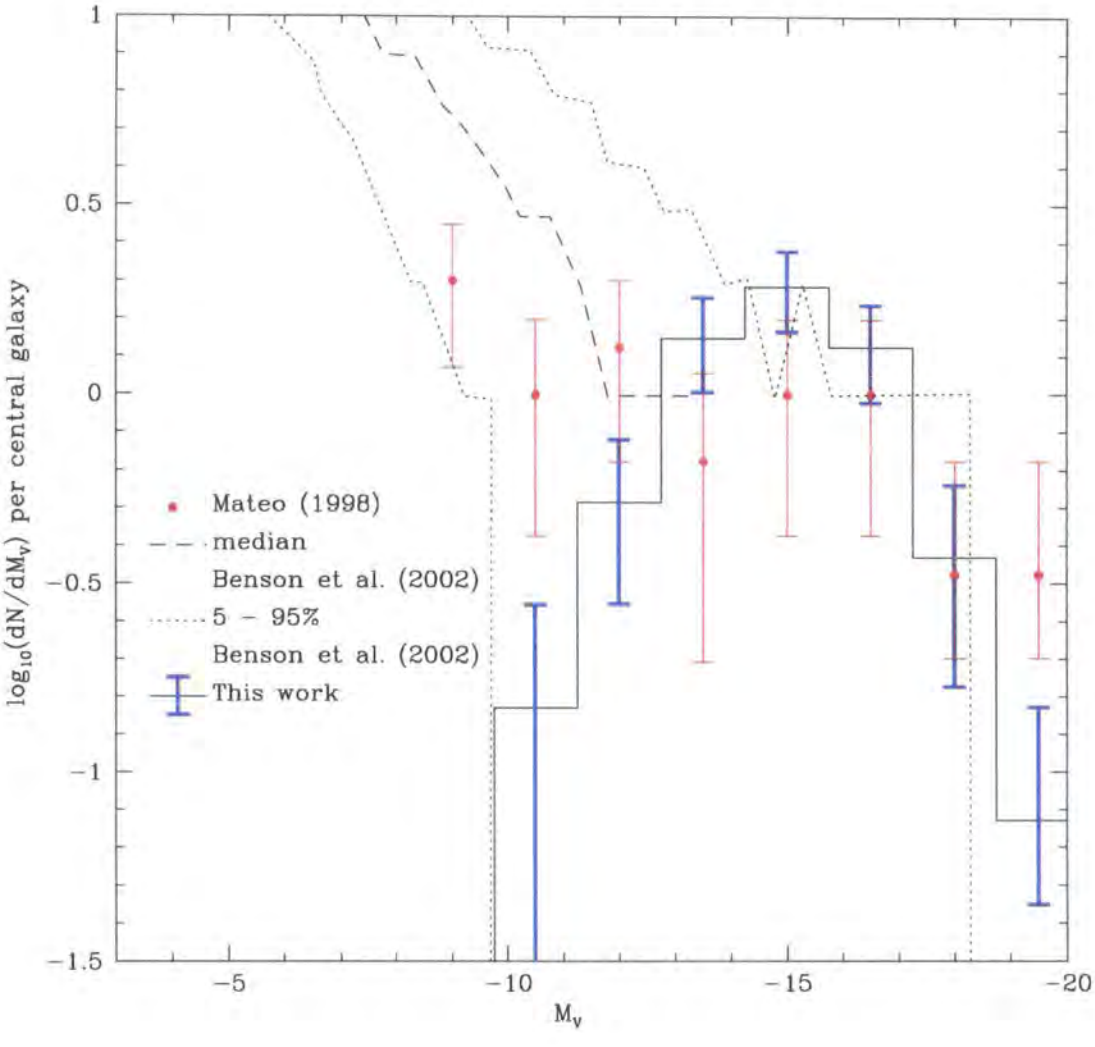

Figure 3.2: The differential V-band luminosity function of satellites per central galaxy in our simulations. The blue errorbars are 1σ Poisson errors per magnitude bin. (For bins with more than one count the errors are simply $\sqrt{N}$, but for bins with only one count, we take $+\sqrt{N}$ as the upper errorbar and determine the lower errorbar by finding the mean of a Poisson distribution whose integral from 1 to infinity corresponds to 16% of the distribution.) The Local Group satellite luminosity function, obtained from the compilation of Mateo (1998), supplemented with data from Irwin, is shown as red circles. The dashed line shows the median luminosity function of 70 realisations of Milky Way type halos calculated using a semi-analytic model by Benson et al (2002b) with the dotted lines indicating the 5 – 95 percentile width of their distribution.

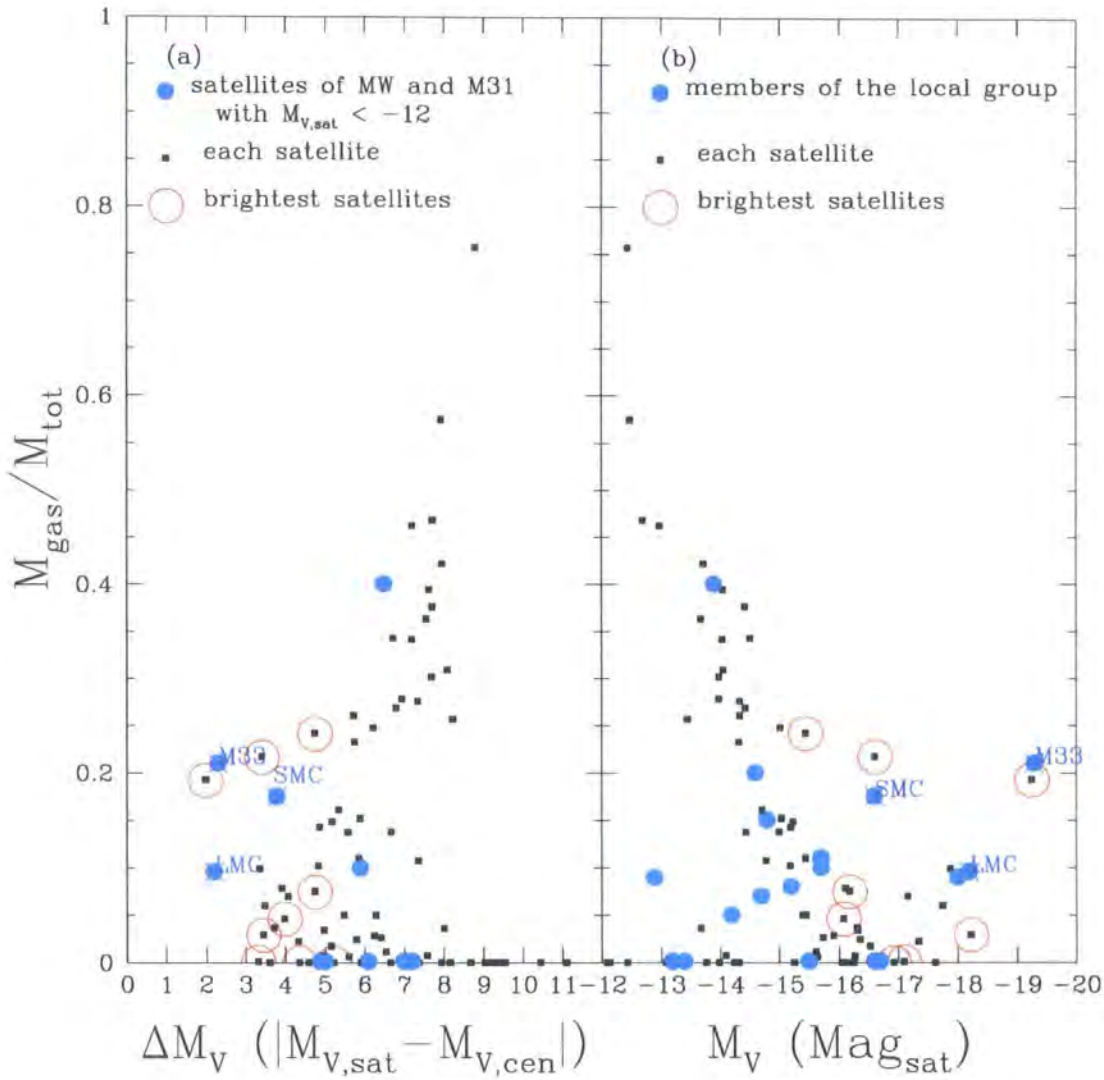

Figure 3.3: Gas fraction in satellites as a function of V-band luminosity. The satellites in the simulation are shown as squares and the brightest satellite in each system is surrounded by a red circle. The Local Group satellites are shown as filled cyan circles and the LMC and SMC are indicated by crosses and labelled. *Panel (a).* Gas fraction as a function of the magnitude difference between the satellite and its central galaxy. For both simulations and data, only satellites with $M_V < -12$ that lie within the virial radius of the central galaxy (the Milky way or M31 in the case of the real data) are plotted; in addition, for the real data a reliable gas fraction measurements is required. *Panel (b).* Gas fraction as a function of absolute V band magnitude. Here all Local Group members with reliable gas fraction measurements or upper limits are plotted. Local Group data are from Mateo (1998); SMC data is from Stanimorovi, Staveley-Smith & Jones (2003), LMC data is from Staveley-Smith et al. (2003), and M33 data is from McGaugh (2005)

latter, we require also a reliable measurement of or upper limit for the gas fraction. The simulations show a trend of increasing gas fraction with decreasing luminosity which, as far as the scant data for the real satellites permit, seems consistent with the measurements. In particular, the brightest satellites in the simulations bracket the values measured for the LMC, the SMC, and M33 with 3 out of 9 simulated satellites having a larger gas fraction. In panel (b) we extend the comparison by including not only satellites within the virial radius, but all the satellites in the Local Group that have reliable gas fraction measurements. In this case, we plot the gas fraction against the V-band magnitude of the satellite. The trend of increasing gas fraction with decreasing luminosity is now clearer in the data and the locus they define agrees well with the locus traced by the simulated satellite galaxies (although note that not all the points plotted are strictly speaking satellites, according to our definition, which requires satellites to lie within the virial radius.)

3.4 The spatial distribution of satellite galaxies

In Fig. 3.4, we show the radial density profile of the dark matter and the radial number density profile of satellites averaged over the 9 central galaxies in our simulations. Both profiles have been normalised to their respective values at the virial radius. The dark matter density profile, shown as the dashed line, closely follows the NFW form (Navarro et al. 1996; Navarro et al. 1997). As found in previous studies (Stoehr et al. 2002; Gao et al. 2004; Chapter 4), the satellite galaxy profile, shown as the solid line in the figure, is flatter than the dark matter profile, as a result of dynamical effects in the inner region of the halo.

To characterise our simulations further, we investigate the flattening of the distributions of dark matter, satellites and stars in the central galaxy. We define the tensor of second moments,

$$I_{jk} = \sum_{\mu} x_j^{\mu} x_k^{\mu}, \tag{3.1}$$

where x_j^{μ} is the j coordinate of μth particle in a reference frame centred on the centre of mass of the central galaxy. To determine the flattening of the central galaxy, we consider only the innermost 98% of the stars and exclude the outermost 2% that make up the diffuse stellar halo. (Our results are insensitive to the exact fraction

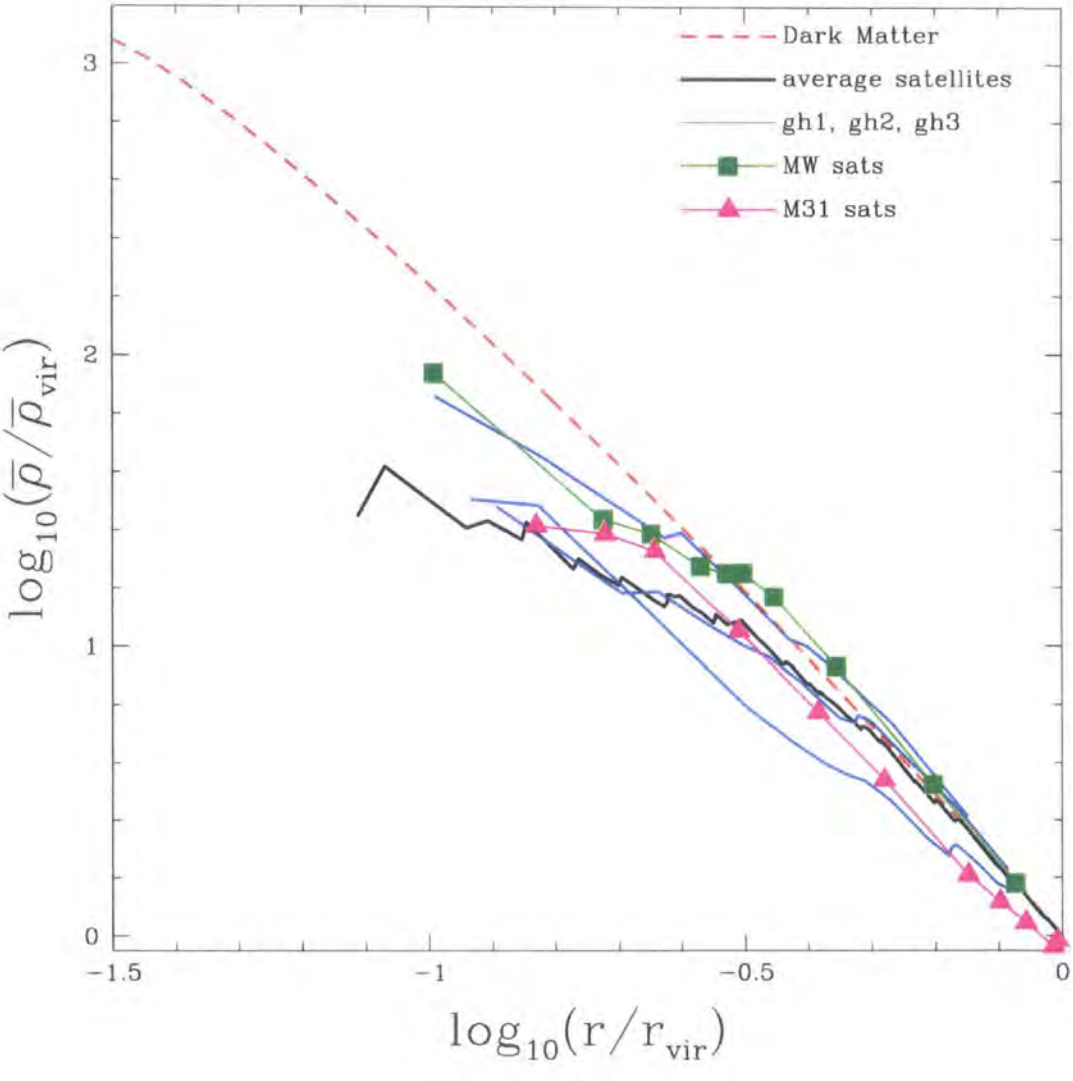

Figure 3.4: Density profiles averaged over the 9 central galaxies in our simulations. The halo dark matter profile is shown with a dashed line while the number density profile of satellites is shown with the solid line. The radial coordinate is in units of the virial radius, $r_{\rm vir}$ and both profiles have been normalised to their respective values at the virial radius.

of excluded stars, provided this is small.) To determine the principal axes of each distribution, we diagonalise the tensor I_{jk}. Its eigenvalues, a^2, b^2, c^2, give the mean square deviation of the x, y and z coordinates along the principle axes. We define $a > b > c$ as the major, intermediate and minor axes of the system, and use the notation $\{a_{\rm dm}, b_{\rm dm}, c_{\rm dm},\}$, $\{a_{\rm sat}, b_{\rm sat}, c_{\rm sat}\}$, $\{a_{\rm gal}, b_{\rm gal}, c_{\rm gal}\}$ to refer to the distributions of dark matter, satellite galaxies and stars in the central galaxy respectively.

It is important to keep in mind that estimates of a, b and c using small numbers of objects are generally biased towards higher anisotropy. For example, if a system has only three members (e.g. satellite galaxies), our method would always return $c = 0$ since three objects will always lie on a plane. Tests of the statistical robustness of our results are performed below.

The Milky Way has 11 satellite galaxies within its virial radius with reliably measured positions and magnitudes. Of our sample of nine simulated central galaxies, three have 11 or more satellites and can be compared with the Milky Way. The axial ratios of each central galaxy in our simulations, its dark matter halo and, for systems with 11 or more members within the virial radius, its satellite distribution are shown in Fig. 3.5.

It is immediately apparent that, in the three sufficiently rich systems, the distribution of the 11 most massive satellites is considerably flatter than the dark matter halo, although the signal is stronger in systems 1 and 3. This is consistent with previous studies (Chapter 2, Kang et al. 2005; Zentner et al. 2005) which also found large flattenings in simulated satellite systems, although in those studies, the satellites were identified in dark matter simulations using a semi-analytic galaxy formation model rather than the full hydrodynamic calculations that we are analysing here. In Chapter 2 we ascribed this anisotropy to the preferential infall of substructures along the spines of filaments as they collapse to make a galaxy.

In order to test the statistical robustness of our results, we perform three tests whose results are displayed in Table 3.2. For the first test, we constructed a spherically symmetric NFW halo with 10^6 particles. We then selected 11 particles at random from the halo 1000 times, and calculated the cumulative distributions of minor-to-major and intermediate-to-major axis ratios. The probability of drawing more extreme values that those measured for the satellite distributions in the simu-

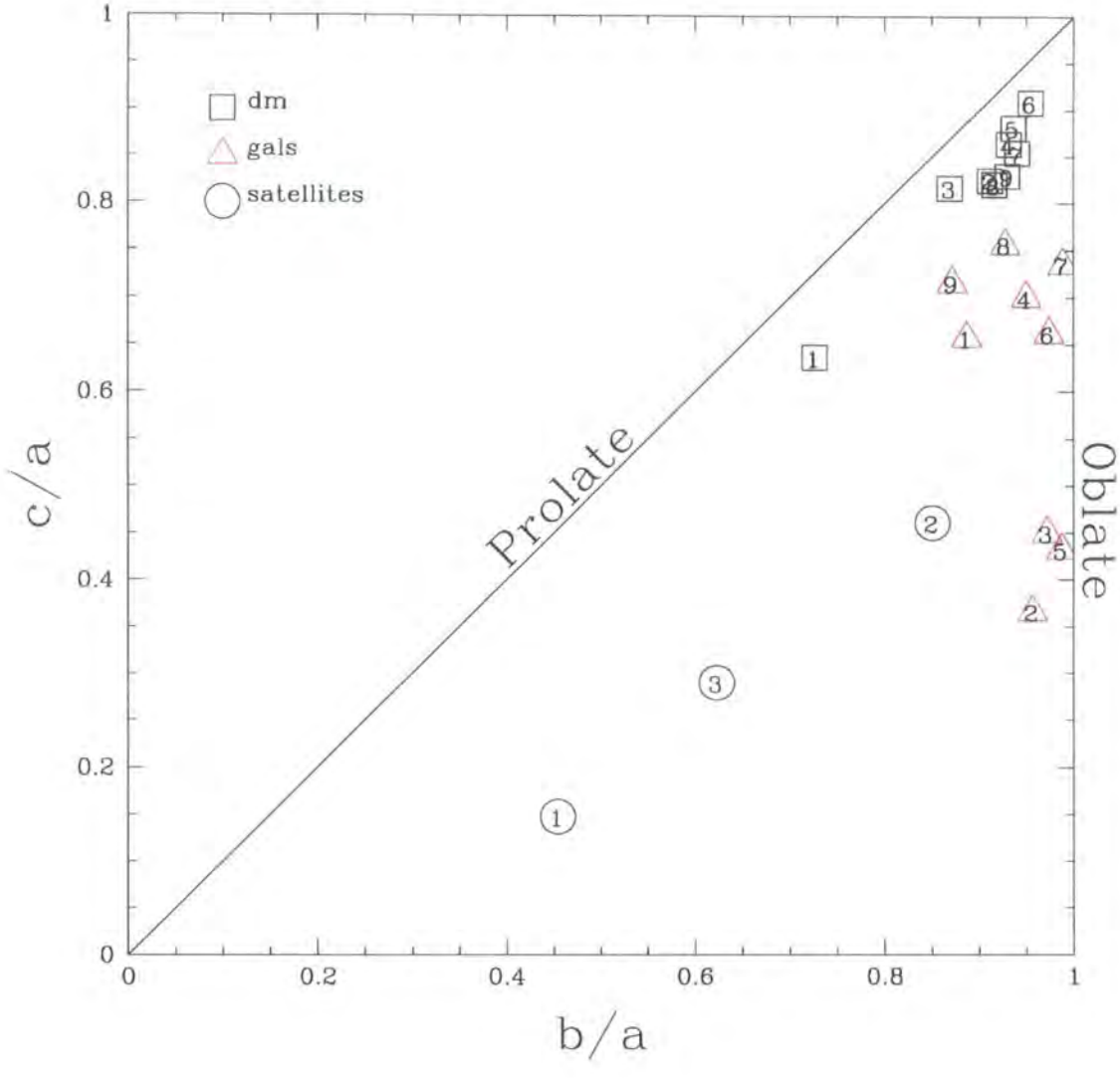

Figure 3.5: Minor-to-major (c/a) versus intermediate-to-major (b/a) axial ratios for all the galaxy halos in our simulations. Since $a > b > c$, the upper left triangular half of this plot cannot contain any points. Prolate objects lie along the diagonal while oblate objects lie along the right vertical axis. The numbers inside each symbol identify the galaxy. Axial ratios for stellar discs and for dark matter halos are shown for all nine systems by red triangles and black squares respectively. For the three systems with 11 or more members, the axial ratios of the satellite distribution of the 11 most massive satellites is shown by the black circles.

Table 3.2: The probability of randomly drawing values of the minor-to-major (c/a) and intermediate-to-major (b/a) axis ratio which are more extreme than those measured for the satellite sytems in the simulations according to the three test described in the text. The three halos with 11 or more satellites within the virial radius are labelled gh1, gh2 and gh3 respectively.

	gh1	gh2	gh3
Isotropic NFW sphere	0.1%	47.6%	5.4%
Squashed NFW profile	0.4%	51.5%	6.4%
Simulated dark halo	0.6%	66.2%	10.5%

lations is given in the first row of Table 3.2, for each of the three galaxy haloes with 11 or more satellites (labelled gh1, gh2 and gh3 respectively). For the second test, we construct flattened NFW halos by squashing a sphere according to the values of $a_{\rm dm}$, $b_{\rm dm}$, and $c_{\rm dm}$ for each of the three simulated halos. We then performed the same test as before; the results are displayed in the second row in Table. 3.2. Finally, we selected 11 dark matter particles directly from each of the three halos (again 1000 times) and performed the same test with results given in the third row of the table.

With the exception of galaxy gh2, whose satellite system is the least flattened of the three (see Fig.3.5), the numbers in Table 3.2 rule out with high confidence the null-hypothesis that the satellite systems in the simulations were randomly drawn from either a spherical or a squashed NFW halo or from the dark matter distribution of the halo itself. This result agrees well with those obtained in Chapter 2 and Zentner et al. (2005).

The flattening and relative orientations of the disk, halo and satellite system of each of our three well populated simulations are shown schematically in cross section in Fig. 3.6. While the relative flattening and orientation of each component has been rendered according to the measured values, for clarity the relative sizes have been chosen arbitrarily. The central galaxy is represented by a yellow ellipsoid

embedded within two larger ellipsoids, a blue one representing the satellite system and a red one representing the dark halo. The poles (i.e. direction of the $\hat{c}$ axis) are visible as the point at which the lines of "longitude" converge. The various systems display a variety of orientations which we quantify below.

The central galaxy orientations displayed in Fig. 3.6 were calculated simply from the innermost 98% of stars. To refine our estimate of orientation and for other purposes, we have performed a dynamical bulge-disc decomposition for each of the nine central galaxies in our simulations. We apply the method proposed by Abadi et al. (2003) and used also by Okamoto et al. (2005). The net angular momentum, relative to the centre of mass of the galaxy, of the material in the inner $10h^{-1}$ kpc is used to define a "z" axis. The angular momentum, J_z, about this axis is computed for each star particle and compared to the angular momentum of a circular orbit with the same energy, $J_c(E)$. All stars with $J_z/J_c(E) \geq 0.75$ are assigned to a disc component whose orientation is taken to be the direction of the nett angular momentum of the disc stars. This method tends to overestimate the amount of material in the disc, as some bulge stars whose orbits are similar to disc star orbits, will be counted as part of the disc. Generally, this direction coincides with that of the short axis of the overall stellar distribution, except in two case (galaxies gh8 and gh9) which are bulge-dominated galaxies with very small disks whose orientation is ill-defined. In what follows, we take the orientation of the galaxy to be that of the disk except for gh8 and gh9 for which we take the direction of their minor axis.

The angles between the different components of each of the three galaxies with 11 or more satellites are plotted in Fig. 3.7. The top panel shows that in two of the galaxies, the disk is inclined about $\sim 45°$ relative to the minor axis of the dark halo. Surprisingly, in the third galaxy, the disk is orthogonal to the minor axis of the halo. The middle panel shows that in two cases (including the one with the orthogonal disk), the satellite systems are, within 20°, perpendicular to the galactic disk. This is also surprising but it is exactly the alignment seen in the Milky Way galaxy, where the satellites lie approximately along a great circle on the sky whose pole is in the galactic plane (e.g. Kroupa et al. 2005). In the third system (gh3), the satellite system is almost perfectly aligned with the galactic disk. Finally, the bottom panel shows that in two of the three systems, the long axis of the satellite

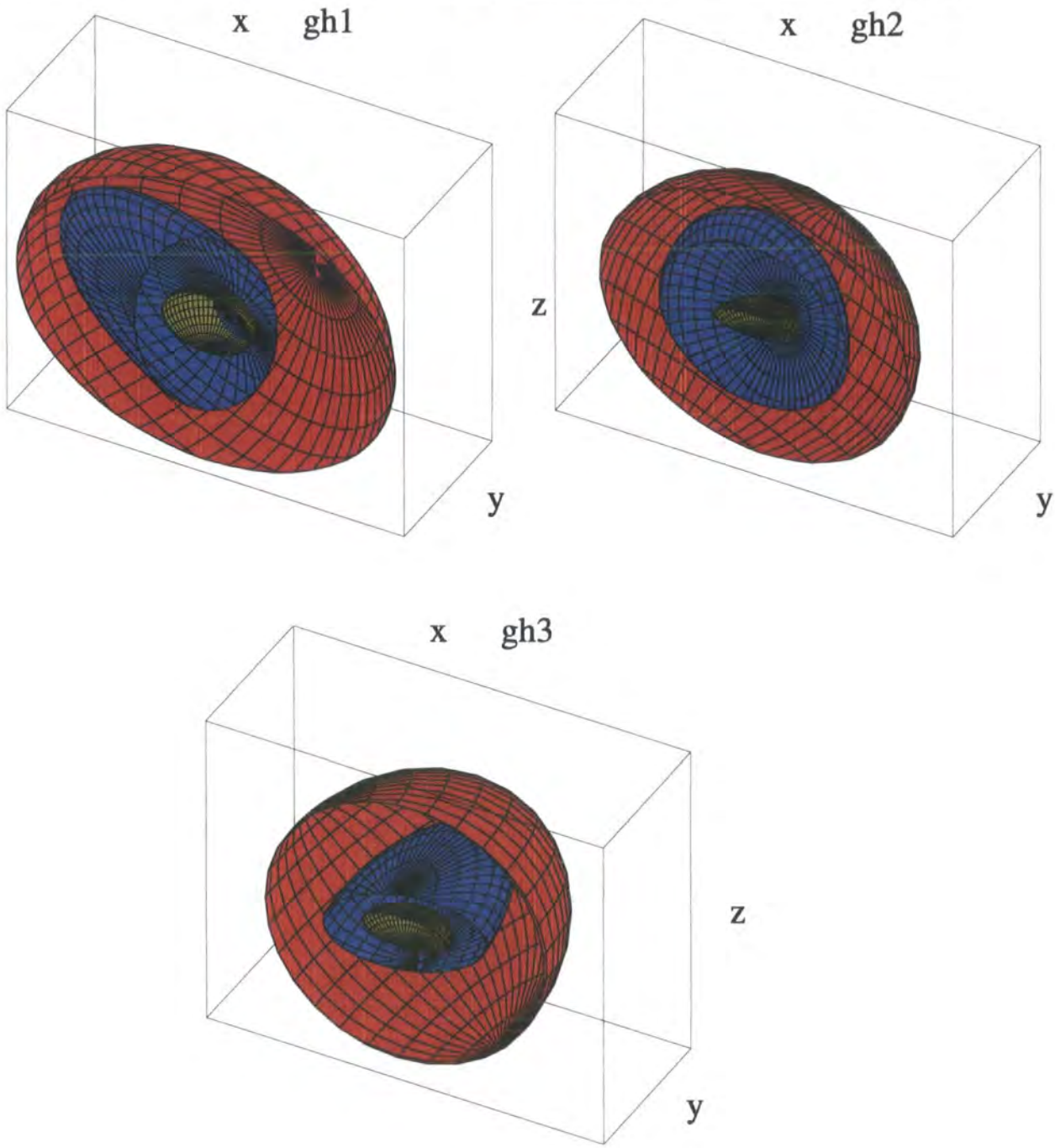

Figure 3.6: The three simulated galaxies with 11 or more satellites. Clockwise, from the top-left, the plots shows galaxies gh1, gh2 and gh3 respectively. The central galaxy, the satellite system and the dark matter halo are represented by the yellow, blue and red ellipsoids respectively. While each ellipsoid has been flattened and oriented according to the measured parameters, their relative sizes have been arbitrarily chosen for clarity. Note that the long, medium and short axes of the central galaxy are always aligned with the x, y, and z axis.

system is well aligned with the long axis of the dark halo. This is consistent with the conclusions reached in Chapter 2 from our (diskless) dark matter simulations. The lack of alignment in system gh2 is probably due to the fact that this has the least aspherical dark halo whose long axis is consequently poorly determined. The alignments of the short axes of the dark halos and satellite systems tell the same story as the alignments of the long axes.

3.5 Alignment of the angular momenta

In this section, we extend our study of alignments to include the possible correlations between the angular momenta of the dark matter halo, $\hat{\underline{J}}_{\rm dm}$, the satellite galaxy population, $\hat{\underline{J}}_{\rm sat}$, and the stars of the central galaxy, $\hat{\underline{J}}_{\rm gal}$. Unless otherwise noted, we consider a number-weighted mean angular momentum, $\underline{J} = \langle \underline{r} \times \underline{v} \rangle$. For the dark matter halo and the central galaxy for which all the particles have roughly the same mass, this "specific" angular momentum is very close to the standard, mass-weighted angular momentum ($\langle \underline{r} \times \underline{p} \rangle$). For the satellite system, however, this definition gives equal weight to each satellite, preventing the statistics from becoming dominated by one or two very large satellites.

The angle between $\hat{\underline{J}}_{\rm dm}$ and $\hat{\underline{J}}_{\rm gal}$ (obtained by computing $\cos(\theta) = \hat{\underline{J}}_{\rm dm} \cdot \hat{\underline{J}}_{\rm gal}$), evaluated for all the material within the virial radius, is plotted in Fig. 3.8. Since the number of satellites is immaterial in this case, we expand our sample to include the six other galaxy halos (identified according to the criteria outlined in Sec. 3.2.2) that were excluded from the satellite analysis in the preceding section. The angular momentum of the galaxy and the dark matter within the virial radius are aligned to within $\sim 30°$, i.e. the galaxy spins in essentially the same direction as the dark matter halo. The single exception is system gh9 in which the galaxy and the dark matter are counter-rotating. A KS test shows that the probability of obtaining the distribution of $\cos\theta$ shown in the figure from nine objects drawn at random from a larger sample of randomly oriented galaxies is only $\sim 0.016\%$. We conclude that there is a significant alignment between the angular momenta of the galaxy and that of the dark halo it inhabits. This is consistent with the acquisition of angular momentum prior to the collapse of the system, when dark matter and gas were well

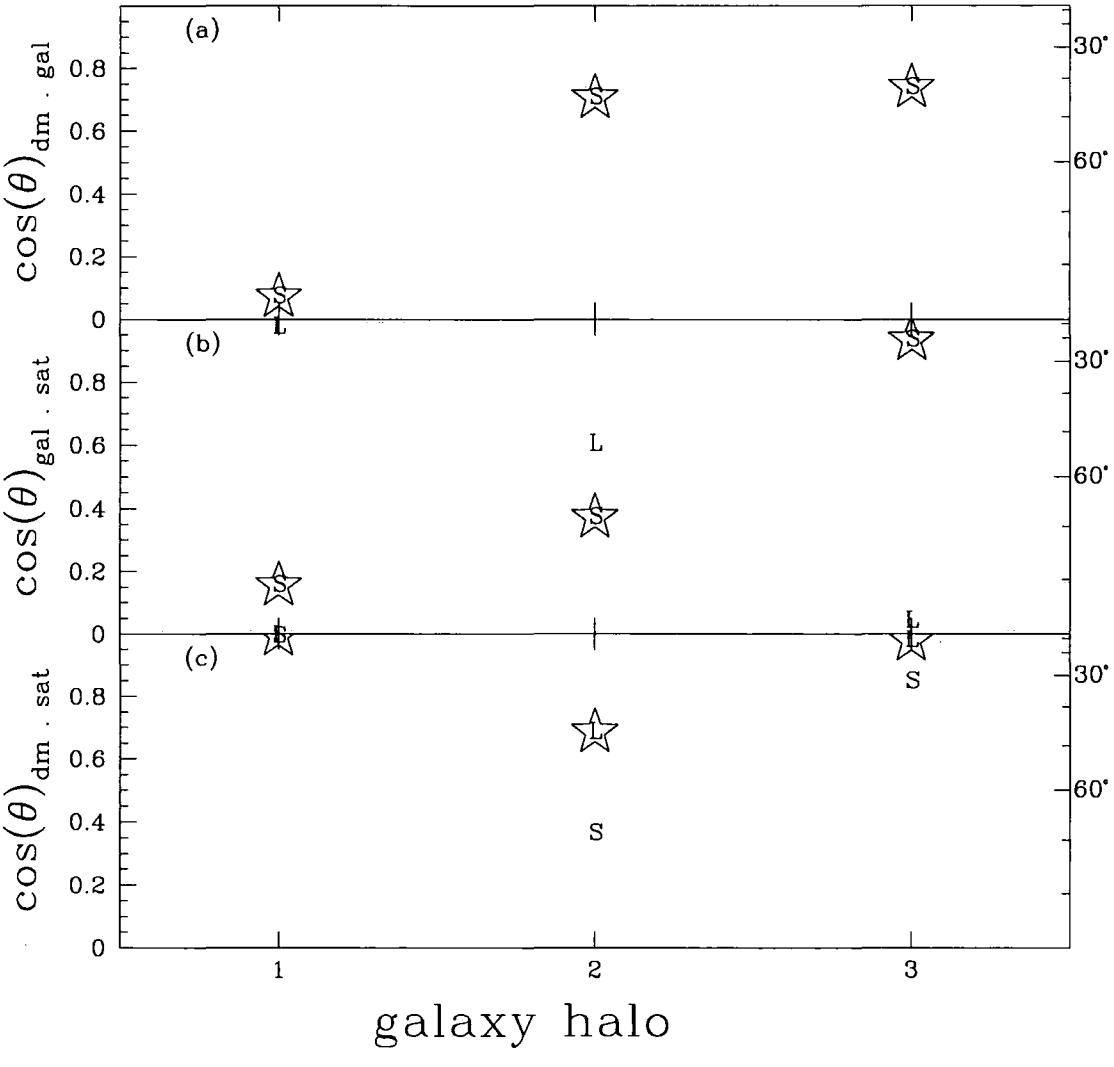

Figure 3.7: Alignments between the long (L) and short (S) axes of the different components of the three galaxies with 11 or more satellites. *Panel (a):* The cosine of the angle between the orientation of the dark halo and of the galaxy. Since galaxies tend to be axis-symmetric the distinction between the intermediate and long axes is poorly defined. Therefore, only the angle between the short axes is shown in this panel. *Panel (b):* The cosine of the angle between the orientation of the galaxy and of the satellite distribution. *Panel (c):* The cosine of the angle between the orientation of the dark halo and of the satellite distribution. The right-hand coordinates are labelled with the value of the angle. The most interesting relation are highlighted with stars.

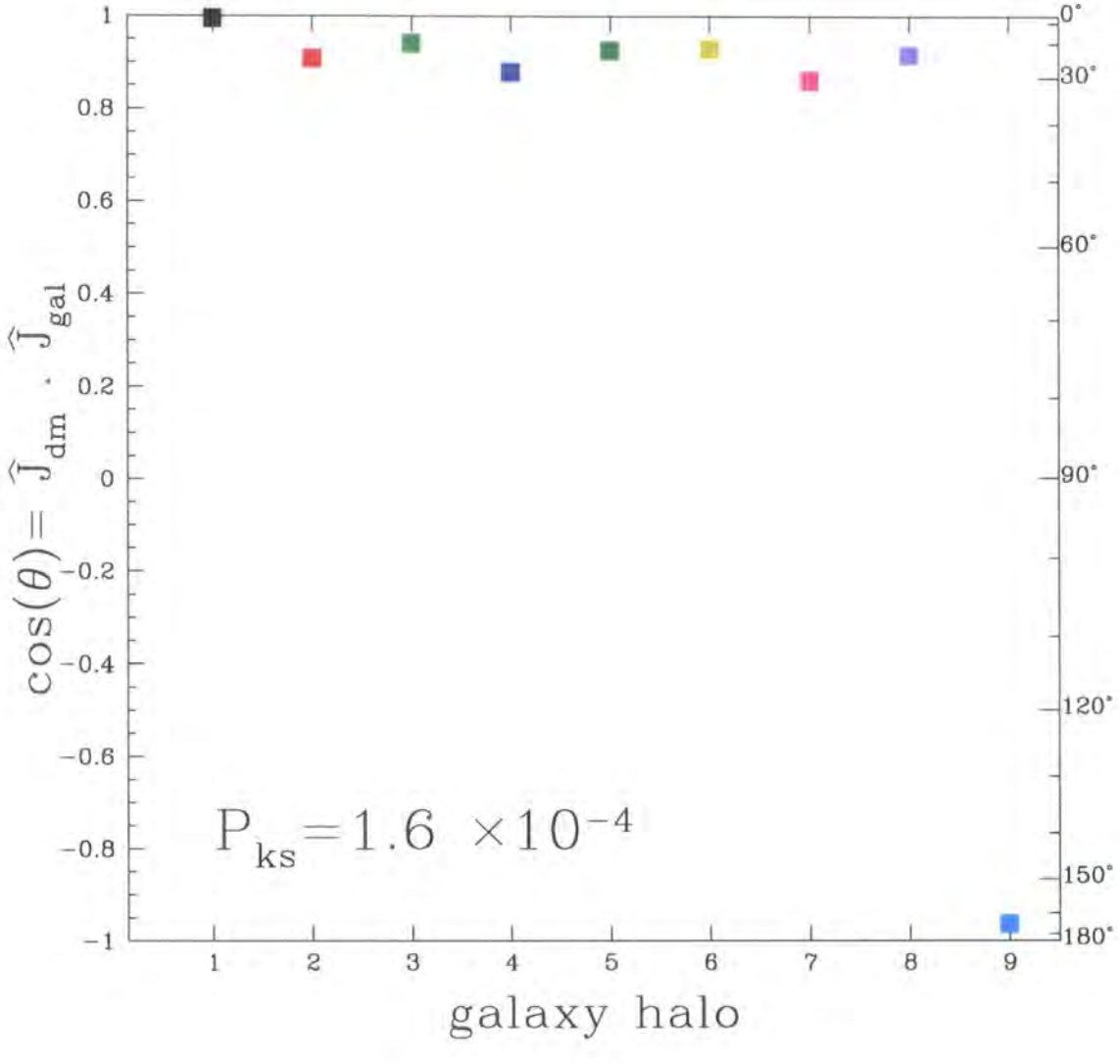

Figure 3.8: Alignment of the angular momentum vectors of the galaxy ($\hat{\mathbf{J}}_{\rm gal}$) and the dark halo ($\hat{\mathbf{J}}_{\rm dm}$) for material within the virial radius for our nine simulated galaxy systems. The right-hand axis gives the value of the angle. Each galactic system has been assigned a colour that will be retained throughout the remainder of this paper.

mixed, as expected in tidal torque theory (e.g. White 1984) and as usually assumed in semi-analytic models of galaxy formation (e.g. Cole et al. 2000).

The radial dependence of the galaxy-halo spin alignment is shown in Fig. 3.9 where we plot the cosine of the angle between $\hat{\underline{J}}_{\rm gal}$ and $\hat{\underline{J}}_{\rm dm}$ $(< r)$ for our nine systems. In 7 out of 9 cases, the alignment persists out to the virial radius of the halo, never straying beyond $\sim 30°$. The two exceptions are systems gh9 and gh8. In the first of these, a tight alignment persists for $r < 0.7r_{\rm vir}$, but it rapidly disappears beyond this radius. A visual inspection of this system shows that the reason for the rapid change in spin direction is simply the presence of a large counter-rotating fragment of dark matter in the outer parts of the halo which has recently been accreted, causing the halo angular momentum to flip in the outer parts. The other anomalous system owes its strange behaviour to the fact that the galaxy is almost a pure spheroid with very little angular momentum. In this case, the direction of $\hat{\underline{J}}_{\rm gal}$ is poorly defined.

Previous studies (e.g. Warren et al. 1992; Bailin and Steinmetz 2005) have found that the halo angular momentum, $\hat{\underline{J}}_{\rm dm}$, tends to be aligned with the halo minor axis, $\hat{\underline{c}}_{\rm dm}$. The simulations of Warren et al. (1992) clearly show such an alignment in the inner parts of the dark halo. Bailin & Steinmetz (2005; see their Fig. 16) demonstrate that the alignment becomes weaker with radius but is still significant ($\sim 30°$) at the virial radius. By contrast, Bailin et al. (2005) report an absence of alignment between $\hat{\underline{c}}_{\rm dm}$ and $\hat{\underline{J}}_{\rm gal}$ at the virial radius in seven hydrodynamic simulations. We now consider the angle subtended by $\hat{\underline{J}}_{\rm dm}$ and $\hat{\underline{c}}_{\rm dm}$ in our own simulations.

In Fig. 3.10 we plot the angle between $\hat{\underline{J}}_{\rm dm}$ and $\hat{\underline{c}}_{\rm dm}$ for all the material within the virial radius and, in Fig. 3.11, the run of this angle with radius. We also plot the KS probability that the distribution of angles for the nine systems at each radius is consistent with a uniform distribution. Our results are qualitatively in good agreement with both Warren et al. (1992) and Bailin and Steinmetz (2005). The radial dependence of $\hat{\underline{J}}_{\rm dm} \cdot \hat{\underline{c}}_{\rm dm}$, displayed in Fig. 3.11, shows that, apart from one anomalous system gh9 (discussed below), there is a good alignment between these two vectors in the inner parts of the halo, within a few tenths of $r_{\rm vir}$. In the outer parts this correlation becomes much weaker, which is perhaps not surprising

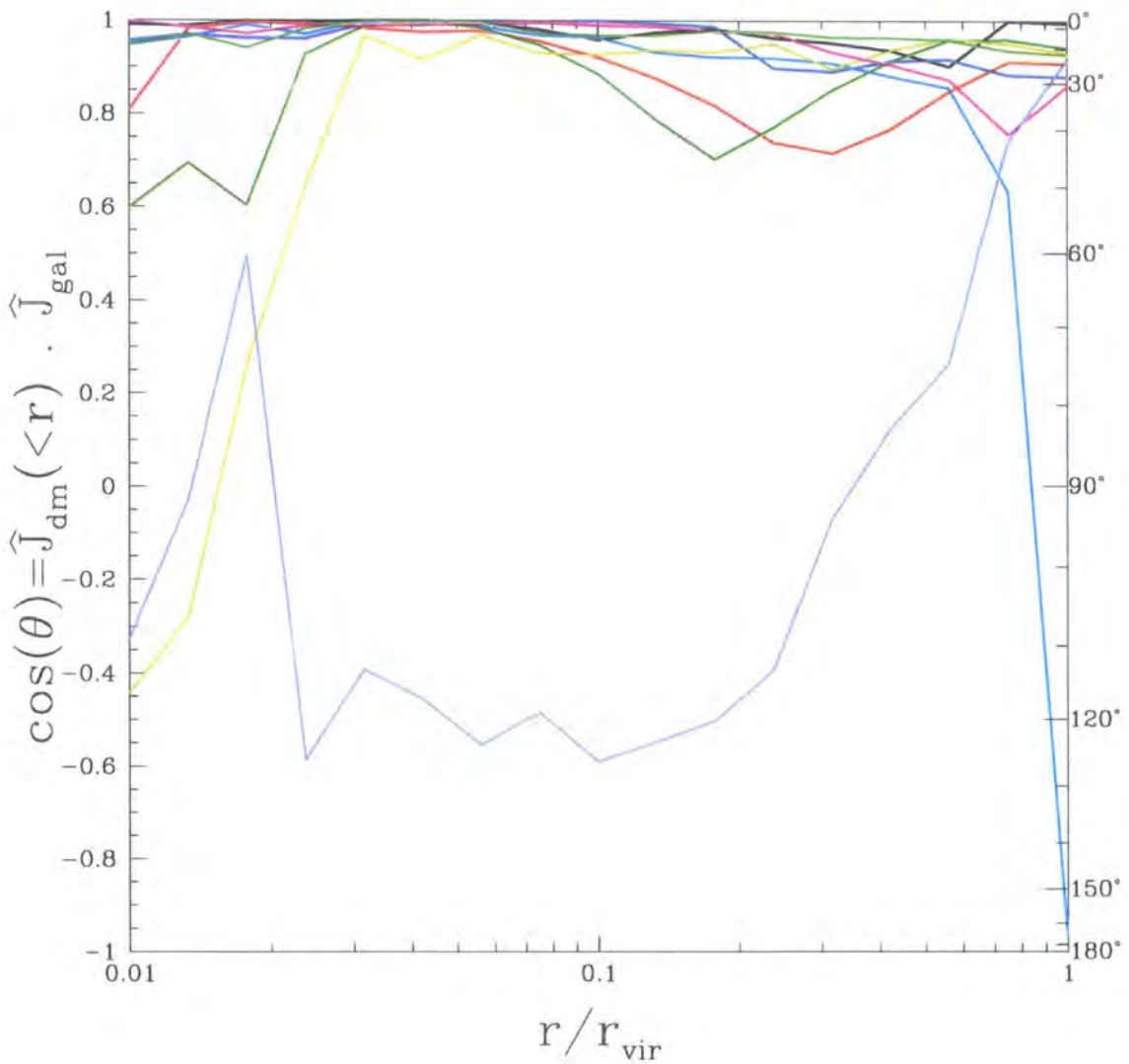

Figure 3.9: The angle between the angular momentum of the disc ($\underline{J}_{\rm disc}$) and the dark matter halo ($\hat{\underline{J}}_{\rm dm}$ $(< r)$) as a function of radius. Each colour represents a single system according to the same code used in Fig 3.8.

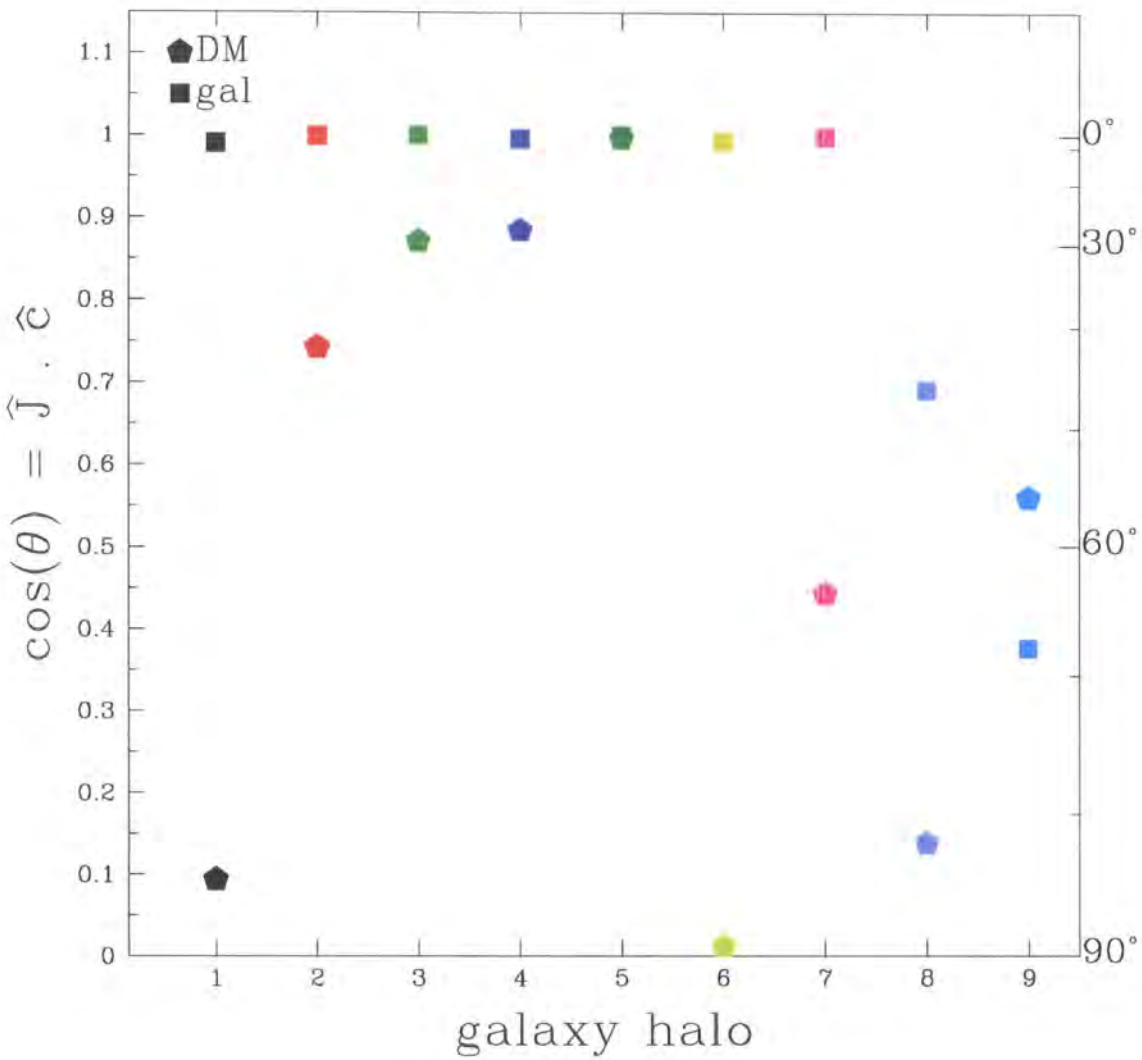

Figure 3.10: The angle between the angular momentum and the short axis of the dark matter halo ($\hat{\underline{J}}_{dm} \cdot \hat{\underline{c}}_{dm}$, pentagons) and of the galaxies ($\hat{\underline{J}}_{gal} \cdot \hat{\underline{c}}_{gal}$, squares) for the nine galaxy halos. The angular momentum vector in most of the galaxies points in the direction of the shortest galactic axis. For the halos, however, no such correlation exists.

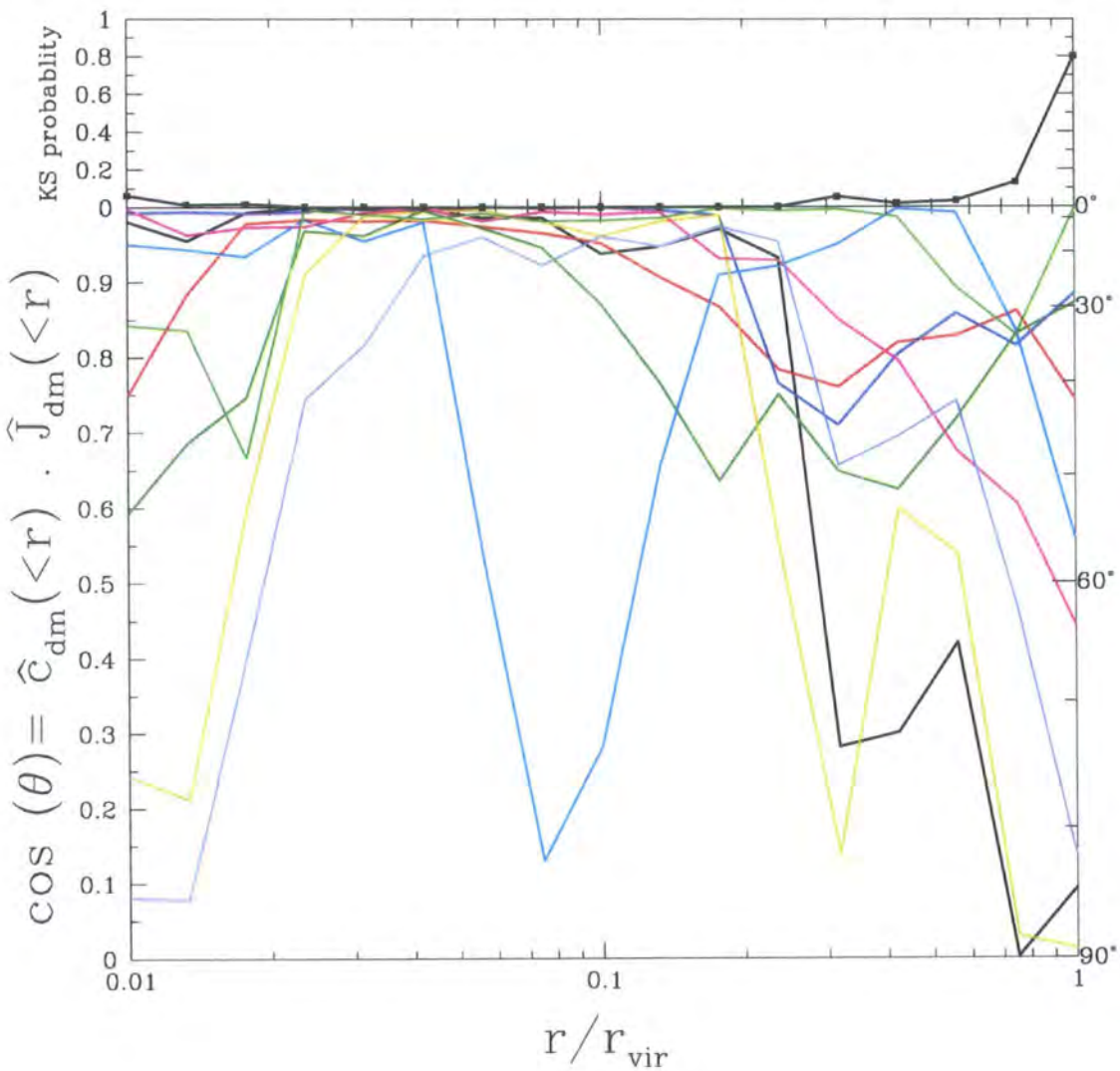

Figure 3.11: The angle between $\hat{\mathrm{J}}_{\mathrm{dm}}$ and $\hat{\mathrm{c}}_{\mathrm{dm}}$ for material within a given radius. Each of the nine galactic haloes is plotted using a different colour, according to the same code used in Fig. 8.

for systems whose shape is supported by an anisotropic velocity dispersion tensor rather than by rotation (Frenk et al. 1985; Warren et al. 1992). While Warren et al. (1992) and Bailin and Steinmetz (2005) find a weak correlation at the virial radius our small sample of 9 halos is consistent with no correlation. Thus the KS probability that the cosine of the angle for these 9 halos is consistent with a uniform distribution jumps from $\sim 15\%$ at $> 0.7r_{\rm vir}$ to $\sim 80\%$ at $r_{\rm vir}$.

Turning to the galaxies, Fig. 3.10 shows that in all but two of the galaxies, the angular momentum vector points in the direction of the shortest galactic axis, as expected for systems flattened by rotation. Of the two discrepant galaxies, gh8 is a nearly perfect spheroid with very little rotation while gh9 is a rapidly rotating spheroid, whose angular momentum is dominated by the bulge's bulk rotation.

Fig. 3.12 where we plot the angle between $\hat{\underline{c}}_{\rm dm}$ and $\hat{\underline{J}}_{\rm gal}$ as a function of radius. Since $\hat{\underline{J}}_{\rm gal}$ is always parallel to $\hat{c}_{\rm gal}$, this is equivalent to plotting the angle between $\hat{\underline{c}}_{\rm dm}$ and $\hat{c}_{\rm gal}$. Apart, again from the anomalous gh9, the angular momentum vector of the galaxy points along the short axis of the halo in the inner parts of the system. This alignment begins to weaken beyond $\sim 0.5r_{vir}$, but even at r_{vir} the KS probability is consistent with a uniform distribution only at the $\sim 15\%$ level. Our results agree well with those of Bailin et al. (2005) in the inner parts of the halo, but they are marginally inconsistent at the virial radius where with their small sample Bailin et al. (2005) find adistribution of cosines consistent with uniform and having a median of 0.5,

We now turn to the alignment of the angular momentum of the satellite system with those of the galaxy and the dark matter halo. In this case, we can use only the three systems with a large satellite population. The results are plotted Fig. 3.13(a) as filled and empty squares.

For all three systems, there is some alignment (within $\sim 40°$) between the spin vectors of the satellite systems and the dark halo. However, in only one case (gh3) is the spin of the satellites aligned with that of the galaxy.

Finally, we ask whether the net angular momentum of the satellite system is related to the shape of the system, i.e. whether the satellites tend to orbit in the approximate plane that they define. If this were the case, we would expect $\hat{\underline{J}}_{\rm sat}$ to point along the short axis of their distribution, $\hat{\underline{c}}_{\rm sat}$. In fact, this is not what we find.

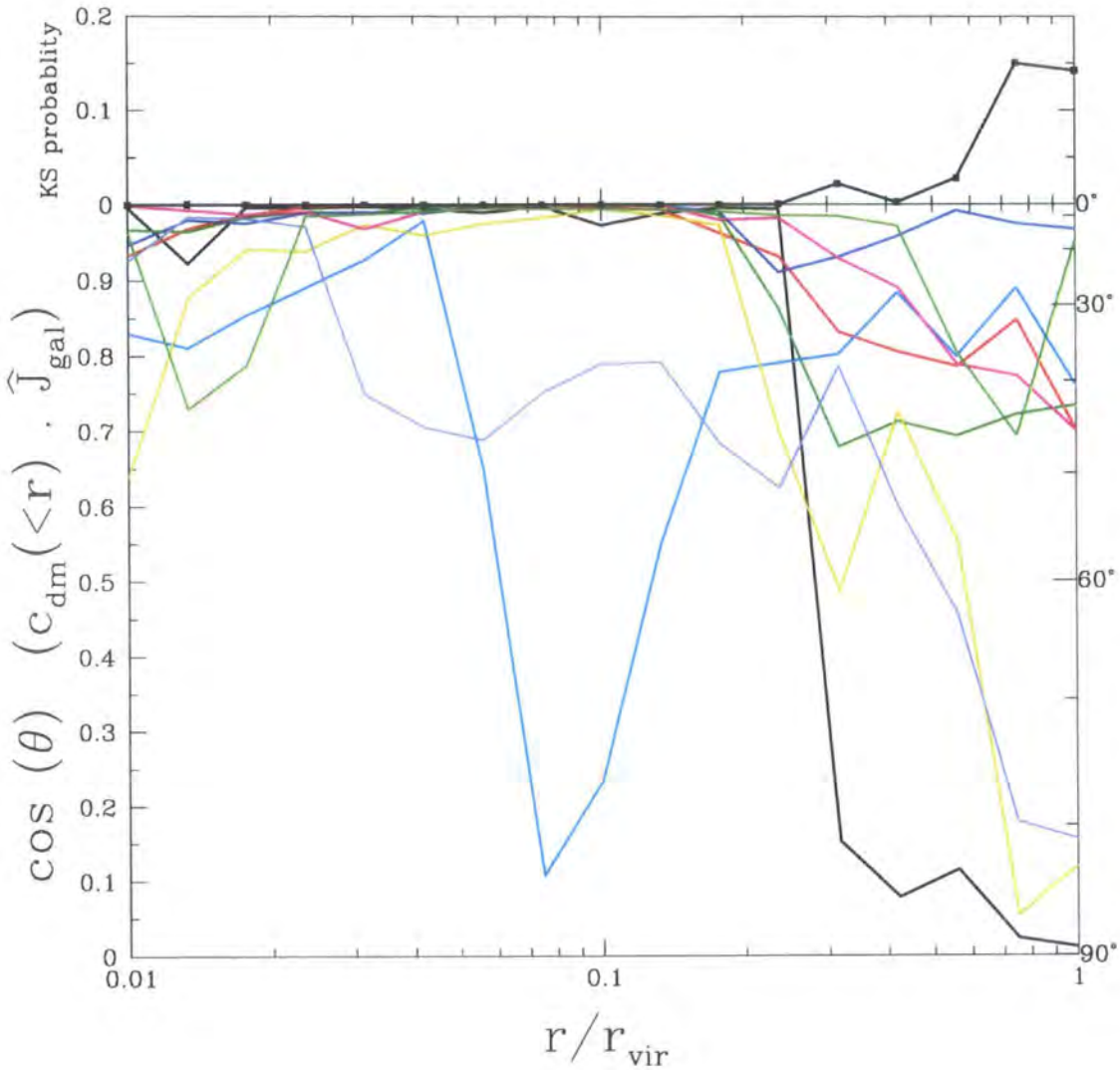

Figure 3.12: The angle between the angular momentum of the disc ($\hat{J}_{gal}$) and the short axis of the dark matter halo ($\hat{c}_{dm}$) for the 9 galaxy halos as a function of radius.

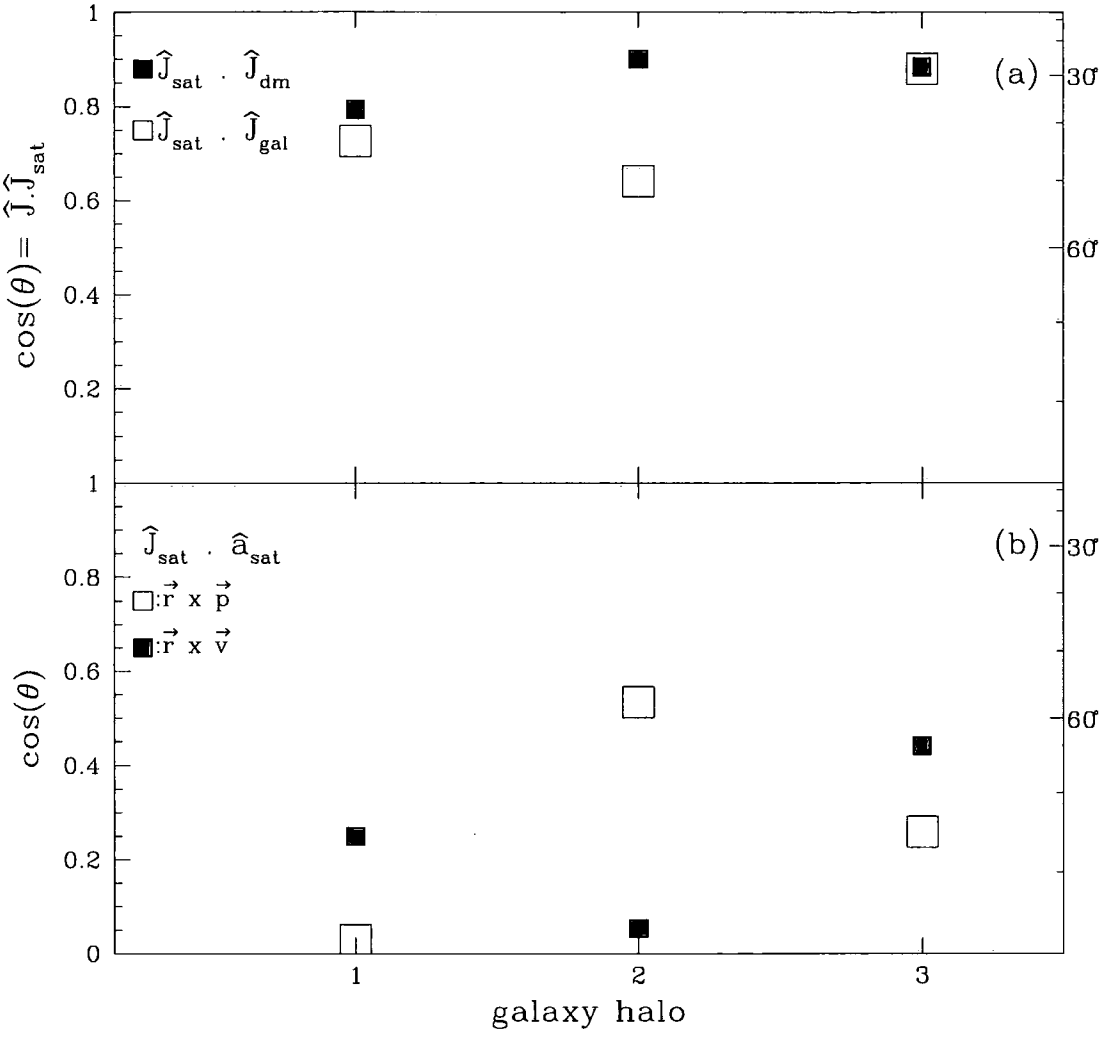

Figure 3.13: *Top Panel* (a): The cosine of the angle between the satellite angular momentum vector, $\hat{\underline{J}}_{sat}$, and $\hat{\underline{J}}_{dm}$ (filled squares) and between $\hat{\underline{J}}_{sat}$ and $\hat{\underline{J}}_{gal}$ (empty squares). *Bottom Panel* (b): The cosine of the angle ($\hat{\underline{J}}_{sat}$) and the long axes of its spatial distribution ($\hat{\underline{a}}_{sat}$). The filled squares correspond to the case when the angular momentum is calculated assuming each satellite has the same mass (i.e $\underline{J} = \langle \underline{r} \times \underline{v} \rangle$) while the empty squares correspond to the case when the angular momentum is calculated in the standard way (i.e $\underline{J} = \langle \underline{r} \times \underline{p} \rangle$).

$\hat{\underline{J}}_{sat}$ tends to point in a direction which, while often approximately at right angles to $\hat{\underline{a}}_{sat}$, the long axis of the satellite system (Fig. 3.13(b)), it is nevertheless not along the short axis of the system, $\hat{\underline{c}}_{sat}$. This arrangement is illustrated schematically in Fig. 3.14 where the blue ellipsoid demarks the structure defined by the anisotropic satellite distribution, while the spin axis, $\hat{\underline{J}}_{sat}$, is shown as a red line and its three projections along the three principal axes of the satellite structure are shown as black lines. From Fig. 3.13(b) we find that in all three cases the angular momentum of the satellite distribution never falls to within $\sim 60°$ of its spatial distribution's long axis. The misalignment between $\hat{\underline{J}}_{sat}$ and $\hat{\underline{a}}_{sat}$ indicates that the satellites are never orbiting in the plane defined by $\hat{\underline{b}}_{sat}$ and $\hat{\underline{c}}_{sat}$. The three systems show different behaviours but in no case is there an indication that the satellites orbit in the apparent plane of their distribution. However we note that there is little consistency throughout our 3 galaxy halos and we find ample evidence for a variety of orientations and alignments.

3.6 Conclusion and discussion

We have analysed two N-body/SPH simulations of galaxy formation in a ΛCDM universe, one of a single bright galaxy and the other of a small region. Our simulations include the main physical processes thought to be important in galaxy formation: metal-dependent gas cooling, heating by photoionizing the primordial hydrogen gas, star formation, metal production and feedback due to supernovae energy injection. In total, we obtained a sample of 9 bright galaxies comparable in luminosity to the Milky Way, containing a total of 78 satellites. Three of the central galaxies had a population of satellites numbering at least eleven, similar to the Milky Way. We have used these samples to investigate several interelated properties of the satellite population.

We first investigated the luminosity function of satellites, a property often regarded as a challenge to the cold dark matter model (e.g. Moore et al. 1999). We find, however, that our simulations produce an excellent match to the observed luminosity function of satellites in the Local Group, at least to the resolution limit of the calculation which corresponds to $M_V \sim 12$, close to the luminosity of the

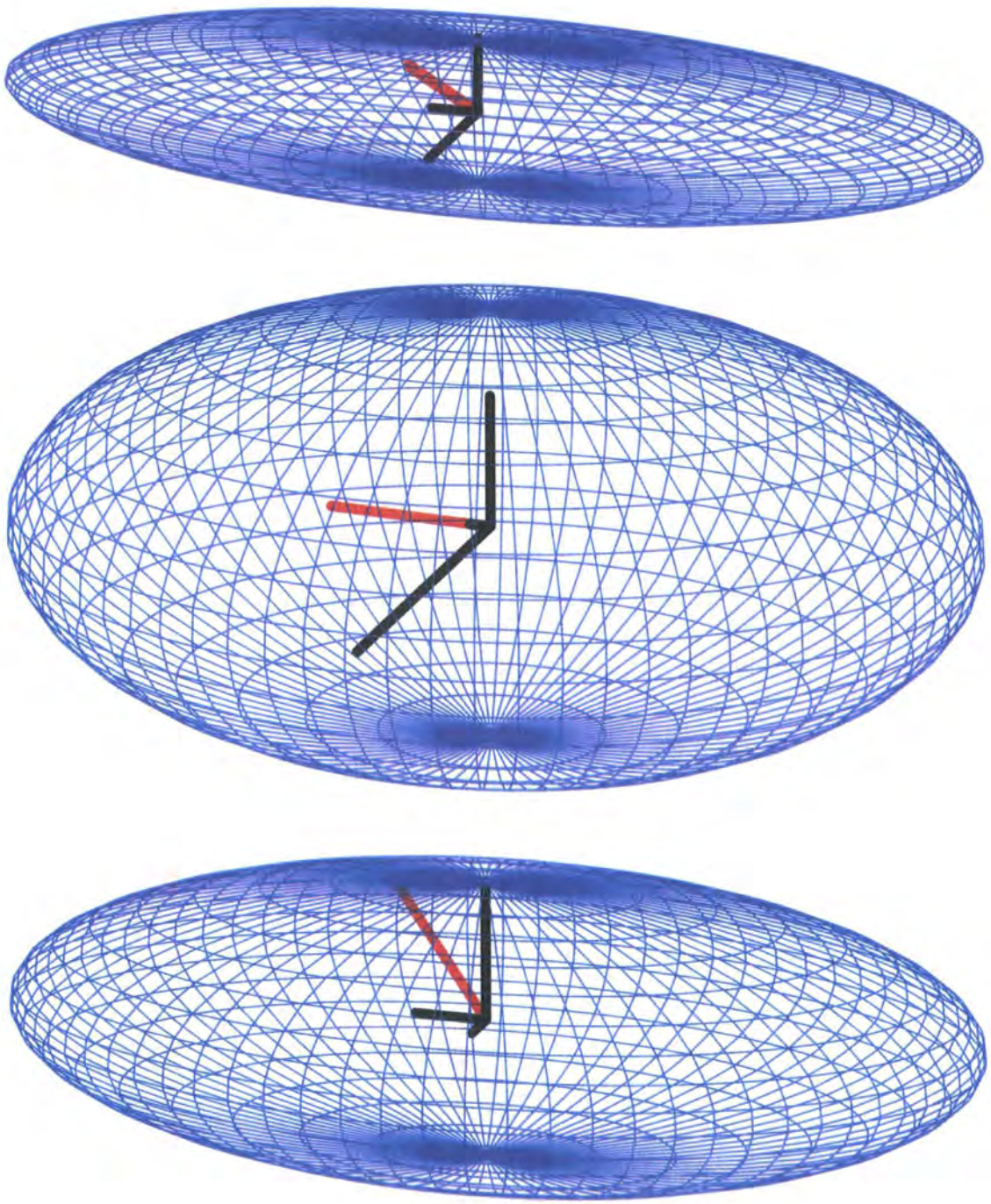

Figure 3.14: Schematic diagram showing the satellite system angular momentum vector, $\hat{\underline{J}}_{\rm sat}$, in three dimension (red line) calculated as $\langle \underline{r} \times \underline{v} \rangle$. The blue ellipsoids illustrate the shape of the satellite distribution. The black lines are the projections of the vector $\hat{\underline{J}}_{\rm sat}$ along the three principal axes of the satellite distribution. From top to bottom we show galaxy halos gh1, gh2 and gh3.

faintest observed satellites. The gas fractions in these satellites agree well with observations, suggesting that their formation paths may be similar to those of real satellites. Many of the small subhalos resolved in the simulations fail to make a substantially bright satellite. As Benson et al. (2002a) have argued star formation is inefficient in small subhalos due to the combined effects of reionization and supernovae feedback which limit the supply of cool gas to the subhalo.

The match of our simulations to the satellite data over most of the observed range suggests that the relative paucity of satellites in the Local Group (the "satellite problem") reflects, not the much larger abundance of subhalos, but rather feedback effects that limit the growth of small galaxies. Furthermore, Benson et al. (2002a) and Stoehr et al. (2002) have argued that the internal dynamics of CDM satellites are also consistent with the data. Overall, our results agree well with the semi-analytic model of Benson et al. (2002a). In the semi-analytic model, however, *bright* satellites, of luminosity similar to the LMC or M33, were rather rare. This is not the case in our simulations which match the bright end of the satellite luminosity function quite well. The differences between the two treatments are no doubt due to the rather different ways in which the physics of galaxy formation are modelled, including differences in the treatment of feedback and star formation and in the satellite merger rates.

We next considered the spatial distribution of the satellites. In the outer half of the system, the density profile of the satellites tracks the dark matter well but, in the inner parts, it falls below the dark matter profile. We find no resolved satellites in the inner $\sim 10\%$ of the halo. These results are consistent with previous purely N-body studies (e.g. Gao et al. 2004; Chapter 4; Shaw et al. 2006).

We can study the distribution of individual satellite systems, particularly their alignments with the halo and disk, for the three systems that formed more than 11 satellites. In agreement with previous purely N-body studies (Chapter 2, Zentner et al. 2005), we find that the satellites tend to be distributed in highly flattened configurations whose major axis is aligned with the major axis of the (generally triaxial) dark halo. In Chapter 2 we argued that this arrangement reflects the preferential infall of satellites along the spine of the filaments of the cosmic web. Our gas dynamic simulations allow us to go further than previous N-body work and

investigate the alignment of satellite systems with galactic disks and the alignment of the latter with dark matter halo. We find that in 2 out or 3 systems, the satellite system is nearly perpendicular (to within 20°) to the plane of the galactic disk. This surprising configuration is exactly what is seen in the Milky Way. The third satellite system ended up well aligned with the disk.

To investigate these alignments further, we calculated the relationship between the disk and the halo, this time using the 9 bright galaxies in our simulations. Previous hydrodynamic simulations have found a good alignment between the disk and the principal plane of the halo (i.e. a good correlation between the directions of the disk axis and the halo minor axis), but only in the inner $\sim 0.2r_{\rm vir}$ of the halo (Kazantzidis et al. 2004; Bailin et al. 2005). Beyond this, these studies find little or no correlation. We also find a good alignment in our simulations between the disk and the halo at small radii but, unlike in the previous studies, the correlation persists, albeit much weakened, out to the virial radius. This sort of alignment is perhaps not unexpected in the simplest interpretation of the tidal torque theory since both the dark halo and the baryon component experience similar tidal torques. The relatively small differences between our results and those of Kazantzidis et al. 2004 and Bailin et al. (2005) are most likely the result of different treatments of star formation and feedback. For example, the strong feedback in our simulations at early times which leads later to a prolonged period of gas accretion and the formation of a large disk in a relatively quiet halo favours the persistence of a relationship between the properties of the halo and the disk.

Of the two cases in which the satellite systems are nearly perpendicular to the disk, in the one which exhibits the strongest alignment (gh1) the disk is also nearly perpendicular to the minor axis of the halo. In the other case, the alignment between the disk and the halo is weaker. In the third system (gh3), in which the satellite system lies in the plane of the disk, the disk is only roughly aligned with the halo. Although our sample is small, it suggests that it should not be surprising that similar kinds of alignments are found in observational studies of satellites in the SDSS and 2dFGRS (Brainerd 2005; Yang et al. 2006; Sales and Lambas 2004).

Finally, we investigated the connection between the angular momenta of the disk and the dark halo. For most systems, the two vectors are very well aligned as

a function of radius, out to the edge of the system. The halo spin tends to be point along the short axis of the halo. However, since the shape of the halo varies with redshift, the spin axis of the disk or of the halo can often loose its alignment with the short halo axis. Thus, care should be taken when interpreting the alignment statistics, either in simulations or in observational data.

In conclusion, our simulations have revealed a number of interesting connections between the properties of central galaxies, their satellite systems and their dark matter halos. They also point to a good overall match between predictions of the ΛCDM model and the observations of galaxy satellite systems that we have considered here such as the luminosity function and the peculiar spatial arrangement of the satellites of the Milky Way. However, due to their high computational cost, our simulations are still too small to provide good statistics. Larger simulations of this kind are required to test the validity of the trends that we have found.

Chapter 4

The effect of gravitational recoil in a Hierarchical universe

4.1 Introduction

The discovery that galactic bulges harbour supermassive black holes whose masses are correlated with the properties of the bulge suggests a close connection between the formation of galaxies and the formation of black holes. The mass of the galactocentric black hole varies approximately linearly with the stellar mass of the bulge (Kormendy and Richstone 1995; Magorrian et al. 1998; Merritt and Ferrarese 2001; McLure and Dunlop 2002) and roughly as the fourth power of the bulge velocity dispersion (Ferrarese and Merritt 2000, Gebhardt et al. 2000, Tremaine et al. 2002). Correlations with the near infrared bulge luminosity (Marconi and Hunt 2003) and with the bulge light concentration (Graham et al. 2001) have also been found. These correlations are remarkable because they link phenomena on widely different scales - from the parsec scale of the black hole's sphere of influence to the kiloparsec scale of bulges - and thus point to a connection between the physics of bulge formation and the physics of black hole accretion and growth (Milosavljević and Merritt 2001). The simplest interpretation is that both, black hole and bulge growth, are driven by the same process whose nature, however, remains unclear.

Various models for the growth of black holes in galaxies have been studied (e.g. Haehnelt and Rees 1993; Silk and Rees 1998; Cattaneo et al. 1999; Kauffmann and Haehnelt 2000; Ostriker 2000; Volonteri et al. 2003; Di Matteo et al. 2005, and others). In the context of the hierarchical cold dark matter model of structure

formation, a plausible explanation for the tight correlation between bulge and black hole properties is that the galaxy mergers or disc instabilities that induce bulge growth via bursts of star formation also feed the central black hole (Kauffmann and Haehnelt 2000; Croton et al. 2006; Bower et al. 2005.) A simple implementation of this model follows from assuming that, as cold gas condenses into stars, a certain percentage of the gas is forced into the centre of the galaxy and accreted by the black hole. Models based on this and related prescriptions successfully reproduce the relation, $m_{\rm BH} - m_{\rm b}$, between black hole mass and stellar bulge mass (Croton et al. 2006; Bower et al. 2005; Malbon in prep).

If a simple model of the kind just mentioned for the simultaneous growth of black holes and bulges is correct, then there are two direct consequences which we explore in this Chapter. The first is that black holes should be expected to exist in bulges of all luminosities including dwarf ellipticals and satellites of brighter galaxies like the Milky Way. Secure measurements of black hole mass to date only span three orders of magnitude, above $m_{\rm BH} \sim 10^6 M_\odot$ for the Milky Way (Merritt and Ferrarese 2001; Tremaine et al. 2002; Schödel et al. 2002). There are claims, however, that the correlation between black hole mass and spheroid properties may extend downwards over three further orders of magnitude in black hole mass mass (Gebhardt et al. 2002; Gerssen et al. 2002).

The second consequence of simple hierarchical models of black hole growth is that central black holes will coalesce as their hosts bulges collide and merge. Binary black holes orbiting each other emit gravitational waves (Peters and Mathews 1963). Using quasi-Newtonian methods to study the orbital decay due to gravitational wave emission, Fitchett (1983) found that the system will eventually enter a plunge phase, causing the black holes to coalesce emitting a burst of gravitational waves. Peres (1962) found that, in addition to transferring energy out of the emitting system, gravitational radiation can also take with it linear momentum. As a result, the centre of mass of the system recoils in a direction specified by the boundary conditions of the last stable orbit.

The astrophysical implication of this linear momentum kick (the "rocket effect" or "gravitational recoil") is that black holes may be ejected from galactic bulges if the potential is shallow and the kick is large enough (Madau and Quataert 2004;

Merritt et al. 2004; Enoki et al. 2004). In theory, this could lead to a sizable population of extragalactic black holes which could, in principle, dominate the black hole mass function. Our aim in this work is to examine the importance of such kicks for the galactic black hole population. In particular, we consider the scatter on the $m_{\rm BH} - m_{\rm b}$ relation in an attempt to constrain the relatively uncertain kick velocity, as well as the nature and spatial distribution of a possible extragalactic population of ejected black holes. We model the growth of black holes using the semi-analytic galaxy formation model of Cole et al. (2000), using two methods for obtaining merger trees: Monte Carlo techniques and high resolution N-body simulations (in which the trajectories of recoiling black holes can be tracked.)

The statistical properties of the population of galactic and intragalactic black holes were recently studied by Volonteri and Perna (2005) who calculated the growth of black holes in a cold dark matter universe taking into account the rocket effect as well as the less common ejection of black holes by 3-body interactions. Like us, they followed the growth of black holes as their host halos merge but they used simplified assumptions for the mass accreted by black holes during mergers instead of the full semi-analytic model of galaxy formation that we employ. Volonteri & Perna also used a simplified model to calculate the spatial distribution of black holes whereas we analyse high-resolution N-body simulations. Their study focused on possible observable signatures of intermediate mass black holes and their relation to observed ultraluminous X-ray sources. In spite of the different methodologies employed in their work and ours, the mass functions and spatial distributions of intermediate mass black holes derived in the two studies are in broad agreement.

This Chapter is organised as follows. In section 4.2, we review the physics of the gravitational recoil. In section 4.3, we describe how we model the formation and ejection of black holes in our semi-analytic model. In section 4.4, we determine the effect of black holes ejected from the progenitors of present day galaxies on the $m_{\rm BH} - m_{\rm b}$ relation. In section 4.5, we use a set of high resolution N-body simulations of galactic halos to track the location of ejected black holes. We conclude in Section 4.6 where we discuss the possible consequences of an extragalactic black hole population.

4.2 The Physics of Kicks

The emission of gravitational radiation is a generic feature of any massive asymmetrically collapsing system (Peres 1962). In order to be accompanied by a linear momentum kick, the gravitational radiation must be asymmetric (Fitchett 1983). For two coalescing black holes of unequal mass this occurs as the gravitational radiation from the lighter, more rapidly moving partner is more strongly beamed. As two black holes orbit each other, gravitational radiation causes their orbits to shrink and circularise until the last stable circular orbit is reached. Using perturbation theory in the weak field approximation, Fitchett (1983) calculated the kick velocity from this final orbit to be:

$$v_{\rm kick} = 1480 \left(\frac{f(q)}{f_{\rm max}}\right) \left(\frac{2G(m_1+m_2)/c^2}{r_{\rm isco}}\right)^4 {\rm km\,s^{-1}} \tag{4.1}$$

where $r_{\rm isco}$ is the radius of the innermost stable circular orbit, $q \equiv m_1/m_2$ is the mass ratio with the convention $m_2 > m_1$, and $f(q) = q^2(1-q)/(1+q)^5$ which reaches a maximum, $f_{\rm max} = 0.0179$, for a mass ratio of $q_{max} \approx 0.382$. Unfortunately, the weak field approximation used by Fitchett becomes invalid as the binary approaches the plunge phase and it is here that the contribution to the recoil velocity becomes largest.

Two decades later, Favata, Hughes & Holz (2004) used perturbation theory to show that, in the presence of strong fields, gravitational kicks are not expected to exceed $600{\rm km\,s^{-1}}$. In a companion paper, Merritt et al. (2004) included the effect of the larger partner's spin and obtained an upper limit of $\sim 500{\rm km\,s^{-1}}$. More recently, Blanchet, Qusailah & Will (2005) performed a higher order calculation of the recoil for the special case of the coalescence of two non-rotating black holes, obtaining an upper limit of $300{\rm km\,s^{-1}}$. However, none these calculations apply to all mass and spin ratios and kick velocities as large as $1000{\rm km\,s^{-1}}$ cannot be definitively ruled out.

In light of the uncertainty in the recoil velocity, we simply assume that the kick is directly proportional to Fitchett's scaling function $f(q)$ and write the recoil velocity in terms of a prefactor velocity $v_{\rm pf}$,

$$v_{\rm kick} = v_{\rm pf} \frac{f(q)}{f_{\rm max}}. \tag{4.2}$$

We then allow $v_{\rm pf}$ to vary between $0\,{\rm km\,s^{-1}}$ (i.e. no kick) to $1000\,{\rm km\,s^{-1}}$ with the aim of constraining this parameter empirically.

4.3 The GALFORM semi-analytic model

In this section, we briefly explain how we use the semi-analytic galaxy formation model GALFORM described in detail by Cole et al. (2000) and Benson et al. (2002a) (and in section 1.3) to model the growth and evolution of galaxies. The growth of dark matter halos by mergers is encoded in a merger tree. Along each branch of the tree, the following physical processes are calculated: (i) shock-heating and virialization of gas within the gravitational potential well of each halo; (ii) radiative cooling of gas onto a galactic disc; (iii) the formation of stars from the cooled gas; (iv) the effects of photoionization on the thermal state and cooling properties of the intergalactic medium; (v) reheating and expulsion of cooled gas through feedback processes associated with stellar winds and supernovae explosions (see Benson et al. 2003b); (vi) the evolution of the stellar populations; (vii) the effects of dust absorption and radiation; (viii) the chemical evolution of the stars and gas; (ix) galaxy mergers (which, depending on the violence of the merger, may be accompanied by starbursts and the formation of a bulge – see Baugh et al. 1998); (x) the evolution of the size of the disc and bulge.

We used two different methods for obtaining dark matter halo merger trees. In the first instance, we constructed the trees using a Monte-Carlo algorithm to determine merger rates (e.g. Lacey and Cole 1993, Cole et al. 2000). In the second instance, we explicitly extracted the merger trees by following the merging of dark matter halos in N-body simulations (Helly et al. 2003). The latter method allows us to apply the semi-analytic formalism directly to the simulations. More details are given in Section 4.5.2.

4.3.1 Discs

Stellar discs are formed as rotating diffuse halo gas cools and settles in a halo. In the GALFORM model, discs are assumed to have an exponential surface density profile,

$$\Sigma(r) = \Sigma_{\rm D} \exp\left(\frac{-r}{r_{\rm D}}\right), \tag{4.3}$$

where $r_{\rm D}$ is a characteristic disc length and $\Sigma_{\rm D}$ is the central surface density. The potential of such a mass distribution as a function of just radius (i.e. in the plane of the disc) is

$$\phi(r, z = 0) = -\pi G \Sigma_{\rm D} r [I_0(y)K_1(y) - I_1(y)K_0(y)] \tag{4.4}$$

where $y \equiv r/2r_{\rm D}$. The functions $I_n(y)$ and $K_n(y)$ are modified Bessel functions of the first and second kind (e.g. Binney and Tremaine 1987). Differencing the potential at $r = 0$ and $r = \infty$, we find that the escape velocity from the centre of the disc is

$$v^2_{\rm D,esc} = 3.36 \frac{GM_{\rm D}}{r_{\rm D,1/2}}, \tag{4.5}$$

where $r_{\rm D,1/2}$ is the half-mass radius of the disc.

4.3.2 Bulges

In the GALFORM model, the principal mechanism for forming both elliptical galaxies and the bulges of luminous spirals is mergers. A merger is termed "major" if the ratio of the mass of the smaller to the larger galaxy exceeds $f_{\rm merge}$; otherwise the merger is termed "minor." In a major merger, all the stars from both merging partners are assumed to form a single spheroid while any gas present is consumed in a burst of star formation. In a minor merger there is no burst of star formation; only the stars from the smaller galaxy are added to the bulge of the larger galaxy, while the gas is added to the disc of the larger galaxy. We adopt $f_{\rm merge} = 0.3$, as recommended by Cole et al. (2000).

In the context of the GALFORM model, Cole et al. (2000) also considered the possibility that dynamical instability in self-gravitating discs could result in the formation of galactic bulges (see also Mo et al. 1999). They found that this mechanism was unlikely to contribute significantly to the formation of large bulges, but

could be important in creating the bulges of lower luminosity galaxies. The criterion they used to determine whether a cold disc was unstable was $\epsilon_{\rm m} \lesssim \epsilon_{\rm m}^{\rm crit} = 1.1$, where

$$\epsilon_{\rm m} = \frac{V_{\rm max}}{(GM_{\rm disc}/r_{\rm D,1/2})^{1/2}} \tag{4.6}$$

(Efstathiou et al., 1982). Here $V_{\rm max}$ is the circular velocity at the disc half-mass radius, $r_{\rm D,1/2}$. We adopt the slightly lower value of $\epsilon_{\rm m}^{\rm crit} = 1.05$ in order to obtain a distribution of bulge to total luminosities similar to that found in the Sloan Digital Sky Survey by Tasca and White (2005). For such unstable discs it was assumed that all the disc stars would be transformed into bulge stars and any cold disc gas would undergo a burst of star formation. The assumption that bulges, and as we discuss later, black holes grow as a result of discs becoming unstable is also assumed in the AGN feedback models incorporated in the latest semi-analytic models of Croton et al. (2006) and Bower et al. (2005). To illustrate the importance of this mechanism, we present models both with and without this secondary route for generating galactic bulges.

The density profile we adopt for bulges is the Hernquist (1990) model,

$$\rho(r) = \frac{M_{\rm B}}{2\pi}\frac{a}{r}\frac{1}{(r+a)^3}, \tag{4.7}$$

where a is a scale length and $M_{\rm B}$ is the total bulge mass. The potential of such a profile is found by integrating the Poisson equation and the escape velocity from the centre of such a spheroid is given by

$$v_{\rm B,esc}^2 = 4.83\frac{GM_{\rm B}}{r_{\rm B,1/2}}, \tag{4.8}$$

where $r_{\rm B,1/2}$ is the bulge's half-mass radius.

4.3.3 Black Holes

We assume that the growth of black holes is proportional to the growth of galactic bulges. Whenever an event that adds stellar mass to the bulge occurs, we assume that a fraction, $f_{\rm BH}$, of that mass is accreted by the central black hole. This assumption is motivated in part by models of black hole growth such as that of Kauffmann and Haehnelt (2000), wherein black holes accrete a proportion of the

cold gas being consumed in a burst of star formation. In our model, black holes grow both as a result of such star formation bursts *and* also by the accretion of stars in mergers or as the result of disc instabilities. We assume that in each case the same mass fraction, $f_{\rm BH}$, is channelled onto the black hole. This simplifying assumption has the virtue that, in the absence of black hole ejection, all bulges will have black holes that sit precisely on the $m_{\rm BH} - m_{\rm b}$ relation and so we can, in principle, use the scatter induced by black hole ejections to set a firm upper limit on the kick velocities. Our model does not require specifying a minimum black hole mass, only the fraction, $f_{\rm BH}$. The precise value of $f_{\rm BH}$ needed to match the data has changed in the literature (e.g. see Magorrian et al. 1998; Merritt and Ferrarese 2001; Merritt et al. 2004) and we choose $f_{\rm BH} = 0.001$, the value published by McLure and Dunlop (2002) from estimates of black hole masses for 72 active galaxies.

During a merger, we assume that a fraction of any new stellar bulge mass is added to the existing black hole,

$$M_{\rm BH,\ new} = M_{\rm BH,\ old} + f_{\rm BH}\,\Delta M_{\rm bulge}. \tag{4.9}$$

If the black hole is ejected during the merger, we assume that a new black hole is born whose mass is equal to the mass fraction that would have been added to the preexisting black hole had it not been ejected, that is:

$$M_{\rm BH,\ new} = f_{\rm BH}\,\Delta M_{\rm bulge}. \tag{4.10}$$

This black hole then becomes the focus of mass accretion during subsequent episodes of bulge growth. In this way, we ensure that all bulges contain a black hole at all times and that, in the absence of gravitational recoil, all black holes at all times have masses directly proportional to their bulges and hence lie on a perfect $m_{\rm BH} - m_{\rm b}$ relation with zero scatter. The implicit assumption that black holes exist only in bulges and not in discs, and that black holes grow during mergers rather than during quiescent star formation is motivated simply by the desire to reproduce the empirical $m_{\rm BH} - m_{\rm b}$ relation.

We assume that once two galaxies have merged, their central black holes coalesce instantaneously. This should be a good approximation as the black holes will merge on a timescale shorter than the time between galaxy mergers, which is determined

by the hierarchical growth of structure (Berczik et al. 2006; Mayer et al. 2006). Note that even when the merger rate of dark matter halos is relatively high, the galaxies orbiting inside the dark halos will only merge once their orbits decay due to energy loss by dynamical friction against the halo material (Lacey and Cole 1993). The assumption of instantaneous black hole coalescence implies that 3-body interactions and associated slingshots (e.g. Saslaw et al. 1974) leading to black ejection are rare (see Volonteri and Perna 2005).

The mass ratio of the merging black holes determines the recoil velocity, $v_{\rm kick}$, according to equation (4.2). Thus, to determine whether the recoiling black hole escapes from the galaxy we add the bulge and disc potentials and require

$$v_{\rm kick}^2 > v_{\rm esc}^2 \equiv 3.36\,\frac{GM_{\rm D}}{r_{\rm D,1/2}} + 4.83\,\frac{GM_{\rm B}}{r_{\rm B,1/2}}. \tag{4.11}$$

Note that we neglect the contribution of the dark matter halo. This is a good approximation over the length scale of the galaxy because the dark matter potential has a very shallow gradient. However, the dark matter potential becomes increasingly important for black holes that escape the galaxy and, in Section 4.5.2, we use an alternative method to follow their orbits. If the recoil velocity, $v_{\rm kick}$, is less then $v_{\rm esc}$ we assume that the black hole will not escape but rapidly return to the centre of the galaxy. This simplifying assumption is motivated by the calculations of Merritt et al. (2004) and Madau and Quataert (2004) who found that if the kinetic energy imparted by the recoil is sufficiently small, then the recoiling black hole undergoes damped oscillations about the galactic nucleus which decay in a few dynamical times.

Our modelling of black hole growth thus automatically reproduces an empirical $m_{\rm BH} - m_{\rm b}$ relation. If the prefactor velocity, $v_{\rm pf}$, in equation (4.2) is zero, the black hole masses are all directly proportional to the bulge mass of their host galaxies. If $v_{\rm pf}$ is not zero, gravitational kicks introduce scatter in the $m_{\rm BH} - m_{\rm b}$ relation which we now investigate and compare with observations.

4.4 The effect of velocity kicks on the $m_{\rm BH}-m_{\rm b}$ relation

In order to investigate how the $m_{\rm BH} - m_{\rm b}$ relation is affected by the ejection of recoiling black hole merger remnants we have studied a sample of 1000 halos of final mass $10^{12}M_{\odot}$. Merger trees for each halo were generated using the Monte-Carlo method described by Cole et al. (2000) and the GALFORM rules of galaxy formation were applied to each branch of the tree. The growth of each central black hole (which tracks the growth of the bulge) was calculated as described in Section 4.3.3. Our fiducial model includes the process of bulge formation by disc instability discussed in Section 4.3.2. For every black hole merger we consider kick velocities corresponding to values of the prefactor, $v_{\rm pf}$, in equation 4.2 in the range 0 - 1000km s^{-1}.

The ejection of a black hole from the bulge is a source of scatter in the $m_{\rm BH} - m_{\rm b}$ relation. Fig. 4.1 shows the $z = 0$ $m_{\rm BH} - m_{\rm b}$ relation for 1000 halos assuming a moderate prefactor kick velocity of 300 km s^{-1}. Note that black hole mass may only be scattered downwards by ejections. Galactic bulges that have never experienced an ejection lie exactly on the diagonal line.

In the absence of kicks, the model, by definition, gives a perfect $m_{\rm BH}-m_{\rm b}$ relation with no scatter. As the kick velocity increases, a tail of bulges that host black holes of reduced mass appears, while the remaining galaxies whose progenitors never lost their black hole still lie precisely on the relation. The form of the scatter about the $m_{\rm BH} - m_{\rm b}$ relation and its dependence on the prefactor $v_{\rm pf}$ are shown in Fig. 4.2. The upper two panels show how deviations from the ideal relation depend on bulge mass for both $v_{\rm pf} = 300\,{\rm km\,s^{-1}}$ and $500\,{\rm km\,s^{-1}}$, while the lower two panels show histograms of these deviations averaged over all bulge masses. We see in these lower panels that the distribution of deviations from the ideal relation is very non-Gaussian, with a tail extending to very low values of $\log_{10}(M_{\rm BH}/M_{\rm ideal,BH})$. For $v_{\rm pf} = 300\,{\rm km\,s^{-1}}$, 2.6% of bulges have black holes with mass smaller than 20% of the ideal $m_{\rm BH} - m_{\rm b}$ value. For $v_{\rm pf} = 500\,{\rm km\,s^{-1}}$ this fraction jumps to 18.9%. The rms width of this distribution is not a good statistical description of the scatter in the $m_{\rm BH} - m_{\rm b}$ relation since the rms is dominated by the noisy tail. We use instead a more robust measure of width. We calculate the widths that contain 68% and

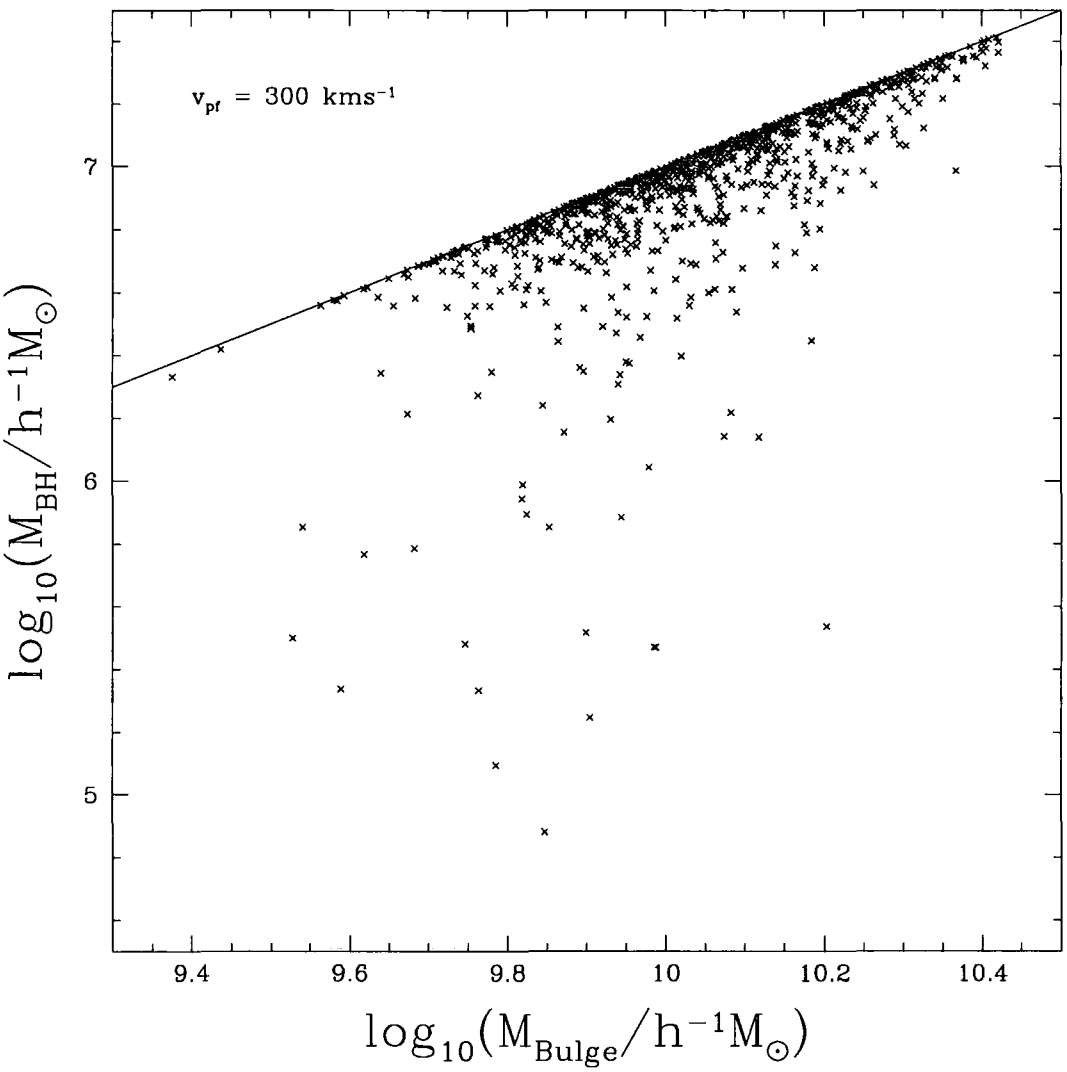

Figure 4.1: The $z = 0$ $m_{\rm BH} - m_{\rm b}$ relation for the case in which black hole merger remnants have the kick velocity given by equation (4.2) with $v_{\rm pf} = 300\,{\rm km\,s^{-1}}$. The diagonal line represents the 'ideal' $m_{\rm BH} - m_{\rm b}$ relation for which $M_{\rm BH}/M_{\rm bulge} = f_{\rm BH} = 10^{-3}$.

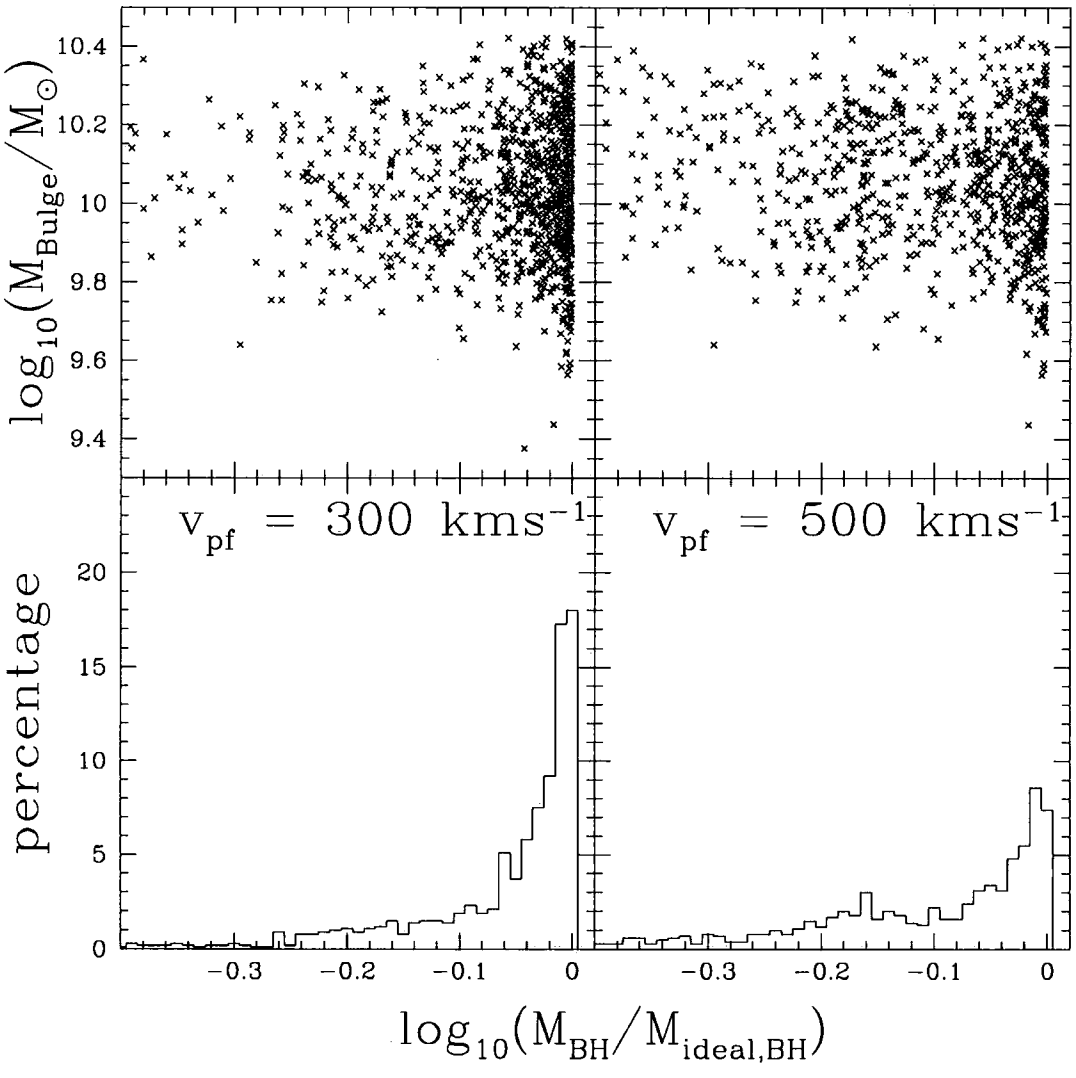

Figure 4.2: Top: residuals from the $m_{\rm BH} - m_{\rm b}$ relation. Plotted here is the dependence on bulge mass of the ratio of the black hole mass to the value for the 'ideal' $m_{\rm BH} - m_{\rm b}$ relation. Bottom: histogram of deviations from the ideal $m_{\rm BH} - m_{\rm b}$ relation.

86% of the distribution, and then define σ_{68} and σ_{86} to be half and one third of these widths respectively. For a Gaussian distribution both of these measures would equal σ, the usual rms width. Fig. 4.3 shows how these measures of scatter vary as a function of $v_{\rm pf}$ and compares them to published observational determinations. The non-Gaussian nature of the scatter results in the two curves being significantly different.

We immediately see that the contribution to the scatter in the $m_{\rm BH}-m_{\rm b}$ relation from ejected black holes is very sensitive to assumptions concerning disc stability. For the case where unstable discs are assumed to form bulges, large values of $v_{\rm pf}$ are strongly ruled out as they would produce more scatter in the $m_{\rm BH}-m_{\rm b}$ relation than is observed. Fig. 4.3 shows that to be consistent with the tightest observational limits (Tremaine et al. 2002; Marconi and Hunt 2003; Häring and Rix 2004) requires $v_{\rm pf} < 450$–$650{\rm km\,s^{-1}}$. This constraint is consistent with the kick velocities predicted by the general relativistic analysis of Favata et al. (2004) and Blanchet et al. (2005). Even so, if the prefactor velocity lies in the range $v_{\rm pf} = 300$ - $500{\rm km\,s^{-1}}$, as these calculations suggest, then gravitational recoil provides a substantial contribution to the scatter in the $m_{\rm BH}-m_{\rm b}$ relation.

In models where discs are assumed to be stable to the formation of a bulge, all the observational estimates of the scatter lie well above the values that result from recoiling black hole ejections. In this case, we conclude that even kicks with velocities exceeding the range expected from current calculations do not produce a significant contribution to the scatter in the $m_{\rm BH}-m_{\rm b}$ relation. There are two reasons for such a large difference between the two models. Firstly, when discs are assumed to be stable there are far fewer ($\sim 10\%$) bulge-bulge mergers and far more disc-bulge and disc-disc mergers involved in the formation of the galaxy. While the total number of mergers is the same in both models, the effect of the gravitational recoil depends only on the number of bulge-bulge mergers because, in our model, black holes only grow if there is a stellar spheroid.

The second reason for the difference between the two cases is that when discs are assumed to be stable, most ejections occur at early times ($z \approx 2$) when the bulges were smaller. The bulge then has enough time to regrow a black hole of the appropriate mass by subsequent galaxy mergers from which black hole ejection

becomes increasingly difficult. When unstable discs are assumed to form bulges, the majority of the ejections occur much later ($z \lesssim 1$) and subsequent mergers are unable to grow a large black hole. Note that no black holes are ejected at $z < 0.7$ and $z < 0.3$ for disc-stable and disc-unstable models respectively.

4.5 The black hole distribution from N-body simulations

In this section, we use high resolution N-body simulations of galactic halos to track the location of subgalactic and galactic black holes as the halo grows by mergers. The simulations provide spatial information that is not available in Monte-Carlo merger trees. We first describe the simulations and the way in which we model black hole escapees.

4.5.1 Galaxies in the N-body simulations

We have used six N-body simulations of galactic-size dark matter halos of final mass $\sim 10^{12} M_{\odot}$ to study the demographics and spatial distribution of their black hole population, including black hole ejections. The simulations were performed using the GADGET code (Springel et al. 2001b) in a flat ΛCDM universe with $\Omega_{\rm m} = 0.3, h = 0.7, \sigma_8 = 0.9$. These simulations have been previously studied by other authors (Power et al. 2003; Hayashi et al. 2004; Navarro et al. 2004b) and we refer the reader to these papers for technical details[1]. Briefly, each simulation follows the formation of structure in a cube of comoving side 35.325 h^{-1}Mpc with a Lagrangian 'high resolution' region around the halo of interest in which the particle mass is $2.64 \times 10^5 h^{-1} M_{\odot}$ and 'low resolution' particles elsewhere. Table 2.2 summarises the parameters of our six simulations.

Halos and their substructures were identified using the algorithm SUBFIND (Springel et al. 2001a). The algorithm first identifies "friends-of-friends" groups using a linking length of 0.2 times the mean interparticle separation which approximately selects particles lying within the virialized region of the halo (Davis et al. 1985). Only ha-

[1]These simulations are the same simulations as used in Chapter 2.

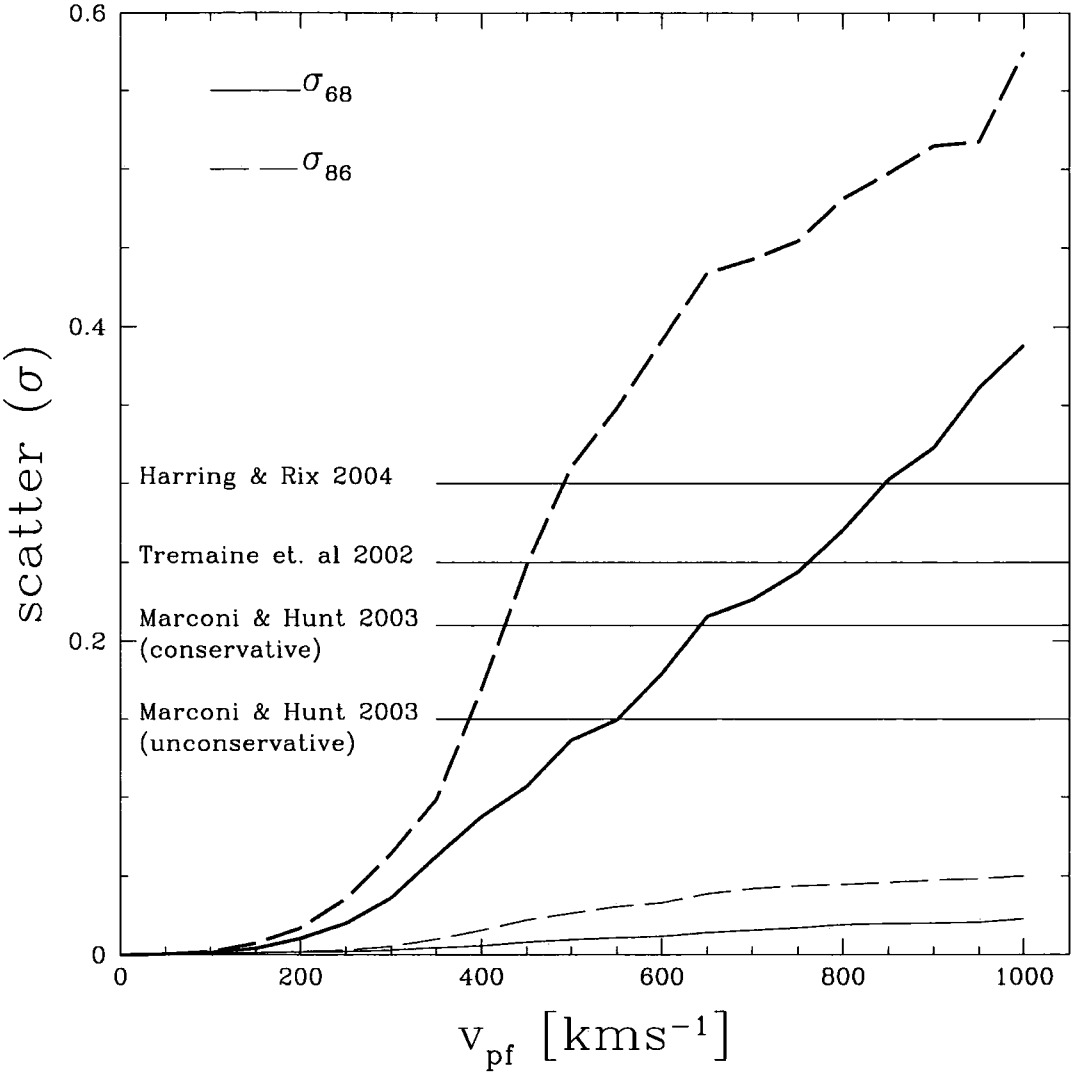

Figure 4.3: The scatter in the $m_{\rm BH} - m_{\rm b}$ relation as a function of the kick velocity prefactor, $v_{\rm pf}$. The curves show our estimates of the width of the distribution of $M_{\rm BH}/M_{\rm ideal,BH}$ induced by black hole ejections as discussed in the text. The solid and dashed curves represent σ_{68} and σ_{86} respectively. The thick lines show the estimates when disc instability produces bulges, while the thin lines represent models when this route for bulge formation is ignored. The horizontal lines show estimates of the scatter from various observational studies. Note that Tremaine et al. (2002) give only an upper limit, while Marconi & Hunt (2003) present two estimates to which they refer as conservative and nonconservative.

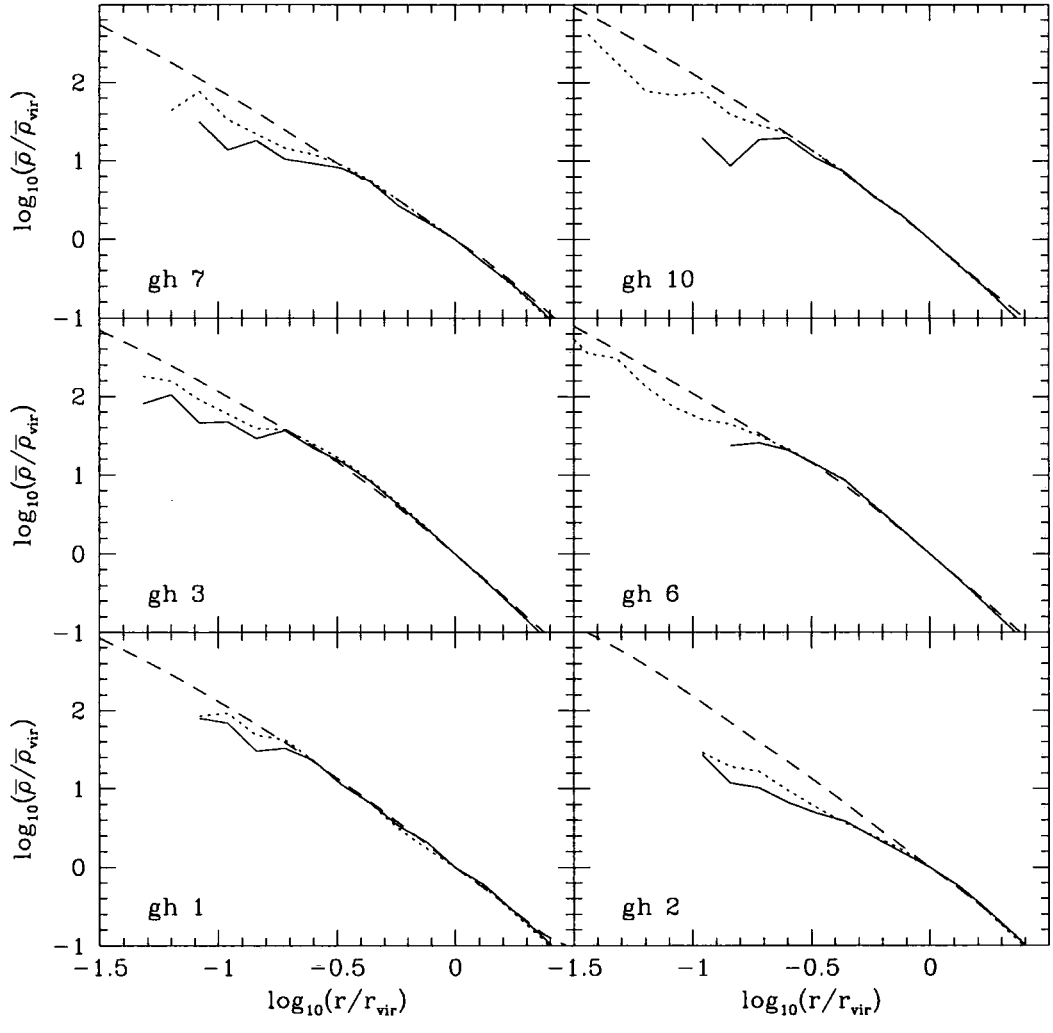

Figure 4.4: The mean interior radial dark matter density profiles for six simulated halos plotted against radius in units of the virial radius, and normalised to the value of the mean interior density at the virial radius (long dashed curve). The solid curves show the mean interior number density of satellites as a function of radius, normalised to the value at the virial radius. The dotted curve shows the mean interior density of all black holes (both those residing in satellites as well as the wandering ones), normalised to the value at the virial radius, assuming a kick velocity, $v_{\rm pf} = 300$ kms^{-1}.

los with more than 10 particles, corresponding to a mass of $2.64 \times 10^6 h^{-1} M_\odot$, are considered. Then, using an excursion set approach, SUBFIND identifies self-bound subgroups within each friends-of-friends halo.

We use the method described by Harker et al. (2006) to construct full merger histories for the dark matter halos. Progenitor and descendant halos are identified at every timestep and tracked throughout the simulation in order to build the merger tree. The semi-analytic galaxy formation code GALFORM (e.g see Cole et al. 2000; Benson et al. 2002a; Baugh et al. 1998) is then applied along each branch of each merger tree to obtain the properties of the central galaxy in each halo and its orbiting satellites. If the subhalo that hosts a satellite survives inside the parent halo, the position of the satellite is identified with the most bound subhalo particle. Some subhalos, however, are disrupted by tidal forces as they sink by dynamical friction and can no longer be identified by SUBFIND. In this case, the satellite is placed at the centre of mass of the particles that made up the subhalo at the last time it was identified. If the harmonic radius of these particles becomes greater than the distance between the satellite and the centre of the parent halo, the satellite is deemed to have merged into the central galaxy.

Fig. 4.4 shows the spherically averaged dark matter density profile of our six halos normalised to the mean dark matter density within the virial radius. The galactrocentric distance is plotted in units of the virial radius (see Table 2.2). We also plot the corresponding number density profile of satellite galaxies with a V band magnitude $M_V < -7$. The dark matter profile follows the NFW form (Navarro et al. 1996, 1997) quite closely (see Navarro et al. 2004b). The radial distribution of the satellites is shallower than that of the dark matter in the inner parts of the halo. This result is broadly in agreement with the density distributions of substructures previously obtained from high resolution N-body simulations (see e.g Ghigna et al. 1998; Ghigna et al. 2000; Gao et al. 2004). Note, however, that the profiles in Fig. 4.4 refer to satellite galaxies, not substructures and that 19.3% of the satellites are not attached to a subhalo. Nevertheless, the radial profile of the satellites is similar to that of subhalos.

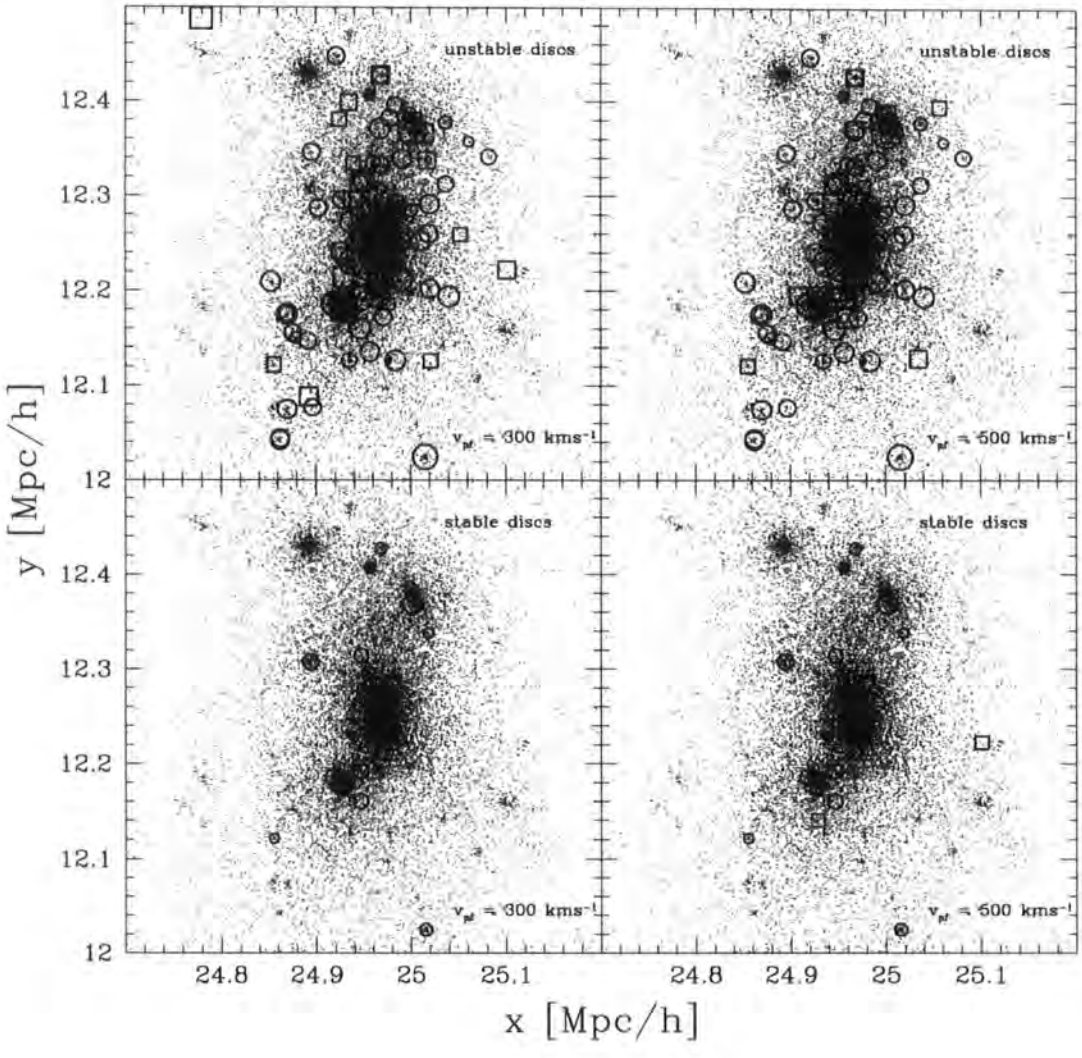

Figure 4.5: The spatial distribution of mass and black holes in simulation gh2. The top two panels correspond to the model in which unstable discs produce bulges, while the lower two panels correspond to the model in which this bulge formation channel is ignored. The left-hand and right-hand panels correspond to kick velocity prefactors of $v_{\rm pf} = 300\,{\rm km\,s^{-1}}$ and $v_{\rm pf} = 500\,{\rm km\,s^{-1}}$ respectively. Black holes are represented by symbols whose area is proportional to their mass. The open circles denote black holes that lie at the centre of a satellite galaxy, while open squares denote wandering black holes that were ejected during a merger. The central galactic supermassive black hole is in the middle of each panel. The virial radius of the halo is indicated by the dashed circle. The subset of intergalactic black holes (i.e. black holes ejected from the halo) that are tagged with simulation particles (75.0% in the left-hand panels and 45.7% in the right-hand panels) are plotted.

4.5.2 The black hole population

The growth of galactic bulges and their associated black holes is calculated along each branch of the merger tree as described in Section 4.3.3. At the final time, each central galaxy contains a black hole typically of mass $10^7 h^{-1} M_\odot$ for models where unstable discs form bulges and $10^6 h^{-1} M_\odot$ for models where disc instability is ignored. There are, in addition, two other populations of black holes. Firstly, there are "galactic black holes" that reside in the bulges of satellites in the halo; secondly, there are black holes that have been ejected from their host galaxy and which we term "wandering" black holes (Volonteri and Perna 2005). The population of wandering black holes, in turn, is made up of "intrahalo black holes" that are still inside the host halo's virial radius at $z = 0$, and "intergalactic black holes" which have been ejected from the halo and lie outside the virial radius at $z = 0$.

Tracking black holes

Black holes that remain within their host bulge are always assumed to be located at the centre of the galaxy. When a black hole is ejected from its galaxy as a result of a recoil, we search for a particle in the simulation in the neighbourhood of the galaxy with appropriate velocity which, we assume, tracks the orbit of the black hole. To find as close a match as possible, we define a cost function and attach the escaping black hole to the particle that minimises the cost. The cost function we adopt is:

$$C_i^2 = \left(\frac{v_{\rm ej} - v_{i,\hat{r}}}{v_{i,\hat{r}}} \right)^2 + \left(\frac{\Delta r_i}{r_\star} \right)^2 , \tag{4.12}$$

where Δr_i and $v_{i,\hat{r}}$ are the position and radial velocity of the ith particle relative to the initial black hole position and velocity, $v_{\rm ej} = (v_{\rm kick}^2 - v_{\rm esc}^2)^{1/2}$ is the velocity the black hole has when it escapes from the galaxy and $r_\star = 0.33$ Mpc.

For modest kick velocities, $v_{\rm pf} \lesssim 300\,{\rm km\,s^{-1}}$, a suitable particle is usually found and 75% of the ejected black holes are identified with particles with $C_i < 0.5$. As $v_{\rm pf}$ is increased, the identification becomes increasingly difficult. Black holes with such large kick velocities, however, are likely to be ejected from the halo in any case. Thus, if no particle with $C_i < 0.5$ is found, we assume that the black hole has been lost from the halo to become part of a population of intergalactic black holes.

	Stable discs		Unstable discs	
$\bar{N}_{sat}$ with bulges	17.3		52.5	
Median M_{blg}	$2.42 \times 10^6 h^{-1} M_\odot$		$6.5 \times 10^5 h^{-1} M_\odot$	
Smallest M_{blg}	$1.68 \times 10^5 h^{-1} M_\odot$		$1.4 \times 10^5 h^{-1} M_\odot$	
	$300\,\mathrm{km\,s^{-1}}$	$500\,\mathrm{km\,s^{-1}}$	$300\,\mathrm{km\,s^{-1}}$	$500\mathrm{km\,s^{-1}}$
$\bar{N}_{BH}$	17.3	17.0	64.5	59.3
$\bar{N}_{sat\ BH}$	15.2	15.2	44.0	43.3
$\bar{N}_{intrahalo\ BH}$	2.2	1.8	20.5	16.0
$\bar{N}_{intergalactic\ BH}$	3.2	4.0	15.0	23.5

Table 4.1: The mean number of satellite galaxies and black holes for both the fiducial model in which unstable discs form bulges and the model in which disc instability is ignored. In all cases we only consider satellites within r_{vir} with $M_v < -7$ and black holes with $M_{BH} > 10^2 h^{-1} M_\odot$. The first section of the table lists the mean number of satellites with bulges and their median and minimum total stellar masses. The second section lists, for both $v_{pf} = 300\,\mathrm{km\,s^{-1}}$ and $v_{pf} = 500\,\mathrm{km\,s^{-1}}$, the mean total number of black holes within the virial radius, $\bar{N}_{BH}$, of which $\bar{N}_{satBH}$ are galactic black holes residing in satellite galaxies, and $\bar{N}_{intrahaloBH}$ are wandering black holes within the main galaxy halo. The last row gives $\bar{N}_{intergalactic\ BH}$, the mean number of wandering black holes that have escaped beyond the virial radius of the main halo.

The general properties (number density, luminosity function) and spatial distribution of the satellite population depend somewhat on whether or not we assume that unstable discs generate galactic bulges. The statistics of the associated black holes, on the other hand, depend strongly on this assumption since many more bulges and black holes are formed when disc instability is taken into account. As above, in what follows, we take the unstable disc case as our fiducial model, but summarise also results when only mergers are assumed to give rise to bulges.

The distribution of black holes

The spatial distribution of black holes and dark matter in one of our simulations is illustrated in Fig. 4.5. The top two panels correspond to the model with unstable discs and the lower two to the model without unstable discs. In both cases, the left-hand column shows results for a kick velocity prefactor of $v_{\rm pf} = 300\,{\rm km\,s^{-1}}$ and the right-hand column for a kick velocity prefactor of $v_{\rm pf} = 500\,{\rm km\,s^{-1}}$. The greater efficiency of bulge formation in the unstable disc case is reflected in the larger number of black holes in this model. Those black holes that are still associated with a satellite galaxy are indicated by circles while those that have been ejected (the "wandering" black holes) are indicate by squares.

Tests of the mass resolution of our calculation in which we artificially increased the minimum halo mass used in the merger trees indicate that our catalogues are essentially complete for satellite galaxies with V-band luminosity brighter than -7 (corresponding to a mass larger than $1.4 \times 10^5 h^{-1} M_\odot$). To this limit we find that, for the unstable disc model, each simulated galaxy halo at $z = 0$ contains, on average, 52 satellites within its virial radius. The median bulge stellar mass of this population is $6.5 \times 10^6 h^{-1} M_\odot$ with a corresponding black hole mass of $6.5 \times 10^3 h^{-1} M_\odot$ in the ideal $m_{\rm BH} - m_{\rm b}$ relation. The fraction of these satellites that retain a central black hole at the final time depends weakly on the assumed prefactor for the kick velocities. For $v_{\rm pf} \lesssim 300\,{\rm km\,s^{-1}}$ 85.4% of satellites retain a central black hole at the final time, but this fraction is reduced to 84.2% for $v_{\rm pf} \lesssim 500\,{\rm km\,s^{-1}}$.

The number density profiles of the black hole populations of each of our simulations, assuming our fiducial $v_{\rm pf} = 300\,{\rm km\,s^{-1}}$, are shown by the dotted lines in

Fig. 4.4. These can be compared with the dark matter density profiles and the corresponding number density profiles of satellite galaxies with a V band magnitude $M_V < -7$. In order to compare wandering and satellite black hole populations of similar masses, for this plot we selected only black holes with mass greater than that of the black hole in the lowest mass bulge of the satellite sample. The density profile of black holes is seen to be intermediate between that of the dark matter and that of the satellites and, in a couple of cases, wandering black holes are found as far in as $r_{\rm vir}/30$. Our understanding of this behaviour is that these black holes are ejected from the progenitors of both present day satellite galaxies and the progenitors of galaxies which by the present have merged with the central galaxy. As the ejection velocities are not large, these wandering black holes initially have orbits similar to the galaxies that ejected them but, being lighter, they are not subject to dynamical friction and so, unlike the satellite galaxies, those near the centre are not removed by merging with the central galaxy.

The black hole mass function

In the case of the fiducial model (in which unstable discs form bulges), each Milky-Way mass halo generated on average 80 black holes of mass greater than $10^2 h^{-1} M_\odot$ for $300 \lesssim v_{\rm pf} \lesssim 500\,{\rm km\,s^{-1}}$ during the course of its formation. Of these, at $z = 0$ approximately half were wandering black holes and the other half were galactic black holes retained by their host satellite galaxies. Of the wandering black holes, the fraction that are ejected with sufficient velocity to completely escape the halo depends more sensitively on $v_{\rm pf}$. For $v_{\rm pf} = 300{\rm km\,s^{-1}}$, 42% become intergalactic wandering black holes while for $v_{\rm pf} = 500{\rm km\,s^{-1}}$ this fraction increases to 60%. These numbers and the corresponding ones for the model in which disc instability is ignored are given in Table 4.1.

At the present day, there are only 50 black holes more massive than $10^2 h^{-1} M_\odot$ within the central 100 h^{-1}kpc of the halo. Black hole passages through the disc are therefore rare and unlikely to have affected the structure of the disc substantially. A large population of intergalactic black holes exists beyond the virial radius of the halo. Some of these are attached to small galaxies that will eventually become satellites, but others are black holes that were ejected from the halo altogether.

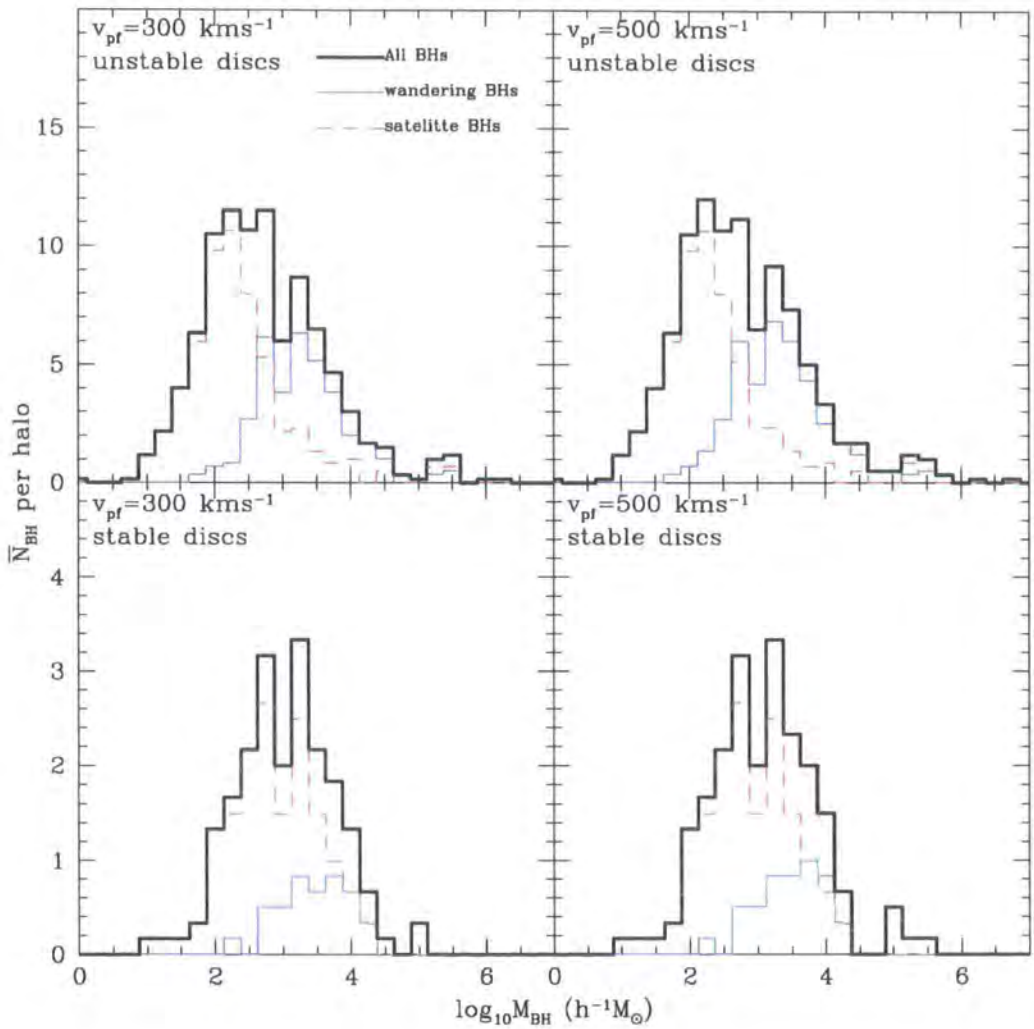

Figure 4.6: The total mass functions for halo black holes. The left-hand panels show the average number of black holes per halo for $v_{\rm pf} = 300\,{\rm km\,s^{-1}}$ while the right-hand panels show the same quantity for $v_{\rm pf} = 500\,{\rm km\,s^{-1}}$. The upper two panels show histograms for models where discs are unstable to bulge formation while the bottom two panels show data for models where disc instability is ignored. The red dashed histogram represents the mass function of black holes that reside in satellite galaxies; the blue solid histrogram represents the mass function of wandering black holes that have been ejected from their host bulges. The black histogram is the combined mass function.

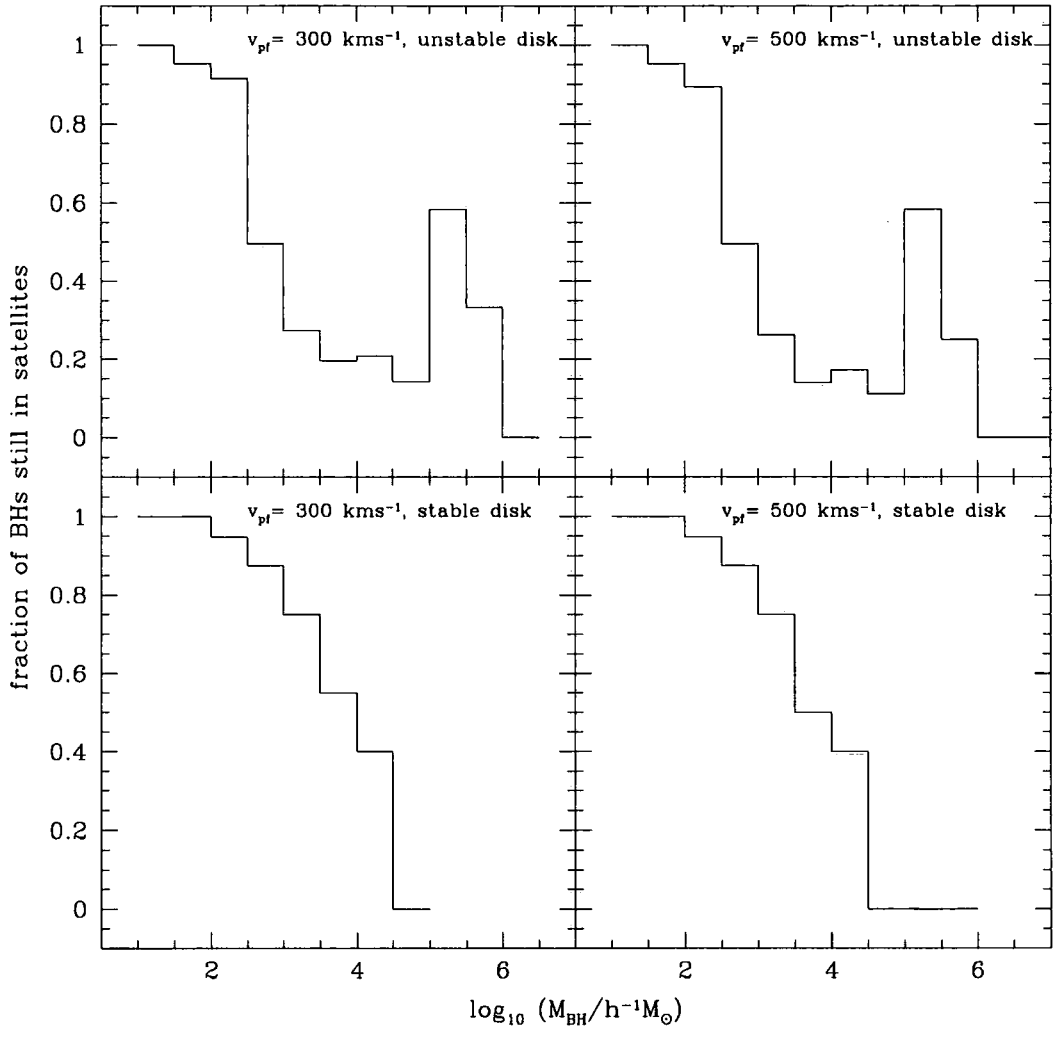

Figure 4.7: The fraction of black holes that remain in satellites as a function of black hole mass. The left two panels are for $v_{\rm pf} = 300\,{\rm km\,s^{-1}}$ and the right two for $v_{\rm pf} = 500\,{\rm km\,s^{-1}}$. The upper two panels are for unstable disc models, while the lower two are for stable disc models.

(Only the fraction of these that were tagged with a particle are shown in Fig. 4.5.)

Fig. 4.6 shows the mass function of halo black holes, averaged over all six simulations, for two assumed values of $v_{\rm pf}$ in the models with and without unstable discs. Black holes in satellites within the virial radius whose host galaxy is brighter then $M_V < -7$ and all wandering black holes are included. In all cases, the central supermassive black hole of mass $\sim 10^6 - 10^7\,M_\odot$ has been omitted from the sample. In the unstable disc case, the medians of the distribution are $10^{2.52}h^{-1}M_\odot$ and $10^{2.56}h^{-1}M_\odot$ for $v_{\rm pf} = 300$ and $500\,{\rm km\,s^{-1}}$ respectively. In both cases, we expect a typical halo to have ~ 3 black holes of mass $M > 10^5 h^{-1}M_\odot$. The mass distribution is slightly wider for the larger value of $v_{\rm pf}$, reflecting the larger efficiency of black hole ejection in this case. In the case where disc instabilities are ignored, there are fewer black holes (note the difference in the scales of the y-axes in the upper and lower panels of this figure), but the distributions are shifted to slightly higher black hole masses with a median of $\sim 10^{3.0}h^{-1}M_\odot$ and virtually no black holes of mass $M > 10^5 h^{-1}M_\odot$. The reason why the median is shifted to slightly higher masses in the stable disc case is because in this case there are fewer ejections, thus allowing satellite galaxy black holes to grow larger.

Also shown in Fig. 4.6 is the result of splitting the black hole mass function into the two populations: the satellite galaxy black holes and wandering black holes (red dashed and blue solid line respectively). The bimodal nature of the total mass function is visible as the result of these two distinct populations. The median of the satellite black hole mass distribution is $\sim 10^{2.24}h^{-1}M_\odot$ while the wandering black hole population peaks at $\sim 10^{3.25}h^{-1}M_\odot$ for unstable disc modes. In the stable disc models, the bimodality is also visible although slightly less pronounced. This tendency for the wandering black holes to be more massive than those retained in the satellites is shown clearly in Fig. 4.7, which plots the fraction of black holes of each mass that are associated with satellite galaxies as a function of black hole mass. We see that below $10^5 M_\odot$ the fraction associated with satellite galaxies is a decreasing function of black hole mass. For low masses ($M < 10^{2.5}h^{-1}M_\odot$), more than 90% of black holes are in satellites. However, at higher masses ($10^{3.5} < M < 10^5 h^{-1}M_\odot$), the majority of black holes are found to be wandering. The reason for this bias in the masses of wandering black holes compared to satellite black holes is the fact

that larger satellites are more likely to merge and experience a kick then smaller ones. Since the dynamical friction timescale is inversely dependent on satellite mass (eq. 4.16 in Cole et al. 2000), we expect the physics of kicks to have a larger effect on the higher mass satellites and bulges than on the lower mass ones. The lower mass satellites will have experienced few if any ejections and their central black holes will be unaffected by velocity kicks.

In principle, a large population of wandering black holes could affect the match between the total mass in black holes at the present day and the mass in quasar remnants inferred from energy considerations (Soltan 1982). In our calculations, however, wandering black holes make up, on average, only 2.6% and 3.9% of the total black hole mass in our simulated galactic halos for $v_{\rm pf} = 300{\rm km\,s^{-1}}$ and $500{\rm km\,s^{-1}}$ respectively. Wandering black holes do, however, make up a large fraction of the intrahalo black hole population (ie. all halo black holes excluding the central one). For these two values of $v_{\rm pf}$, unattached wandering intrahalo black holes make up 31.8% and 48.4% of the total intrahalo satellite black hole mass.

Another noteworthy feature of the black hole mass functions of Fig. 4.6 is the presence of a small population of very massive black holes with $M_{\rm BH} > 10^5 h^{-1} M_\odot$. This population is primarily composed of wandering black holes, although a portion of it in the unstable disc model consists of black holes in massive satellites whose bulge masses are $\sim 10^{8.24} h^{-1} M_\odot$, as evidenced by the high mass peak in the upper panels of Fig. 4.7. In stable disc models, this population is composed entirely of wandering black holes. These massive wandering black holes originate from ejections from the central galaxy that occurred when the central galaxies bulge had a mass of $\sim 10^9 h^{-1} M_\odot$. The central galaxy has since undergone subsequent phases of bulge formation to bring its mass to $\sim 10^{10} h^{-1} M_\odot$ and, in the process, has regrown a central black hole of mass $\lesssim 10^7 h^{-1} M_\odot$.

4.6 Discussion and conclusions

The gravitational recoil of merging black holes is an important physical effect in a universe built up hierarchically through the repeated merging of galactic units. Whenever galaxies that host black holes merge, the black holes themselves will

coalesce and there exists the potential for the remnant black hole to be ejected from the galaxy, provided the recoil velocity is high enough and the galactic potential shallow enough.

We have examined the role that gravitational recoil plays on the demographics of black holes. We find that the process of ejecting black holes from galaxies is efficient if bulges and black holes grow both in galaxy mergers and as a result of discs becoming unstable, because in this case nearly all bulges contain a black hole. In models where disc instability is ignored, this process is not as efficient because fewer bulges and associated black holes exist and because black hole - black hole mergers tend to occur late when the galactic potential wells are deeper. In the former case, black hole ejections produce a significant contribution to the scatter in the $m_{\rm BH} - m_{\rm b}$ relation. In fact, conservative estimates of the scatter in the observed relation constrain the recoil prefactor velocity to $v_{\rm pf} < 500\,{\rm km\,s^{-1}}$, which is consistent with the general relativistic calculations of Favata et al. (2004) and Blanchet et al. (2005).

Our results regarding the demographics and spatial distribution of black holes are in broad agreement with those of Volonteri and Perna (2005) in spite of the different assumptions and methodologies employed in the two studies. For example, the respective radial profiles of intrahalo satellites are similar and Volonteri & Perna find that the population of ejected intrahalo black holes extends further into the centre of the halo than that of satellite-resident black holes, just as in three of our six N-body simulations. Our predicted black hole mass function in the disc-unstable model is similar to the Volonteri & Perna mass function although this agreement is, in part, a coincidence since in their model black holes grow only during merger events.

Is there any empirical evidence for the kind of black hole processes present in our model? Coccato et al. (2006) have recently reported the discovery of a black hole in NGC 4435 whose mass is smaller than about 20% of the value expected from the $m_{\rm BH} - m_{\rm b}$ relation. Black holes with a smaller than expected mass arise naturally in our model, although masses as extreme as this could be rare. For example, in our model with $v_{\rm pf} = 300\,{\rm km\,s^{-1}}$, only $2 - 3\%$ of black holes have a mass that deviates as much or more from the mean relation as that of the black hole in NGC 4435.

However, if $v_{\rm pf} = 500\,{\rm km\,s^{-1}}$ this fraction raises to $\sim 20\%$.

Indirect evidence for black holes with masses below those expected from the $m_{\rm BH} - m_{\rm b}$ relation has been presented by Colbert and Mushotzky (1999). They argue that the compact X-ray sources often seen near the centre of elliptical and spiral galaxies could be black holes of mass $\sim 10^2 - 10^4 M_\odot$. Interestingly, these sources are often displaced from the centre by a few hundred parsecs. Similarly, Neff et al. (2003) have discovered a group of off-centre compact X-ray sources in the merger remnant NGC 3256 which, they argue, could be intermediate-mass black holes. In our model, these objects might be identified with the black holes of infalling satellites or with recently merged black holes that have been kicked out of the galactic centre, their growth stunted as a result.

To investigate the spatial distribution of black holes in Milky-Way like galactic halos we used a set of N-body simulations to track both the satellite galaxies that host black holes and also the black holes that are ejected from their host galaxies. We find that the black hole mass function is bimodal, being composed of two overlapping populations. The lower mass population consists of black holes at the centre of orbiting low mass satellites that have not undergone recent mergers, while the slightly higher mass population is composed of wandering black holes that have been ejected from mergers that formed the central galaxies and the more massive satellites. Among the latter population, we find a few supermassive ($< 10^6 h^{-1} M_\odot$) black holes that were ejected from the main progenitor of the central galaxy sufficiently early such that the bulge of the central galaxy has had enough time to regrow a sizable black hole. There is also an intergalactic population consisting of black holes whose recoil velocity was large enough not only to unbind them from their host galaxy but also from its halo.

In the future it may be possible to detect the formation of wandering black holes directly using instruments such as *LISA*[2] that can directly measure the gravitational radiation emitted in the black hole – black hole merger that ejects the remnant. In the meantime, detecting these black holes presents an interesting challenge. In practise, an ejected intergalactic or intrahalo black hole is likely to bring along a small cusp of stars tightly bound to it as it escapes the halo's potential. These

[2] `http://lisa.jpl.nasa.gov/`

stars would provide the only measurable way of detecting such black holes. Most likely, there would not be any gas that could be accreted and hence the black holes would not be observable in the conventional way. However, if the orbits of the stars that are bound to the black hole are gravitationally perturbed, some of them may be accreted by the black hole. In addition to emitting a burst of gravitational radiation, this type of infall would tidally disrupt the star and create a small accretion disc which would radiate according to the standard physics of accretion discs. The gravitational radiation signature and accretion disc emission would provide the best way to identify these black holes.

Magain et al. (2005) have recently discovered a quasar, HE0450-2958, which has no visible host galaxy and, at first sight, is a good candidate for an escaped black hole. Haehnelt et al. (2006) have indeed suggested that the quasar may have been ejected from a nearby ultraluminous infrared galaxy (ULIRG) either through the gravitational recoil process we are considering here or through a gravitational slingshot associated with three or more black holes involved in the merger responsible for the ULIRG. Hoffman and Loeb (2006) have argued that the quasar is much too far from the companion galaxy, ~ 7 kpc, to have been ejected with a velocity of $300\,\mathrm{km\,s^{-1}}$ and favour the slingshot mechanism. From kinematic information derived from the spectra of the quasar and companion galaxy, Merritt et al. (2005) also derive a large putative kick velocity ~ 500 kms^{-1}. They further argue that the presence of a narrow emission line region at a distance of ~ 1.5 kpc is incompatible with such a large ejection velocity. Hoffman and Loeb (2006), however, point out that the emission line region could plausibly be generated by cold gas clouds left over from an active "feedback" AGN phase and which lie in the vicinity of the quasar. Clearly, further observations of this interesting object are required in order to establish whether or not an ejected black hole is involved.

Ultraluminous X-ray sources (ULXs) or micro-quasars have long been regarded as candidates for intermediate-mass black holes, $M_{\mathrm{BH}} \sim 100 - 1000 M_{\odot}$, radiating near the Eddington limit (see e.g. Fabbiano 1989; Mushotzky 2004 and references therein). This is exactly the kind of object that would be naturally identified with the orbiting intrahalo black holes predicted by our model. This interpretation, however, has two difficulties. Firstly, ULXs tend to be associated with star-forming

regions and their frequency seems to be correlated with the galactic star formation rate (see e.g. Kaaret et al. 2004 and references therein). These facts lend support to the view that ULXs are stellar mass black holes emitting beamed radiation at highly super-Eddington rates or perhaps intermediate mass black holes formed in a young star cluster (Portegies Zwart et al. 2004). The second argument against identifying ULXs with the intrahalo black holes in our model is the difficulty of finding a suitable source of material for the black hole to accrete (Volonteri and Perna 2005). There are, however, some examples of ULXs, most notably the ULX in M82 (Kaaret et al. 2001) and that in the interacting galaxy NGC 7714 (Smith et al. 2005), that are probably much too bright to be explained even as exotic super-Eddington luminosity stellar mass black holes (King et al. 2001). King and Dehnen (2005) call objects like this "Hyperluminous X-ray sources" (HLX) and argue that these objects are precisely the intrahalo black holes associated with satellites in our model which switch on when they come close to the galactic centre. Since the exact mechanism by which these black holes would be activated is uncertain, we cannot predict how common this phenomenon should be. However, our model contains, in principle, a plentiful supply of intermediate mass black holes orbiting in the halo of every galaxy which is sufficient to account for the presence of a few ULXs or HLXs in most galaxies.

Chapter 5

Conclusions and Future Work

5.1 Conclusions and Future Work: Satellites

In this thesis we have posited and attempted to answer two questions, likely to be important in understanding the galaxy formation puzzle. The first concerns the fact that the 11 known satellite galaxies within 250 kpc of the Milky Way lie close to a great circle on the sky. Kroupa et al. (2005) noted that this anisotrpoic alignment is a highly unlikely outcome in the CDM model. In Chapter 2 we used six high resolution N-body simulations of galactic dark matter halos to investigate whether this remarkable property can be understood within the context of the cold dark matter cosmology. We constructed halo merger trees from the simulations and used a semi-analytic model to follow the formation of satellite galaxies. We found that in all 6 of our simulations, the 11 brightest satellites are indeed distributed along thin, disk-like structures analogous to that traced by the Milky Way's satellites. This feature was also seen in simulations executed with a different prescription for star formation and gas cooling (see Chapter 3). This is in sharp contrast to the overall distributions of dark matter in the halo and of subhalos within it which, although triaxial, are not highly aspherical. We found that the spatial distribution of satellites is significantly different from that of the most massive subhalos, but is similar to that of the subset of subhalos that had the most massive progenitors at earlier times. We also found that the elongated disk-like structure delineated by the satellites has its long axis aligned with the major axis of the dark matter halo. In the dark matter only runs we verified our results were robust by changing some of the physics (e.g. reionization) modelled by the semi-analytics. However in

principle, our work in Chapter 2 was still limited by having only six simulations at our disposal.

With the advent of the Sloan Digital Sky Survey, many new Milky Way satellites have been discovered in rapid succession. This has occured because the survey is able to, for the first time, observe very low surface brightness objects. The discovery of eight such objects over the summer of 2006 (Zucker et al. 2006, Belokurov et al. 2006a, Belokurov et al. 2006b, Willman et al. 2006), increases the number of known Milky Way satellites by nearly a factor of 2. However, all the newly discovered satellites are much fainter than the previously know 11 and have very low absolute magnitudes ($M_V \geq -7.8$). Hence the sample of the 11 brightest satellites we use (which is identical to the sample used by Kroupa et al. 2005), is uneffected by the discovery of additional low surface brightness satellites.

The lack of a statistically large sample was also present in Chapter 3 where we used two cosmological hydrodynamic simulations to study the alignments of the angular momenta and the spatial distribution of satellite galaxies, dark matter haloes and the central galaxies. In Chapter 3 we were able to resolve slightly more galactic systems (nine) than in Chapter 2, however the same small sample size problem meant only three of these had enough satellites to make a comparison with the Milky Way meaningful. Since we used the galaxy formation simulations of Okamoto et al. (2005) (which are able to produce realistically sized galaxy discs), we were able to study not only the sense of the satellite galaxy anisotropy (i.e. whether it is perpendicular to the galactic disc) but also the alignment between the angular momentum of the galactic disc and various components of the halo. We found that for galaxies with a significant disc component, the disc and the dark halo's angular momenta are aligned out to the virial radius. We also found that the total angular momentum of the satellite distribution is within 30° of being perpendicular to the long axis of its spatial distribution. As in Chapter 2 we found that the anisotropic satellite galaxy distribution tends to align itself with the long axis of the dark matter halo. We also found that the short axis of two of our satellite systems were perpendicular to the short axis of their central galaxies, implying that two out of three of our systems had a similar configuration to the Milky Way and its satellite system.

Since these simulations were gas-dynamical we were also able to investigate the luminosity function and gas content of the satellite galaxies. We found that unlike the semi-analytic models, the hydrodynamic simulations are more efficient in making large gas rich satellites and come close to matching the observed distribution. The bright end of the luminosity function is well matched, but at the faint end our simulations do not produce enough objects. This is due to our resolution limit, and any results at the very faint end are unlikely to be complete.

In order to make a statistically substantiated statement about the co-evolution of galaxies and their satellites, a larger sample is clearly needed. Indeed, if we wish to compare our theoretical work with, for example, observational studies made with the SDSS, we will need to simulate on the order of 10^4 central galaxies (the SDSS analysis by Yang et al. (2006) contained $\sim 4 \times 10^4$ unique central galactic systems). At present this seems unlikely, however as our computational ability to simulate large cosmological regions increases, new faster codes will be able to achieve this level of precision within the next few years. The largest dark matter simulation conducted to date, the *Millennium Simulation* (Springel et al. 2005), produces an order of magnitude more galaxies in Milky Way sized haloes than the observational work of Yang et al. (2006) ($\sim 8 \times 10^5$ central galaxies in haloes of mass $5 \times 10^{11} M_\odot < M_{\rm H} < 1 \times 10^{13} M_\odot$; Helly, *private communication*). However, the *Millennium* simulation's resolution is far too low to reliably resolve satellites much dimmer then the LMC (the particle resolution is $\sim 10^9 M_\odot$). Likewise, in order to make definitive predictions on the alignment between satellites and central galaxies, or the alignment between the angular momenta of halo and central galaxies, many more well resolved galactic discs are needed. This is likely to be achieved with the advent of large hydrodynamic simulations of cosmological regions.

5.2 Conclusions and Future Work: Black Holes

The second question we have attempted to address concerns the role of gravitational radiation in expelling black holes from galaxies. Galactic bulges are known to harbour central black holes whose mass is tightly correlated with the stellar mass and velocity dispersion of the bulge. In a hierarchical universe, galaxies are built up

through successive mergers of subgalactic units, a process that is accompanied by the amalgamation of bulges and the likely coalescence of galactocentric black holes. In these mergers, the beaming of gravitational radiation during the plunge phase of the black hole collision can impart a linear momentum kick or "gravitational recoil" to the remnant. If large enough, this kick will eject the remnant from the galaxy entirely and populate intergalactic space with wandering black holes. In Chapter 4 we used a semi-analytic model of galaxy formation to investigate the effect of black hole ejections on the scatter of the relation between black hole and bulge mass. We found that while not the dominant source of the measured scatter, this mechanism does provide a significant contribution and may be used to set a constraint, $v_{\rm kick} \lesssim 500 {\rm km\,s^{-1}}$, on the typical kick velocity, in agreement with values found from general relativistic calculations. Even for the more modest kick velocities implied by these calculations, we found that a substantial number of central black holes are ejected from the progenitors of present day galaxies, giving rise to a population of wandering intrahalo and intergalactic black holes whose distribution we were able to qualify. Although we found that intergalactic black holes make up only $\sim 2-3\%$ of the total galactic black hole mass within a halo, wandering black holes can contribute up to about half of the total black hole mass orbiting the central galaxy.

In our black hole work in Chapter 4, we used a cost function to tag particles which had the same velocity and position as our ejected black holes. For the limited set of properties we investigated, this proved to be accurate enough for a quantitative study. To study more details of the ejected black hole population, it would be beneficial if one could introduce a "new" particle into the simulation with the exact mass, position and velocity of the ejected black hole. To do this would require re-running the simulation at each time step, after inserting the requisite black hole. The computational cost of such a technique is at the moment, far too expensive. However, it might be possible to incorporate such ideas into the simulation code itself, and calculate the dynamics of ejected black holes on-the-fly, as the simulation advances. Such work has yet to be attempted mostly due to the uncertainty regarding the gravitational recoil velocity kick. However, as progress in minimising the uncertainties in the recoil calculation, as well as an extension in understanding

the influence, this calculation may in the future be possible.

Bibliography

S. J. Aarseth, E. L. Turner, and J. R. Gott. N-body simulations of galaxy clustering. I - Initial conditions and galaxy collapse times. ApJ, 228:664–683, March 1979.

M. G. Abadi, J. F. Navarro, M. Steinmetz, and V. R. Eke. Simulations of Galaxy Formation in a Λ Cold Dark Matter Universe. II. The Fine Structure of Simulated Galactic Disks. ApJ, 597:21–34, November 2003.

Abazajian et al. and The SDSS collaboration. The Third Data Release of the Sloan Digital Sky Survey. AJ, 129:1755–1759, March 2005.

A. Aguirre, J. Schaye, and E. Quataert. Problems for Modified Newtonian Dynamics in Clusters and the Lyα Forest? ApJ, 561:550–558, November 2001.

J. Bailin, D. Kawata, B. K. Gibson, M. Steinmetz, J. F. Navarro, C. B. Brook, S. P. D. Gill, R. A. Ibata, A. Knebe, G. F. Lewis, and T. Okamoto. Internal Alignment of the Halos of Disk Galaxies in Cosmological Hydrodynamic Simulations. ApJ, 627:L17–L20, July 2005.

J. Bailin and M. Steinmetz. Internal and External Alignment of the Shapes and Angular Momenta of ΛCDM Halos. ApJ, 627:647–665, July 2005.

J. Barnes and P. Hut. A Hierarchical O(NlogN) Force-Calculation Algorithm. Nature, 324:446–449, December 1986.

C. M. Baugh, A. J. Benson, S. Cole, C. S. Frenk, and C. G. Lacey. Modelling the evolution of galaxy clustering. MNRAS, 305:L21–L25, May 1999.

C. M. Baugh, S. Cole, C. S. Frenk, and C. G. Lacey. The Epoch of Galaxy Formation. ApJ, 498:504–+, May 1998.

C. M. Baugh, C. G. Lacey, C. S. Frenk, A. J. Benson, S. Cole, G. L. Granato, L. Silva, and A. Bressan. Predictions for the SKA from hierarchical galaxy formation models. *New Astronomy Review*, 48:1239–1246, December 2004.

C. M. Baugh, C. G. Lacey, C. S. Frenk, G. L. Granato, L. Silva, A. Bressan, A. J. Benson, and S. Cole. Can the faint submillimetre galaxies be explained in the Λ cold dark matter model? MNRAS, 356:1191–1200, January 2005.

J. D. Bekenstein. Relativistic gravitation theory for the modified Newtonian dynamics paradigm. Phys. Rev. D, 70(8):083509–+, October 2004.

V. Belokurov, D. B. Zucker, N. W. Evans, J. T. Kleyna, S. Koposov, S. T. Hodgkin, M. J. Irwin, G. Gilmore, M. I. Wilkinson, M. Fellhauer, D. M. Bramich, P. C. Hewett, S. Vidrih, J. T. A. De Jong, J. A. Smith, H. . Rix, E. F. Bell, R. F. G. Wyse, H. J. Newberg, P. A. Mayeur, B. Yanny, C. M. Rockosi, O. Y. Gnedin, D. P. Schneider, T. C. Beers, J. C. Barentine, H. Brewington, J. Brinkmann, M. Harvanek, S. J. Kleinman, J. Krzesinski, D. Long, A. Nitta, and S. A. Snedden. Cats and Dogs, Hair and A Hero: A Quintet of New Milky Way Companions. *ArXiv Astrophysics e-prints*, August 2006a.

V. Belokurov, D. B. Zucker, N. W. Evans, M. I. Wilkinson, M. J. Irwin, S. Hodgkin, D. M. Bramich, J. M. Irwin, G. Gilmore, B. Willman, S. Vidrih, H. J. Newberg, R. F. G. Wyse, M. Fellhauer, P. C. Hewett, N. Cole, E. F. Bell, T. C. Beers, C. M. Rockosi, B. Yanny, E. K. Grebel, D. P. Schneider, R. Lupton, J. C. Barentine, H. Brewington, J. Brinkmann, M. Harvanek, S. J. Kleinman, J. Krzesinski, D. Long, A. Nitta, J. A. Smith, and S. A. Snedden. A Faint New Milky Way Satellite in Bootes. *ArXiv Astrophysics e-prints*, April 2006b.

A. J. Benson. Orbital parameters of infalling dark matter substructures. MNRAS, 358:551–562, April 2005.

A. J. Benson, R. G. Bower, C. S. Frenk, C. G. Lacey, C. M. Baugh, and S. Cole. What Shapes the Luminosity Function of Galaxies? ApJ, 599:38–49, December 2003a.

A. J. Benson, C. S. Frenk, C. M. Baugh, S. Cole, and C. G. Lacey. The effects of photoionization on galaxy formation - III. Environmental dependence in the luminosity function. MNRAS, 343:679–691, August 2003b.

A. J. Benson, C. S. Frenk, C. G. Lacey, C. M. Baugh, and S. Cole. The effects of photoionization on galaxy formation - II. Satellite galaxies in the Local Group. MNRAS, 333:177–190, June 2002a.

A. J. Benson, C. G. Lacey, C. M. Baugh, S. Cole, and C. S. Frenk. The effects of photoionization on galaxy formation - I. Model and results at z=0. MNRAS, 333:156–176, June 2002b.

P. Berczik, D. Merritt, R. Spurzem, and H.-P. Bischof. Efficient Merger of Binary Supermassive Black Holes in Non-Axisymmetric Galaxies. *ArXiv Astrophysics e-prints*, January 2006.

J. Binney. The physics of dissipational galaxy formation. ApJ, 215:483–491, July 1977.

J. Binney and S. Tremaine. *Galactic dynamics.* Princeton, NJ, Princeton University Press, 1987, 747 p., 1987.

L. Blanchet, M. S. S. Qusailah, and C. M. Will. Gravitational Recoil of Inspiraling Black Hole Binaries to Second Post-Newtonian Order. ApJ, 635:508–515, December 2005.

J. R. Bond, S. Cole, G. Efstathiou, and N. Kaiser. Excursion set mass functions for hierarchical Gaussian fluctuations. ApJ, 379:440–460, October 1991.

J. R. Bond, G. Efstathiou, and J. Silk. Massive neutrinos and the large-scale structure of the universe. *Physical Review Letters*, 45:1980–1984, December 1980.

R. G. Bower. The evolution of groups of galaxies in the Press-Schechter formalism. MNRAS, 248:332–352, January 1991.

R. G. Bower, A. J. Benson, R. Malbon, J. C. Helly, C. S. Frenk, C. M. Baugh, S. Cole, and C. G. Lacey. The broken hierarchy of galaxy formation. *ArXiv Astrophysics e-prints*, November 2005.

T. G. Brainerd. Anisotropic Distribution of SDSS Satellite Galaxies: Planar (Not Polar) Alignment. ApJ, 628:L101–L104, August 2005.

A. H. Broeils. *Ph.D. Thesis, University of Groningen*, 1992.

J. S. Bullock. Shapes of dark matter halos. In P. Natarajan, editor, *The shapes of galaxies and their dark halos, Proceedings of the Yale Cosmology Workshop "The Shapes of Galaxies and Their Dark Matter Halos", New Haven, Connecticut, USA, 28-30 May 2001. Edited by Priyamvada Natarajan. Singapore: World Scientific, 2002, ISBN 9810248482, p.109*, pages 109–+, 2002.

J. S. Bullock, T. S. Kolatt, Y. Sigad, R. S. Somerville, A. V. Kravtsov, A. A. Klypin, J. R. Primack, and A. Dekel. Profiles of dark haloes: evolution, scatter and environment. MNRAS, 321:559–575, March 2001.

J. S. Bullock, A. V. Kravtsov, and D. H. Weinberg. Reionization and the Abundance of Galactic Satellites. ApJ, 539:517–521, August 2000.

E. M. Burbidge, G. R. Burbidge, W. A. Fowler, and F. Hoyle. Synthesis of the Elements in Stars. *Reviews of Modern Physics*, 29:547–650, 1957.

S. Burles and D. Tytler. The Deuterium Abundance toward QSO 1009+2956. ApJ, 507:732–744, November 1998.

A. Cattaneo, M. G. Haehnelt, and M. J. Rees. The distribution of supermassive black holes in the nuclei of nearby galaxies. MNRAS, 308:77–81, September 1999.

A. Cavaliere and R. Fusco-Femiano. X-rays from hot plasma in clusters of galaxies. A&A, 49:137–144, May 1976.

S. Chandrasekhar. Stochastic Problems in Physics and Astronomy. *Reviews of Modern Physics*, 15:1–89, 1943.

D. Clowe, A. Gonzalez, and M. Markevitch. Weak-Lensing Mass Reconstruction of the Interacting Cluster 1E 0657-558: Direct Evidence for the Existence of Dark Matter. ApJ, 604:596–603, April 2004.

L. Coccato, M. Sarzi, A. Pizzella, E. M. Corsini, E. D. Bontà, and F. Bertola. NGC 4435: a bulge-dominated galaxy with an unforeseen low-mass central black hole. MNRAS, 366:1050–1066, March 2006.

E. J. M. Colbert and R. F. Mushotzky. The Nature of Accreting Black Holes in Nearby Galaxy Nuclei. ApJ, 519:89–107, July 1999.

S. Cole. *Ph.D. Thesis, Univeristy of Cambridge*, 1989.

S. Cole. Modeling galaxy formation in evolving dark matter halos. ApJ, 367:45–53, January 1991.

S. Cole, A. Aragon-Salamanca, C. S. Frenk, J. F. Navarro, and S. E. Zepf. A Recipe for Galaxy Formation. MNRAS, 271:781–+, December 1994.

S. Cole and N. Kaiser. Biased clustering in the cold dark matter cosmogony. MNRAS, 237:1127–1146, April 1989.

S. Cole and C. Lacey. The structure of dark matter haloes in hierarchical clustering models. MNRAS, 281:716–+, July 1996.

S. Cole, C. G. Lacey, C. M. Baugh, and C. S. Frenk. Hierarchical galaxy formation. MNRAS, 319:168–204, November 2000.

S. Cole, W. J. Percival, J. A. Peacock, P. Norberg, C. M. Baugh, C. S. Frenk, I. Baldry, J. Bland-Hawthorn, T. Bridges, R. Cannon, M. Colless, C. Collins, W. Couch, N. J. G. Cross, G. Dalton, V. R. Eke, R. De Propris, S. P. Driver, G. Efstathiou, R. S. Ellis, K. Glazebrook, C. Jackson, A. Jenkins, O. Lahav, I. Lewis, S. Lumsden, S. Maddox, D. Madgwick, B. A. Peterson, W. Sutherland, and K. Taylor. The 2dF Galaxy Redshift Survey: power-spectrum analysis of the final data set and cosmological implications. MNRAS, 362:505–534, September 2005.

M. Colless, G. Dalton, S. Maddox, W. Sutherland, P. Norberg, S. Cole, J. Bland-Hawthorn, T. Bridges, R. Cannon, C. Collins, W. Couch, N. Cross, K. Deeley, R. de Propris, S. P. Driver, G. Efstathiou, R. S. Ellis, C. S. Frenk, K. Glazebrook, C. Jackson, O. Lahav, I. Lewis, S. Lumsden, D. Madgwick, J. A. Peacock, B. A.

Peterson, I. Price, M. Seaborne, and K. Taylor. The 2dF Galaxy Redshift Survey 100k Data Release (2dFGRS Team, 2001). *VizieR Online Data Catalog*, 7226: 0–+, June 2003.

F. Combes, F. Debbasch, D. Friedli, and D. Pfenniger. Box and peanut shapes generated by stellar bars. A&A, 233:82–95, July 1990.

M. W. Craig and M. Davis. The structure of dark matter halos in an annihilating dark matter model. *New Astronomy*, 6:425–436, October 2001.

D. J. Croton, V. Springel, S. D. M. White, G. De Lucia, C. S. Frenk, L. Gao, A. Jenkins, G. Kauffmann, J. F. Navarro, and N. Yoshida. The many lives of active galactic nuclei: cooling flows, black holes and the luminosities and colours of galaxies. MNRAS, 365:11–28, January 2006.

M. Davis, G. Efstathiou, C. S. Frenk, and S. D. M. White. The evolution of large-scale structure in a universe dominated by cold dark matter. ApJ, 292:371–394, May 1985.

T. Di Matteo, V. Springel, and L. Hernquist. Energy input from quasars regulates the growth and activity of black holes and their host galaxies. Nature, 433: 604–607, February 2005.

G. Efstathiou, M. Davis, S. D. M. White, and C. S. Frenk. Numerical techniques for large cosmological N-body simulations. ApJS, 57:241–260, February 1985.

G. Efstathiou, G. Lake, and J. Negroponte. The stability and masses of disc galaxies. MNRAS, 199:1069–1088, June 1982.

A. Einstein. Die Grundlage der allgemeinen Relativitätstheorie. *Annalen der Physik*, 49:769-822, 1916.

D. J. Eisenstein, I. Zehavi, D. W. Hogg, R. Scoccimarro, M. R. Blanton, R. C. Nichol, R. Scranton, H.-J. Seo, M. Tegmark, Z. Zheng, S. F. Anderson, J. Annis, N. Bahcall, J. Brinkmann, S. Burles, F. J. Castander, A. Connolly, I. Csabai, M. Doi, M. Fukugita, J. A. Frieman, K. Glazebrook, J. E. Gunn, J. S. Hendry,

G. Hennessy, Z. Ivezić, S. Kent, G. R. Knapp, H. Lin, Y.-S. Loh, R. H. Lupton, B. Margon, T. A. McKay, A. Meiksin, J. A. Munn, A. Pope, M. W. Richmond, D. Schlegel, D. P. Schneider, K. Shimasaku, C. Stoughton, M. A. Strauss, M. SubbaRao, A. S. Szalay, I. Szapudi, D. L. Tucker, B. Yanny, and D. G. York. Detection of the Baryon Acoustic Peak in the Large-Scale Correlation Function of SDSS Luminous Red Galaxies. ApJ, 633:560–574, November 2005.

V. Eke, G. Efstathiou, and L. Wright. The cosmological dependence of galactic specific angular momenta. MNRAS, 315:L18–L22, June 2000.

V. R. Eke, S. Cole, and C. S. Frenk. Cluster evolution as a diagnostic for Omega. MNRAS, 282:263–280, September 1996.

V. R. Eke, S. Cole, C. S. Frenk, and J. Patrick Henry. Measuring Omega_0 using cluster evolution. MNRAS, 298:1145–1158, August 1998.

V. R. Eke, C. S. Frenk, C. M. Baugh, S. Cole, P. Norberg, J. A. Peacock, I. K. Baldry, J. Bland-Hawthorn, T. Bridges, R. Cannon, M. Colless, C. Collins, W. Couch, G. Dalton, R. de Propris, S. P. Driver, G. Efstathiou, R. S. Ellis, K. Glazebrook, C. A. Jackson, O. Lahav, I. Lewis, S. Lumsden, S. J. Maddox, D. Madgwick, B. A. Peterson, W. Sutherland, and K. Taylor. Galaxy groups in the Two-degree Field Galaxy Redshift Survey: the luminous content of the groups. MNRAS, 355:769–784, December 2004.

M. Enoki, K. T. Inoue, M. Nagashima, and N. Sugiyama. Gravitational Waves from Supermassive Black Hole Coalescence in a Hierarchical Galaxy Formation Model. ApJ, 615:19–28, November 2004.

A. E. Evrard and J. P. Henry. Expectations for X-ray cluster observations by the ROSAT satellite. ApJ, 383:95–103, December 1991.

G. Fabbiano. X rays from normal galaxies. ARA&A, 27:87–138, 1989.

M. Favata, S. A. Hughes, and D. E. Holz. How Black Holes Get Their Kicks: Gravitational Radiation Recoil Revisited. ApJ, 607:L5–L8, May 2004.

A. Ferrara, S. Bianchi, A. Cimatti, and C. Giovanardi. An Atlas of Monte Carlo Models of Dust Extinction in Galaxies for Cosmological Applications. ApJS, 123: 437–445, August 1999.

L. Ferrarese and D. Merritt. A Fundamental Relation between Supermassive Black Holes and Their Host Galaxies. ApJ, 539:L9–L12, August 2000.

M. J. Fitchett. The influence of gravitational wave momentum losses on the centre of mass motion of a Newtonian binary system. MNRAS, 203:1049–1062, June 1983.

W. L. Freedman, B. F. Madore, B. K. Gibson, L. Ferrarese, D. D. Kelson, S. Sakai, J. R. Mould, R. C. Kennicutt, H. C. Ford, J. A. Graham, J. P. Huchra, S. M. G. Hughes, G. D. Illingworth, L. M. Macri, and P. B. Stetson. Final Results from the Hubble Space Telescope Key Project to Measure the Hubble Constant. ApJ, 553:47–72, May 2001.

C. S. Frenk, A. E. Evrard, S. D. M. White, and F. J. Summers. Galaxy Dynamics in Clusters. ApJ, 472:460–+, December 1996.

C. S. Frenk, S. D. M. White, M. Davis, and G. Efstathiou. The formation of dark halos in a universe dominated by cold dark matter. ApJ, 327:507–525, April 1988.

C. S. Frenk, S. D. M. White, G. Efstathiou, and M. Davis. Cold dark matter, the structure of galactic haloes and the origin of the Hubble sequence. Nature, 317: 595–597, October 1985.

G. Gamow. The physics of the expanding universe. *Vistas in Astronomy*, 2:1726–1732, 1956.

L. Gao, S. D. M. White, A. Jenkins, F. Stoehr, and V. Springel. The subhalo populations of ΛCDM dark haloes. MNRAS, 355:819–834, December 2004.

R. Gavazzi. Constraints on MOND from the lensing cluster MS2137-23. *New Astronomy Review*, 46:783–789, November 2002.

K. Gebhardt, R. Bender, G. Bower, A. Dressler, S. M. Faber, A. V. Filippenko, R. Green, C. Grillmair, L. C. Ho, J. Kormendy, T. R. Lauer, J. Magorrian,

J. Pinkney, D. Richstone, and S. Tremaine. A Relationship between Nuclear Black Hole Mass and Galaxy Velocity Dispersion. ApJ, 539:L13–L16, August 2000.

K. Gebhardt, R. M. Rich, and L. C. Ho. A 20,000 $M_{\rm solar}$ Black Hole in the Stellar Cluster G1. ApJ, 578:L41–L45, October 2002.

J. Gerssen, R. P. van der Marel, K. Gebhardt, P. Guhathakurta, R. C. Peterson, and C. Pryor. Hubble Space Telescope Evidence for an Intermediate-Mass Black Hole in the Globular Cluster M15. II. Kinematic Analysis and Dynamical Modeling. AJ, 124:3270–3288, December 2002.

S. Ghigna, B. Moore, F. Governato, G. Lake, T. Quinn, and J. Stadel. Dark matter haloes within clusters. MNRAS, 300:146–162, October 1998.

S. Ghigna, B. Moore, F. Governato, G. Lake, T. Quinn, and J. Stadel. Density Profiles and Substructure of Dark Matter Halos: Converging Results at Ultra-High Numerical Resolution. ApJ, 544:616–628, December 2000.

R. A. Gingold and J. J. Monaghan. Smoothed particle hydrodynamics - Theory and application to non-spherical stars. MNRAS, 181:375–389, November 1977.

N. Y. Gnedin. Effect of Reionization on Structure Formation in the Universe. ApJ, 542:535–541, October 2000.

F. Governato, C. M. Baugh, C. S. Frenk, S. Cole, C. G. Lacey, T. Quinn, and J. Stadel. The seeds of rich galaxy clusters in the Universe. Nature, 392:359–361, 1998.

F. Governato, L. Mayer, J. Wadsley, J. P. Gardner, B. Willman, E. Hayashi, T. Quinn, J. Stadel, and G. Lake. The Formation of a Realistic Disk Galaxy in Λ-dominated Cosmologies. ApJ, 607:688–696, June 2004.

A. W. Graham, P. Erwin, N. Caon, and I. Trujillo. A Correlation between Galaxy Light Concentration and Supermassive Black Hole Mass. ApJ, 563:L11–L14, December 2001.

A. H. Guth. Inflationary universe: A possible solution to the horizon and flatness problems. Phys. Rev. D, 23:347–356, January 1981.

F. Haardt and P. Madau. Radiative Transfer in a Clumpy Universe. II. The Ultraviolet Extragalactic Background. ApJ, 461:20–+, April 1996.

M. G. Haehnelt, M. B. Davies, and M. J. Rees. Possible evidence for the ejection of a supermassive black hole from an ongoing merger of galaxies. MNRAS, 366: L22–L25, February 2006.

M. G. Haehnelt and M. J. Rees. The formation of nuclei in newly formed galaxies and the evolution of the quasar population. MNRAS, 263:168–178, July 1993.

N. Häring and H.-W. Rix. On the Black Hole Mass-Bulge Mass Relation. ApJ, 604: L89–L92, April 2004.

G. Harker, S. Cole, J. Helly, C. Frenk, and A. Jenkins. A marked correlation function analysis of halo formation times in the Millennium Simulation. MNRAS, 367:1039–1049, April 2006.

D. L. Hawley and P. J. E. Peebles. Distribution of observed orientations of galaxies. AJ, 80:477–491, July 1975.

E. Hayashi, J. F. Navarro, C. Power, A. Jenkins, C. S. Frenk, S. D. M. White, V. Springel, J. Stadel, and T. R. Quinn. The inner structure of ΛCDM haloes - II. Halo mass profiles and low surface brightness galaxy rotation curves. MNRAS, 355:794–812, December 2004.

J. C. Helly, S. Cole, C. S. Frenk, C. M. Baugh, A. Benson, and C. Lacey. Galaxy formation using halo merger histories taken from N-body simulations. MNRAS, 338:903–912, February 2003.

A. Helmi. Velocity Trends in the Debris of Sagittarius and the Shape of the Dark Matter Halo of Our Galaxy. ApJ, 610:L97–L100, August 2004.

L. Hernquist. An analytical model for spherical galaxies and bulges. ApJ, 356: 359–364, June 1990.

L. Hoffman and A. Loeb. Three-Body Kick to a Bright Quasar Out of Its Galaxy during a Merger. ApJ, 638:L75–L78, February 2006.

E. Holmberg. A study of physical groups of galaxies. *Arkiv for Astronomi*, 5: 305–343, 1969.

E. Hubble. A Relation between Distance and Radial Velocity among Extra-Galactic Nebulae. *Proceedings of the National Academy of Science*, 15:168–173, March 1929a.

E. P. Hubble. A spiral nebula as a stellar system, Messier 31. ApJ, 69:103–158, March 1929b.

Y. I. Izotov, T. X. Thuan, and V. A. Lipovetsky. The primordial helium abundance from a new sample of metal-deficient blue compact galaxies. ApJ, 435:647–667, November 1994.

Y. P. Jing. The Density Profile of Equilibrium and Nonequilibrium Dark Matter Halos. ApJ, 535:30–36, May 2000.

Y. P. Jing and Y. Suto. Triaxial Modeling of Halo Density Profiles with High-Resolution N-Body Simulations. ApJ, 574:538–553, August 2002.

P. Kaaret, A. Alonso-Herrero, J. S. Gallagher, G. Fabbiano, A. Zezas, and M. J. Rieke. Displacement of X-ray sources from star clusters in starburst galaxies. MNRAS, 348:L28–L32, February 2004.

P. Kaaret, A. H. Prestwich, A. Zezas, S. S. Murray, D.-W. Kim, R. E. Kilgard, E. M. Schlegel, and M. J. Ward. Chandra High-Resolution Camera observations of the luminous X-ray source in the starburst galaxy M82. MNRAS, 321:L29–L32, February 2001.

M. Kamionkowski and A. R. Liddle. The Dearth of Halo Dwarf Galaxies: Is There Power on Short Scales? *Physical Review Letters*, 84:4525–4528, May 2000.

X. Kang, S. Mao, L. Gao, and Y. P. Jing. Are great disks defined by satellite galaxies in Milky-Way type halos rare in ΛCDM? A&A, 437:383–388, July 2005.

I. Kant. *Allgemeine Naturgeschichte und Theorie des Himmels.* Zeitz, Bei W. Webel, 1798. Neue aufl., 1798.

N. Katz and S. D. M. White. Hierarchical galaxy formation - Overmerging and the formation of an X-ray cluster. ApJ, 412:455–478, August 1993.

G. Kauffmann and S. Charlot. The K-band luminosity function at z=1: a powerful constraint on galaxy formation theory. MNRAS, 297:L23+, June 1998.

G. Kauffmann, J. M. Colberg, A. Diaferio, and S. D. M. White. Clustering of galaxies in a hierarchical universe - I. Methods and results at z=0. MNRAS, 303: 188–206, February 1999.

G. Kauffmann and M. Haehnelt. A unified model for the evolution of galaxies and quasars. MNRAS, 311:576–588, January 2000.

G. Kauffmann, A. Nusser, and M. Steinmetz. Galaxy formation and large-scale bias. MNRAS, 286:795–811, April 1997.

G. Kauffmann, S. D. M. White, and B. Guiderdoni. The Formation and Evolution of Galaxies Within Merging Dark Matter Haloes. MNRAS, 264:201–+, September 1993.

S. T. Kay and R. G. Bower. Measuring Ω_0 from the entropy evolution of clusters. MNRAS, 308:664–676, September 1999.

S. Kazantzidis, A. V. Kravtsov, A. R. Zentner, B. Allgood, D. Nagai, and B. Moore. The Effect of Gas Cooling on the Shapes of Dark Matter Halos. ApJ, 611:L73–L76, August 2004.

R. C. Kennicutt. The rate of star formation in normal disk galaxies. ApJ, 272: 54–67, September 1983.

A. R. King, M. B. Davies, M. J. Ward, G. Fabbiano, and M. Elvis. Ultraluminous X-Ray Sources in External Galaxies. ApJ, 552:L109–L112, May 2001.

A. R. King and W. Dehnen. Hierarchical merging, ultraluminous and hyperluminous X-ray sources. MNRAS, 357:275–278, February 2005.

A. Klypin, A. V. Kravtsov, O. Valenzuela, and F. Prada. Where Are the Missing Galactic Satellites? ApJ, 522:82–92, September 1999.

A. Knebe, S. P. D. Gill, B. K. Gibson, G. F. Lewis, R. A. Ibata, and M. A. Dopita. Anisotropy in the Distribution of Satellite Galaxy Orbits. ApJ, 603:7–11, March 2004.

J. Kormendy and D. Richstone. Inward Bound—The Search For Supermassive Black Holes In Galactic Nuclei. ARA&A, 33:581–+, 1995.

A. V. Kravtsov, O. Y. Gnedin, and A. A. Klypin. The Tumultuous Lives of Galactic Dwarfs and the Missing Satellites Problem. ApJ, 609:482–497, July 2004.

P. Kroupa, C. Theis, and C. M. Boily. The great disk of Milky-Way satellites and cosmological sub-structures. A&A, 431:517–521, February 2005.

W. E. Kunkel and S. Demers. The Magellanic Plane. In *The Galaxy and the Local Group*, pages 241–+, 1976.

W. E. Kunkel and S. Demers. The sculptor dwarf galaxy. Photoelectric sequence and a preliminary colour-magnitude diagram. ApJ, 214:21–+, May 1977.

H. Kurki-Suonio. Big Bang Nucleosynthesis Calculation. *Space Science Reviews*, 100:249–261, January 2002.

C. Lacey and S. Cole. Merger rates in hierarchical models of galaxy formation. MNRAS, 262:627–649, June 1993.

L. B. Lucy. A numerical approach to the testing of the fission hypothesis. AJ, 82: 1013–1024, December 1977.

D. Lynden-Bell. Dwarf galaxies and globular clusters in high velocity hydrogen streams. MNRAS, 174:695–710, March 1976.

D. Lynden-Bell. The Fornax-Leo-Sculptor system. *The Observatory*, 102:202–208, October 1982.

H. T. MacGillivray, R. J. Dodd, B. V. McNally, and H. G. Corwin, Jr. Orientations of galaxies in the Local Supercluster. MNRAS, 198:605–615, February 1982.

P. Madau and E. Quataert. The Effect of Gravitational-Wave Recoil on the Demography of Massive Black Holes. ApJ, 606:L17–L20, May 2004.

P. Magain, G. Letawe, F. Courbin, P. Jablonka, K. Jahnke, G. Meylan, and L. Wisotzki. Discovery of a bright quasar without a massive host galaxy. Nature, 437:381–384, September 2005.

J. Magorrian, S. Tremaine, D. Richstone, R. Bender, G. Bower, A. Dressler, S. M. Faber, K. Gebhardt, R. Green, C. Grillmair, J. Kormendy, and T. Lauer. The Demography of Massive Dark Objects in Galaxy Centers. AJ, 115:2285–2305, June 1998.

S. R. Majewski. The Fornax-Leo-Sculptor stream revisited. ApJ, 431:L17–L21, August 1994.

A. Marconi and L. K. Hunt. The Relation between Black Hole Mass, Bulge Mass, and Near-Infrared Luminosity. ApJ, 589:L21–L24, May 2003.

P. Marigo. Chemical yields from low- and intermediate-mass stars: Model predictions and basic observational constraints. A&A, 370:194–217, April 2001.

M. L. Mateo. Dwarf Galaxies of the Local Group. ARA&A, 36:435–506, 1998.

L. Mayer, S. Kazantzidis, P. Madau, M. Colpi, T. Quinn, and J. Wadsley. Multiscale simulations of merging galaxies with supermassive black holes. *ArXiv Astrophysics e-prints*, February 2006.

R. J. McLure and J. S. Dunlop. On the black hole-bulge mass relation in active and inactive galaxies. MNRAS, 331:795–804, April 2002.

D. Merritt and L. Ferrarese. Black hole demographics from the M-σ relation. MNRAS, 320:L30–L34, January 2001.

D. Merritt, M. Milosavljević, M. Favata, S. A. Hughes, and D. E. Holz. Consequences of Gravitational Radiation Recoil. ApJ, 607:L9–L12, May 2004.

D. Merritt, T. Storchi Bergmann, A. Robinson, D. Batcheldor, D. Axon, and R. Cid Fernandes. The nature of the HE0450-2958 System. *ArXiv Astrophysics e-prints*, November 2005.

M. Milgrom. A Modification of the Newtonian Dynamics - Implications for Galaxy Systems. ApJ, 270:384–+, July 1983.

M. Milosavljević and D. Merritt. Formation of Galactic Nuclei. ApJ, 563:34–62, December 2001.

H. J. Mo, S. Mao, and S. D. M. White. The formation of galactic discs. MNRAS, 295:319–336, April 1998.

H. J. Mo, S. Mao, and S. D. M. White. The structure and clustering of Lyman-break galaxies. MNRAS, 304:175–184, March 1999.

B. Mobasher, R. Guzman, A. Aragon-Salamanca, and S. Zepf. The near-infrared Fundamental Plane of elliptical galaxies. MNRAS, 304:225–234, April 1999.

J. J. Monaghan. Smoothed particle hydrodynamics. ARA&A, 30:543–574, 1992.

B. Moore, S. Gelato, A. Jenkins, F. R. Pearce, and V. Quilis. Collisional versus Collisionless Dark Matter. ApJ, 535:L21–L24, May 2000.

B. Moore, S. Ghigna, F. Governato, G. Lake, T. Quinn, J. Stadel, and P. Tozzi. Dark Matter Substructure within Galactic Halos. ApJ, 524:L19–L22, October 1999.

R. Mushotzky. Ultra-Luminous Sources in Nearby Galaxies. *Progress of Theoretical Physics Supplement*, 155:27–44, 2004.

M. Nagashima, C. G. Lacey, C. M. Baugh, C. S. Frenk, and S. Cole. The metal enrichment of the intracluster medium in hierarchical galaxy formation models. MNRAS, 358:1247–1266, April 2005a.

M. Nagashima, C. G. Lacey, T. Okamoto, C. M. Baugh, C. S. Frenk, and S. Cole. The metal enrichment of elliptical galaxies in hierarchical galaxy formation models. MNRAS, 363:L31–L35, October 2005b.

J. F. Navarro, M. G. Abadi, and M. Steinmetz. Tidal Torques and the Orientation of Nearby Disk Galaxies. ApJ, 613:L41–L44, September 2004a.

J. F. Navarro and W. Benz. Dynamics of cooling gas in galactic dark halos. ApJ, 380:320–329, October 1991.

J. F. Navarro, C. S. Frenk, and S. D. M. White. Simulations of X-ray clusters. MNRAS, 275:720–740, August 1995.

J. F. Navarro, C. S. Frenk, and S. D. M. White. The Structure of Cold Dark Matter Halos. ApJ, 462:563–+, May 1996.

J. F. Navarro, C. S. Frenk, and S. D. M. White. A Universal Density Profile from Hierarchical Clustering. ApJ, 490:493–+, December 1997.

J. F. Navarro, E. Hayashi, C. Power, A. R. Jenkins, C. S. Frenk, S. D. M. White, V. Springel, J. Stadel, and T. R. Quinn. The inner structure of ΛCDM haloes - III. Universality and asymptotic slopes. MNRAS, 349:1039–1051, April 2004b.

J. F. Navarro and S. D. M. White. Simulations of dissipative galaxy formation in hierarchically clustering universes-2. Dynamics of the baryonic component in galactic haloes. MNRAS, 267:401–412, March 1994.

S. G. Neff, J. S. Ulvestad, and S. D. Campion. Radio Emission Associated with Ultraluminous X-Ray Sources in the Galaxy Merger NGC 3256. ApJ, 599:1043–1048, December 2003.

T. Okamoto, V. R. Eke, C. S. Frenk, and A. Jenkins. Effects of feedback on the morphology of galaxy discs. MNRAS, 363:1299–1314, November 2005.

J. P. Ostriker. Collisional Dark Matter and the Origin of Massive Black Holes. *Physical Review Letters*, 84:5258–5260, June 2000.

P. J. E. Peebles. Rotation of Galaxies and the Gravitational Instability Picture. A&A, 11:377–+, April 1971.

A. A. Penzias and R. W. Wilson. A Measurement of Excess Antenna Temperature at 4080 Mc/s. ApJ, 142:419–421, July 1965.

A. Peres. Classical Radiation Recoil. *Physical Review*, 128:2471–2475, December 1962.

S. Perlmutter, S. Gabi, G. Goldhaber, A. Goobar, D. E. Groom, I. M. Hook, A. G. Kim, M. Y. Kim, J. C. Lee, R. Pain, C. R. Pennypacker, I. A. Small, R. S. Ellis, R. G. McMahon, B. J. Boyle, P. S. Bunclark, D. Carter, M. J. Irwin, K. Glazebrook, H. J. M. Newberg, A. V. Filippenko, T. Matheson, M. Dopita, W. J. Couch, and The Supernova Cosmology Project. Measurements of the Cosmological Parameters Omega and Lambda from the First Seven Supernovae at $Z > 0.35$. ApJ, 483:565–+, July 1997.

P. C. Peters and J. Mathews. Gravitational Radiation from Point Masses in a Keplerian Orbit. *Physical Review*, 131:435–440, July 1963.

S. F. Portegies Zwart, H. Baumgardt, P. Hut, J. Makino, and S. L. W. McMillan. Formation of massive black holes throughrunaway collisions in dense young star clusters. Nature, 428:724–726, April 2004.

L. Portinari, C. Chiosi, and A. Bressan. Galactic chemical enrichment with new metallicity dependent stellar yields. A&A, 334:505–539, June 1998.

C. Power, J. F. Navarro, A. Jenkins, C. S. Frenk, S. D. M. White, V. Springel, J. Stadel, and T. Quinn. The inner structure of ΛCDM haloes - I. A numerical convergence study. MNRAS, 338:14–34, January 2003.

W. H. Press and P. Schechter. Formation of Galaxies and Clusters of Galaxies by Self-Similar Gravitational Condensation. ApJ, 187:425–438, February 1974.

M. J. Rees and J. P. Ostriker. Cooling, dynamics and fragmentation of massive gas clouds - Clues to the masses and radii of galaxies and clusters. MNRAS, 179: 541–559, June 1977.

A. G. Riess, A. V. Filippenko, P. Challis, A. Clocchiatti, A. Diercks, P. M. Garnavich, R. L. Gilliland, C. J. Hogan, S. Jha, R. P. Kirshner, B. Leibundgut, M. M. Phillips, D. Reiss, B. P. Schmidt, R. A. Schommer, R. C. Smith, J. Spyromilio, C. Stubbs, N. B. Suntzeff, and J. Tonry. Observational Evidence from Supernovae for an Accelerating Universe and a Cosmological Constant. AJ, 116: 1009–1038, September 1998.

B. Robertson, N. Yoshida, V. Springel, and L. Hernquist. Disk Galaxy Formation in a Λ Cold Dark Matter Universe. ApJ, 606:32–45, May 2004.

V. C. Rubin, N. Thonnard, and W. K. Ford. Rotational properties of 21 SC galaxies with a large range of luminosities and radii, from NGC 4605 /R = 4kpc/ to UGC 2885 /R = 122 kpc/. ApJ, 238:471–487, June 1980.

L. Sales and D. G. Lambas. Anisotropy in the distribution of satellites around primary galaxies in the 2dF Galaxy Redshift Survey: the Holmberg effect. MNRAS, 348:1236–1240, March 2004.

E. E. Salpeter. Nuclear Reactions in Stars Without Hydrogen. ApJ, 115:326–328, March 1952.

W. C. Saslaw, M. J. Valtonen, and S. J. Aarseth. The Gravitational Slingshot and the Structure of Extragalactic Radio Sources. ApJ, 190:253–270, June 1974.

R. Schödel, T. Ott, R. Genzel, R. Hofmann, M. Lehnert, A. Eckart, N. Mouawad, T. Alexander, M. J. Reid, R. Lenzen, M. Hartung, F. Lacombe, D. Rouan, E. Gendron, G. Rousset, A.-M. Lagrange, W. Brandner, N. Ageorges, C. Lidman, A. F. M. Moorwood, J. Spyromilio, N. Hubin, and K. M. Menten. A star in a 15.2-year orbit around the supermassive black hole at the centre of the Milky Way. Nature, 419:694–696, October 2002.

N. A. Sharp, D. N. C. Lin, and S. D. M. White. A test of the tidal hypothesis for the origin of galactic angular momentum. MNRAS, 187:287–291, April 1979.

L. Shaw, J. Weller, J. P. Ostriker, and P. Bode. A New Definition of Substructure in Dark Matter Halos. *ArXiv Astrophysics e-prints*, March 2006.

J. Silk. On the fragmentation of cosmic gas clouds. I - The formation of galaxies and the first generation of stars. ApJ, 211:638–648, February 1977.

J. Silk and M. J. Rees. Quasars and galaxy formation. A&A, 331:L1–L4, March 1998.

B. J. Smith, C. Struck, and M. A. Nowak. Chandra X-Ray Imaging of the Interacting Starburst Galaxy System NGC 7714/7715: Tidal Ultraluminous X-Ray

Sources, Emergent Wind, and Resolved H II Regions. AJ, 129:1350–1368, March 2005.

G. F. Smoot, C. L. Bennett, A. Kogut, E. L. Wright, J. Aymon, N. W. Boggess, E. S. Cheng, G. de Amici, S. Gulkis, M. G. Hauser, G. Hinshaw, P. D. Jackson, M. Janssen, E. Kaita, T. Kelsall, P. Keegstra, C. Lineweaver, K. Loewenstein, P. Lubin, J. Mather, S. S. Meyer, S. H. Moseley, T. Murdock, L. Rokke, R. F. Silverberg, L. Tenorio, R. Weiss, and D. T. Wilkinson. Structure in the COBE differential microwave radiometer first-year maps. ApJ, 396:L1–L5, September 1992.

A. Soltan. Masses of quasars. MNRAS, 200:115–122, July 1982.

R. S. Somerville and J. R. Primack. Semi-analytic modelling of galaxy formation: the local Universe. MNRAS, 310:1087–1110, December 1999.

J. Sommer-Larsen, S. Gelato, and H. Vedel. Formation of Disk Galaxies: Feedback and the Angular Momentum Problem. ApJ, 519:501–512, July 1999.

D. N. Spergel, R. Bean, O. Dore', M. R. Nolta, C. L. Bennett, G. Hinshaw, N. Jarosik, E. Komatsu, L. Page, H. V. Peiris, L. Verde, C. Barnes, M. Halpern, R. S. Hill, A. Kogut, M. Limon, S. S. Meyer, N. Odegard, G. S. Tucker, J. L. Weiland, E. Wollack, and E. L. Wright. Wilkinson Microwave Anisotropy Probe (WMAP) Three Year Results: Implications for Cosmology. *ArXiv Astrophysics e-prints*, March 2006.

D. N. Spergel and P. J. Steinhardt. Observational Evidence for Self-Interacting Cold Dark Matter. *Physical Review Letters*, 84:3760–3763, April 2000.

D. N. Spergel, L. Verde, H. V. Peiris, E. Komatsu, M. R. Nolta, C. L. Bennett, M. Halpern, G. Hinshaw, N. Jarosik, A. Kogut, M. Limon, S. S. Meyer, L. Page, G. S. Tucker, J. L. Weiland, E. Wollack, and E. L. Wright. First-Year Wilkinson Microwave Anisotropy Probe (WMAP) Observations: Determination of Cosmological Parameters. ApJS, 148:175–194, September 2003.

V. Springel. The cosmological simulation code GADGET-2. MNRAS, 364:1105–1134, December 2005.

V. Springel, C. S. Frenk, and S. D. M. White. The large-scale structure of the Universe. Nature, 440:1137–1144, April 2006.

V. Springel and L. Hernquist. The history of star formation in a Λ cold dark matter universe. MNRAS, 339:312–334, February 2003.

V. Springel, S. D. M. White, A. Jenkins, C. S. Frenk, N. Yoshida, L. Gao, J. Navarro, R. Thacker, D. Croton, J. Helly, J. A. Peacock, S. Cole, P. Thomas, H. Couchman, A. Evrard, J. Colberg, and F. Pearce. Simulations of the formation, evolution and clustering of galaxies and quasars. Nature, 435:629–636, June 2005.

V. Springel, S. D. M. White, G. Tormen, and G. Kauffmann. Populating a cluster of galaxies - I. Results at [formmu2]z=0. MNRAS, 328:726–750, December 2001a.

V. Springel, N. Yoshida, and S. D. M. White. GADGET: a code for collisionless and gasdynamical cosmological simulations. *New Astronomy*, 6:79–117, April 2001b.

F. Stoehr, S. D. M. White, G. Tormen, and V. Springel. The satellite population of the Milky Way in a ΛCDM universe. MNRAS, 335:L84–L88, October 2002.

R. S. Sutherland and M. A. Dopita. Cooling functions for low-density astrophysical plasmas. ApJS, 88:253–327, September 1993.

L. A. M. Tasca and S. D. M. White. Quantitative Morphology of Galaxies from the SDSS I: Luminosity in Bulges and Disks. *ArXiv Astrophysics e-prints*, July 2005.

G. Tormen. The rise and fall of satellites in galaxy clusters. MNRAS, 290:411–421, September 1997.

S. Tremaine, K. Gebhardt, R. Bender, G. Bower, A. Dressler, S. M. Faber, A. V. Filippenko, R. Green, C. Grillmair, L. C. Ho, J. Kormendy, T. R. Lauer, J. Magorrian, J. Pinkney, and D. Richstone. The Slope of the Black Hole Mass versus Velocity Dispersion Correlation. ApJ, 574:740–753, August 2002.

N. Trentham and S. Hodgkin. The luminosity function of the Virgo Cluster from M_B=-22 to -11. MNRAS, 333:423–442, June 2002.

R. B. Tully and J. R. Fisher. A new method of determining distances to galaxies. A&A, 54:661–673, February 1977.

M. Volonteri, F. Haardt, and P. Madau. The Assembly and Merging History of Supermassive Black Holes in Hierarchical Models of Galaxy Formation. ApJ, 582:559–573, January 2003.

M. Volonteri and R. Perna. Dynamical evolution of intermediate-mass black holes and their observable signatures in the nearby Universe. MNRAS, 358:913–922, April 2005.

M. S. Warren, P. J. Quinn, J. K. Salmon, and W. H. Zurek. Dark halos formed via dissipationless collapse. I - Shapes and alignment of angular momentum. ApJ, 399:405–425, November 1992.

R. H. Wechsler, J. S. Bullock, J. R. Primack, A. V. Kravtsov, and A. Dekel. Concentrations of Dark Halos from Their Assembly Histories. ApJ, 568:52–70, March 2002.

M. L. Weil, V. R. Eke, and G. Efstathiou. The formation of disc galaxies. MNRAS, 300:773–789, November 1998.

S. D. M. White. Angular momentum growth in protogalaxies. ApJ, 286:38–41, November 1984.

S. D. M. White and C. S. Frenk. Galaxy formation through hierarchical clustering. ApJ, 379:52–79, September 1991.

S. D. M. White, C. S. Frenk, M. Davis, and G. Efstathiou. Clusters, filaments, and voids in a universe dominated by cold dark matter. ApJ, 313:505–516, February 1987.

S. D. M. White, J. F. Navarro, A. E. Evrard, and C. S. Frenk. The Baryon Content of Galaxy Clusters - a Challenge to Cosmological Orthodoxy. Nature, 366:429–+, December 1993.

S. D. M. White and M. J. Rees. Core condensation in heavy halos - A two-stage theory for galaxy formation and clustering. MNRAS, 183:341–358, May 1978.

B. Willman, F. Governato, J. J. Dalcanton, D. Reed, and T. Quinn. The observed and predicted spatial distribution of Milky Way satellite galaxies. MNRAS, 353: 639–646, September 2004.

B. Willman, M. Masjedi, D. W. Hogg, J. J. Dalcanton, D. Martinez-Delgado, M. Blanton, A. A. West, A. Dotter, and B. Chaboyer. Willman 1 - A Galactic Satellite at 40 kpc With Multiple Stellar Tails. *ArXiv Astrophysics e-prints*, March 2006.

K. K. S. Wu, A. C. Fabian, and P. E. J. Nulsen. Non-gravitational heating in the hierarchical formation of X-ray clusters. MNRAS, 318:889–912, November 2000.

X. Yang, F. C. van den Bosch, H. J. Mo, S. Mao, X. Kang, S. M. Weinmann, Y. Guo, and Y. P. Jing. The alignment between the distribution of satellites and the orientation of their central galaxy. MNRAS, pages 528–+, June 2006.

N. Yoshida, V. Springel, S. D. M. White, and G. Tormen. Weakly Self-interacting Dark Matter and the Structure of Dark Halos. ApJ, 544:L87–L90, December 2000.

D. Zaritsky, R. Smith, C. S. Frenk, and S. D. M. White. Anisotropies in the Distribution of Satellite Galaxies. ApJ, 478:L53+, April 1997.

M. Zeilik and S. Gregory. *Introductory Astronomy and Astrophysics.* Introductory Astronomy and Astrophysics, 4/e, published by Harcourt College Publishers, 1998; ISBN number: 0-03-006228-4, 1998.

Y. B. Zel'Dovich. Gravitational instability: an approximate theory for large density perturbations. A&A, 5:84–89, March 1970.

A. R. Zentner, A. V. Kravtsov, O. Y. Gnedin, and A. A. Klypin. The Anisotropic Distribution of Galactic Satellites. ApJ, 629:219–232, August 2005.

D. H. Zhao, H. J. Mo, Y. P. Jing, and G. Börner. The growth and structure of dark matter haloes. MNRAS, 339:12–24, February 2003.

D. B. Zucker, V. Belokurov, N. W. Evans, M. I. Wilkinson, M. J. Irwin, T. Sivarani, S. Hodgkin, D. M. Bramich, J. M. Irwin, G. Gilmore, B. Willman, S. Vidrih,

M. Fellhauer, P. C. Hewett, T. C. Beers, E. F. Bell, E. K. Grebel, D. P. Schneider, H. J. Newberg, R. F. G. Wyse, C. M. Rockosi, B. Yanny, R. Lupton, J. A. Smith, J. C. Barentine, H. Brewington, J. Brinkmann, M. Harvanek, S. J. Kleinman, J. Krzesinski, D. Long, A. Nitta, and S. A. Snedden. A New Milky Way Dwarf Satellite in Canes Venatici. *ArXiv Astrophysics e-prints*, April 2006.

F. Zwicky. Die Rotverschiebung von extragalaktischen Nebeln. *Helvetica Physica Acta*, 6:110–127, 1933.